Bergische Universität Wuppertal

Fachbereich Mathematik und Naturwissenschaften

Lehrstuhl für Angewandte Mathematik
und Numerische Mathematik

Numerical Algorithms for System Level Electro-Thermal Simulation

Ph.D. thesis

Author: Massimiliano Culpo

Supervisor: Prof. Dr. Michael Günther

October, 2009

http://www-num.math.uni-wuppertal.de

Die Dissertation kann wie folgt zitiert werden:

urn:nbn:de:hbz:468-20090978
[http://nbn-resolving.de/urn/resolver.pl?urn=urn%3Anbn%3Ade%3Ahbz%3A468-20090978]

Preface

This thesis is one among the many results obtained by the European Research and Training Network (RTN) Project “CoMSON” coordinated by Prof. Michael Günther. Within this framework I was employed as an Early Stage Researcher (ESR) by the “Bergische Universität Wuppertal”, being therefore three times indebted to Michael as he was not only my project coordinator, but also the head of my department and my thesis supervisor. I learned a lot form his suggestions and I want to express here my gratitude for that.

During my work in the project I had the pleasure of being constantly supervised by Dr. Andreas Bartel from “Bergische Universität Wuppertal” and Dr. Steffen Voigtmann from “QIMONDA AG, Munich”. I thank Andreas especially for his help in the proof of the well posedness of the electro-thermal coupled system: without his deep knowledge of PDAEs, and the further aid of Michael in fixing the details, I doubt this would have been possible. I am most grateful to Steffen for the many fruitful discussions we had regarding an industrial implementation of the method. I hope his suggestions and teachings will be adequately reflected in the thesis.

I am pleased to thank the former “CoMSON” Experienced Researcher Dr. Carlo de Falco. The knowledge I gathered in these years about numerics and scientific programming is due to him in the most part. I learned a lot from the collaboration with Prof. Giuseppe Alì while working on the analysis of the thermal element . His example was to me an invaluable training. I am also grateful to Dr. Georg Denk for making me feel welcome during the few weeks I spent in QIMONDA, and for the availability he, Steffen and Carlo showed when preparing the work presented at the SCEE conference in Helsinki. Finally I thank all my colleagues at “Bergische Universität Wuppertal”, for the support they gave me in many ways.

Massimiliano Culpo

Contents

Preface iii

Contents v

List of abbreviations ix

Motivation 3

I Modeling 7

1 State of the art in electro-thermal simulation 9

1.1 Challenges in electro-thermal engineering of ICs 9
1.2 State of the art in electro-thermal simulation 12
1.3 Overview and setting of the proposed method 15

2 Electro-thermal models at the system level 19

2.1 Conservation laws 19
2.2 Standard device models and MNA 24
2.3 Extended electrical models 27
2.4 Thermal element model 28
2.5 Coupled electro-thermal system 31

II Analysis 39

3 Analysis of a coupled electro-thermal system 41

3.1 Assumptions on the heat diffusion operator 41

3.2 Well posedness of the thermal element model 43

3.3 Well posedness of the coupled system 54

III Numerical Discretization 65

4 Patched mesh method 67

4.1 Patched space definition and interpolation estimates 67

4.2 Approximation of diffusion-reaction equations 72

5 Numerical solution of the coupled system 83

5.1 Discretization of the electro-thermal model 83

5.2 Solution of non-linear algebraic equation systems 86

5.3 Evaluation of the thermal element 89

IV Numerical validation 93

6 CMOS inverter 95

6.1 Description of the circuit 95

6.2 Simulation results 97

7 Power nMOS-FET 101

7.1 Description of the device 101

7.2 Simulation results 102

V Appendix 111

A Graph theory 113

A.1 Basic definitions 113

A.2 Kirchhoff's laws 114

B DAE theory 115

B.1 Linear DAEs with constant coefficients: Kronecker index 115

B.2 Extension of index concepts to non-linear DAEs 116

C PDE theory 117

C.1 Function spaces 117

C.2 Variational formulation of elliptic problems 118

D Resolution of diffusion-reaction equation layers 121

D.1 Model problem exhibiting internal layers 121

D.2 Solution decomposition 122

D.3 Discretization of the model problem 124

VI Summary and Bibliography 131

Summary 133

Bibliography 135

List of Figures 145

List of Tables 147

Index 149

List of abbreviations

CAD	Computer aided design
CMOS	Complementary Metal Oxide Semiconductor
DAE	Differential Algebraic Equation
ET	Electro-thermal
FET	Field Effect Transistor
IC	Integrated circuit
ITRS	International Technology Roadmap for Semiconductors
KCL	Kirchhoff's current law
KVL	Kirchhoff's voltage law
MNA	Modified nodal analysis
MOS	Metal Oxide Semiconductor
PDAE	Partial differential algebraic equation
PDE	Partial differential equation
SiP	System in Package
SoC	System on Chip
SOI	Silicon on insulator
UTB	Ultra thin body
VLSI	Very Large Scale of Integration

Introduction

Motivation

Electronic circuits are nowadays an integral part of our everyday life. Their applications range from strategic industry sectors (automotive, robotics, telecommunications, etc.) to home-entertainment. The reason for this unavoidable success lies in the exponential rate of improvement in speed, reliability, integration level and power consumption that semiconductor industry was able to maintain in the last decades.

A major role was played in this sense by CMOS technology, that superseded in the early 80's the then dominant bipolar technology. Since then a tremendous pace of technological progress was achieved mainly by an aggressive geometrical scaling of semiconductor devices feature sizes. During the 80's and part of the 90's (*micro-electronic era*) this type of scaling showed no evident side effects but now, with transistor characteristic lengths entering the *nanometer* regime, the major merits of CMOS technology are threatened by the increasing importance of effects that before could have been considered as secondary. In particular one of the most prominent issues regards power consumption in integrated circuits.

In fact, one of the main reasons CMOS technology was adopted as a standard by semiconductor industry was the reduced power consumption required by CMOS circuits if compared to similar ones based on bipolar technology. This was true especially for digital circuits, as CMOS-logic drew almost no power for a steady-state polarization. Unfortunately, with industry approaching the theoretical limits of CMOS scaling, the trend associating new technology generations with a reduced power consumption has been reversed. Pure *geometrical scaling* will not be sustainable anymore, and a candidate technology to substitute CMOS will become necessary in the next decade if the current rate of development is to be maintained.

Whether industry will take the path of migrating functionalities from the system board level to a single System-in-Package (SiP), or it will choose to employ new structures and materials to improve performances of System-on-Chips (SoC), it is foreseen that an accurate electro-thermal analysis will be a key factor to a reliable and cost-effective design. Computer aided design (CAD) tools are therefore asked to precede these innovations and provide dependable means to simulate coupled electro-thermal effects.

The development of a robust algorithm for this purpose requires a high degree of integration inside usual industrial design flows to be effectively usable, and the possibility to account for 2D/3D heat diffusion to properly describe thermal effects at the system level. In particular it should allow an efficient handling of the space-time multiscale effects associated with the problem at hand. Hence, a new strategy to automatically perform system level electro-thermal simulations inside an industrial design flow is presented in this thesis.

In the proposed approach the electrical behavior of possibly each circuit element is modeled by standard compact models with an added temperature node. Mutual heating is then accounted for by a 2D or 3D diffusion-reaction partial differential equation (PDE), which is coupled to the electrical network by enforcing instantaneous energy conservation. To cope with the multi-scale nature of heat diffusion in VLSI circuit a suitable spatial discretization scheme is adopted which allows for efficient meshing of large domains with details at a much smaller scale. Numerical results on both academic and realistic test cases are included as a validation of the model and of the numerical method. The thesis is organized as follows:

Part I: The major technological challenges expected in the design of new generation ICs are introduced. Particular relevance is given to issues concerning power consumption and heat dissipation. The requirements posed by these issues to CAD tools are then drawn, and the shortcomings of current state-of-the-art approaches are briefly investigated. To overcome these problems a new procedure is proposed. The underlying mathematical model fits the structure of standard modified nodal analysis, and is therefore feasible to be employed inside an industrial design flow without any major modification. In particular, a procedure to automatically extract a thermal element (accounting for heat-diffusion at the system level) from available layout or package information is given.

Part II: Theoretical considerations about the mathematical model established in Part I are presented. More specifically, the thermal element is investigated when driven by external independent sources, fixing either the Joule power dissipated in a physical region of the chip or the corresponding average temperature. Results concerning existence and uniqueness of the solution are derived for both steady-state and transient case. Finally the well posedness of the whole coupled system is provided.

Part III: The numerical approximation of the model introduced in Part I and analyzed in Part II is addressed. To cope with spatial multi-scale issues a finite element method employing non-nested unstructured grids is presented. A thorough discussion concerning its setting and applications is held and numerical examples are provided to support theoretical statements. Then the complete space-time discretization and solution procedure of the coupled electro-thermal system is taken into account. The structure commonly adopted in most of the industrial circuit simulators is sketched and the concept of *elemental stamp* is introduced. Finally a complete characterization of the thermal element stamp is given. Means to improve efficiency in an actual industrial implementation are briefly addressed during the chapter.

Part IV: The method proposed in the thesis is tested on two numerical examples. The first one is a simple CMOS-inverter circuit. Particular attention is given in this case to the reduced number of unknowns stemming from the adopted space discretization method and to the natural way in which mutual heating is taken into account by the thermal element. The second example is provided by a n-channel power MOS-FET whose electrical behavior is modeled by a *distributed lumped-element approach.* In this case the possibility to deploy a fine mesh (associated with a thermally active area) at different positions in the die is stressed. This feature may be of practical relevance if an industrial implementation of the method is to be performed. The code used to compute these two examples is released under the GNU-GPL (version 2) license and distributed as part of the `CoMSON DP` environment.

Part V: The basic notions of graph theory (Appendix A), differential-algebraic equations (Appendix B) and partial differential equations (Appendix C) necessary to the understanding of the thesis are here gathered as appendix chapters. Though the subjects are presented in a very schematic form, many references to advanced textbooks or research articles are provided to the reader interested in a deeper treatment of these topics. Moreover in Appendix D a novel extension of the patched finite element method that permits to resolve internal and boundary layers in singularly perturbed diffusion reaction PDEs is given.

Part VI: Finally, the summary and the bibliography can be found in Part VI together with the list of figures and tables, and the alphabetical index.

Part I

Modeling

1

State of the art in electro-thermal simulation

The purpose of Chapter 1 is to introduce the reader to the field of electro-thermal (ET) simulation and sketch its state of the art, providing thus a clear starting point for the research that will be developed next in the thesis.

Strong motivations toward the necessity of a coupled treatment of electrical and thermal effects during the design phase of new generation integrated circuits (ICs) are given in Section 1.1, where major technological challenges are briefly discussed. As numerical simulation of suitable mathematical models is the usual way through which these effects are accounted for in an industrial design environment, in Section 1.2 a list of requirements is derived for a generic Computer Aided Design (CAD) tool aiming at the description of IC electro-thermal behavior. To outline the state of the art in this field a broad review of literature is proposed and categorized on the basis of the adopted models and solution techniques. A discussion concerning the setting of the method developed in this thesis concludes the chapter.

1.1 Challenges in electro-thermal engineering of ICs

Since its birth semiconductor industry has been characterized by the rapid rate of development in its products. For more than four decades improvements in speed, reliability, integration level, compactness and power consumption proceeded uninterrupted. The major part of these achievements is principally due to the exponential decrease in the minimum feature sizes used to fabricate integrated circuits. The most cited fact to establish this trend regards integration level, and is usually stated as *Moore's law* [46, 70, 84]:

> “ The number of components per chip doubles roughly every 24 months”.

In the last few technology generations of Complementary Metal-Oxide-Silicon (CMOS) ICs this miniaturization was pursued via an aggressive *geometrical scaling*: horizontal and vertical feature sizes of the devices were systematically shrunken to improve integration density and thus circuit performance [24]. With industry beginning to approach the theoretical limits of CMOS scaling, this rapid pace of improvements is now threatened and it is forecasted in the 2007 edition of the International Technology Roadmap for Semiconductors (ITRS) [57] that by the end of the next decade it will be necessary to go beyond CMOS technology as it is now.

As circuit performance does not scale only with Moore's law, but depends also on many other design and technology choices, post-CMOS technologies may thus involve not only new devices, but also new manufacturing and design archetypes. On the one hand the path of a greater integration of System-on-Chip (SoC) will be pursued supporting *geometrical scaling* with the new concept of *equivalent scaling* which involves 3D design improvements, new materials usage and the employment of novel structures to enhance the performances on chip. On the other hand there will be an increasing importance of the migration from the system board level into a single System-in-Package (SiP) of all the non-digital functionalities that do not scale with Moore's law (*functional diversification*). The common denominator of all these new approaches is that they require innovations in cross disciplinary fields. In particular for both SoC and SiP applications an accurate electro-thermal analysis will be a key factor to a reliable and cost-effective design [92].

In fact, with transistors entering the nanometer regime, the growth-rate of power dissipation is witnessing an enormous boost due to a substantial increase of effects that before could have been considered as secondary. Peculiarities of these effects are:

1. a strong coupling between temperature and current,
2. the broad space-scale range in which they occur.

Because of these characteristics electro-thermal phenomena may have negative impact at the device, chip and package level. Design processes must therefore take them into account in their very early stages to ensure reliability and performance of the produced circuit. This omni-comprehensive approach towards the understanding of coupled ET issues was named "Electro-Thermal Engineering“ in [6]. Its scope is briefly shown in Figure 1.1, where thermal effects are divided into categories depending on the space-time scale in which they happen. In the following a short description is given based on a paper by Banerjee [6].

Micro-scale Micro-scale effects concern a space-time range of $10n$m-10μm / $0.1n$s-10μs and are mainly associated with the technology processes used to fabricate Silicon chips. As already stated, to maintain the historical trends of performance increase [88], the major integration of SoC requires the introduction of new materials and new design structures to reduce undesired short channel effects or leakage currents and achieve design objectives such as the increase of drain saturation current at lower supply voltage. Among these innovative designs Strained-Silicon devices, as well as Ultra-Thin-Body Silicon-On-Insulator (UTB-SOI) or multiple gates structures are found. However the use of SiGe graded layer in Strained-Silicon devices or of buried oxide in SOI type structures increases the thermal resistance due to the poor thermal conductivity of these materials while confined geometries further exacerbate thermal issues, due to

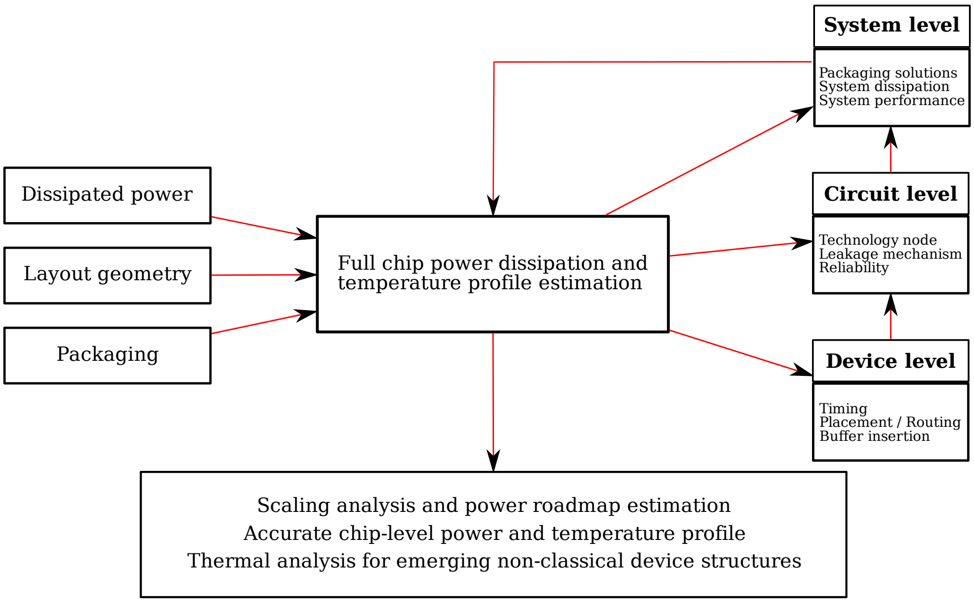
System level
Packaging solutions
System dissipation
System performance
Dissipated power
Layout geometry
Packaging
Full chip power dissipation and temperature profile estimation
Circuit level
Technology node
Leakage mechanism
Reliability
Device level
Timing
Placement / Routing
Buffer insertion
Scaling analysis and power roadmap estimation
Accurate chip-level power and temperature profile
Thermal analysis for emerging non-classical device structures

Figure (1.1): *Schematic overview of electro-thermal engineering broad scope. Geometrical information on the layout and package as well as information on the dissipated power are used to simulate thermal effects at the micro-scale (device and circuit level) and at the macro-scale (system level) in order to obtain a thermally-aware design of ICs.*

the presence of multiple insulating interfaces. The poor thermal properties of these structures result in a major rise in temperature and therefore in lower drive current and higher leakage current than predicted from a purely electrical analysis.

Another technological solution to improve transistor density that is currently being explored by semiconductor industry is the 3D integration of ICs. Here the aim is twofold: a reduced delay is achieved due to the shorter vertical interconnection paths, while the integration of different substrates and technologies is still allowed. A key-barrier becomes in this case the thermal management of internal active layers that suffer from poor thermal dissipation capabilities [2, 7].

Macro-scale Macro-scale effects concern a much bigger space-time scale than micro-scale ones. We can therefore roughly state that while micro-scale effects regard mainly the SoC level, macro-scale ones affect instead the SiP level. A major electrical problem that has to be solved at this scale is the increasing global delay in signal propagation. As a matter of fact, while delay of interconnects is expected to locally decrease with technology scaling, on a global level increased latency is experienced. To keep this problem under control buffers are used to drive signal faster through the various stages of the system. However they contribute significantly to the total power dissipation, and this is becoming a major issue for high-performance ICs. In fact an higher power dissipation causes an increase in the temperature of the devices, which further increases subthreshold leakage currents, going into a feedback that used to be more or less insignificant for earlier generation ICs while it is not in last generation ones.

Another problem is due to extremely high peak temperatures and temperature gradients (hot-spots). These effects appear mainly at the active surface of the chip, and can significantly increase interconnect resistance, which would in turn increase the delay in the interconnect line. In this case an appropriate treatment of the problem is required not to split electrical specifications at the circuit level from thermal specifications at the package level during the design phase.

1.2 State of the art in electro-thermal simulation

Technology modeling and simulation is one of the few methodologies enabling the reduction of development cycle times and costs in industry. As semiconductor fabrication moves toward a major technological innovation, CAD tools have to follow quickly these changes and continue to provide a strong support to the design flow. To achieve this result it is necessary to raise the level of abstraction of simulation softwares [83] allowing:

1. simultaneous treatment of phenomena that were considered separately before,
2. an efficient handling of space-time multiscale effects.

Focusing on the management of ET effects in electronic circuits, this means that thermal components (chip, package or board) should be designed together with the circuit schematic. Due to this necessity any simulation algorithm in the field is asked for some requirements [58] that concern either the integration in an industrial environment or the numerical methods used to simulate ET processes. On the former side an automatic assembly (and simulation) of the coupled ET system from available design data and the possibility to embed easily the algorithm in an optimization loop are surely the most requested features. On the latter side there is a growing need to adopt a 2D or even 3D description of possibly non-linear heat-diffusion processes in SoCs or SiPs: in this case an efficient treatment of the computational mesh is necessary. To the knowledge of the author none of the methods already proposed in literature meet all these requirements at one time.

In the following a broad review of the current state of the art in ET simulation is provided. While a detailed description of every method is out of the scope, the distinctive features of each one are presented and a large number of bibliographical references are given to the interested reader. To simplify the presentation different approaches are categorized according to their treatment of the thermal part in the overall model.

Separate Chip/Package thermal analysis A widespread means to tackle multiphysics issues in ICs is the so-called *V-cycle* design methodology, based on the iteration upon implementation and verification paths. In the simplest case, where only electrical and thermal effects are of concern, this procedure requires:

1. the design of an IC,
2. the simulation of the electrical behavior of the IC, for a given set of guessed device temperatures,
3. the 3D thermal simulation of the Chip or Package, where power densities used as generation terms are computed from previous step results,
4. the verification of design specifications through a second simulation of the electrical behavior, where device temperatures are extracted from previous thermal simulation,
5. the iteration, if verification fails, of the entire procedure.

In this case the coupling is not based upon physical considerations, as two distinct mathematical models are used for the electrical and thermal part and the connection between the two is frequently based on empirical or statistical speculations.

Since electrical simulation of ICs is a quite established subject, scientific literature focuses in this case on improving the efficiency of the thermal solver. In fact this is usually the bottleneck of the entire procedure because of the high computational cost associated with the linearization and discretization of the non-linear partial differential equations (PDEs) used to model heat-diffusion. In [97, 98], for instance, a particular time-stepping technique (Alternate Direction Implicit or ADI) is adopted, that allows for the solution of a sequence of three 1D problems instead of a full 3D one, providing thus an enormous speed-up in the simulation time. The application of this procedure is anyhow restricted to structured mesh and therefore the capabilities to treat unusual geometries are limited. Other proposed strategies involve the employment of multi-grid techniques [65] or space-time adaption [104].

There is however an inherent defect in the *V-cycle* design methodology given by the lack of consistency between electrical and thermal computed data. This was not a major issue with previous generation ICs, where currents exhibit a weak dependence on temperature, but it is becoming a problem nowadays.

Electro-thermal analysis via relaxation method Relaxation methods constitute a possible way to solve the lack of consistency that is the main problem of V-cycle design methodology, while maintaining its peculiarities. In this case a unique mathematical model includes both electrical and thermal effects: the coupling between the two parts is therefore more likely to be based on physical considerations rather than on empirical assumptions. Anyhow the solution of the coupled system is obtained with a relaxation process that still permits to employ two different and specialized tools to cope with the electrical and thermal part. These tools communicate with each other through an appropriate interface [4, 14] and often constitute the kernel of a time-stepping algorithm.

Even though this approach is proven to be the best compromise between accuracy and simulation time for mildly non-linear system, it is widely known that it could cause a deterioration in performance [100] or even failures in converge when applied to systems where currents exhibit a strongly non-linear dependence on temperatures [90].

Electro-thermal analysis via analytical models of Chip/Package Analytical models of Chip/Package aim at a high performance gain paying the price of an over-simplification of the underlying physical problem. They are therefore often tailored to some specific case constituting an optimal ad-hoc solution without any flexibility presumption. For example, in [17] a particular solution for the thermal response of power semiconductors at short power pulses is obtained under the assumption of infinite die surface and negligible removal of heat by convection and radiation. In [67,105] analytical solutions are obtained to describe 1D heat flow in SOI structures and 2D heat loss to the substrate for steady state and fast operating conditions. An attempt to extend the reduced flexibility of analytical approaches providing a semi-analytical, semi-numerical method was presented in [64].

Electro-thermal analysis via RC-network fitting Another way to model thermal response of the Chip/Package is through the fitting of an RC-network with given topology. In this case the RC-network is not required to have any physical interpretation with respect to heat-diffusion processes: it suffices to model the device temperatures dynamical behavior with the required accuracy. The method can thus be interpreted as a black-box system identification method. While giving the possibility to exploit purely electrical solvers (and therefore established mathematical techniques) to simulate a coupled ET system, procedures of that kind introduce a major effort lying in the correct identification of the RC-network parameters (usually involving computationally expensive 3D thermal simulations or even experimental measurements). Examples of the use of RC-network fitting for IC design are in [89], where thermal effects are combined with mixed analog-digital simulation, and in [5], where the approach is used to model by measurements the thermal characterization of power devices.

Electro-thermal analysis via brute-force models The term *brute-force model* refers to the use of some type of discretization of the PDEs describing heat-diffusion on chip or package directly at the circuit simulation level. In this case a frequent assumption is to consider heat-diffusion as a linear process, so that the discretization could be a-priori reinterpreted in terms of linear circuit elements. From the practical point of view this means that a circuit netlist describing the thermal response of the die can be derived once and for all in a pre-processing step, and used afterwards as a standard input to a circuit simulator. The pioneer of this technique was Fukahori [35] who used a particular type of asymmetric finite differences scheme to discretize the linear heat-diffusion equation.

This approach suffers from two main limitations, constituted by the raise in computational cost due to the many variables associated with the discretization of a 3D problem, and by the non-trivial extension to non-linear heat-diffusion. The first of

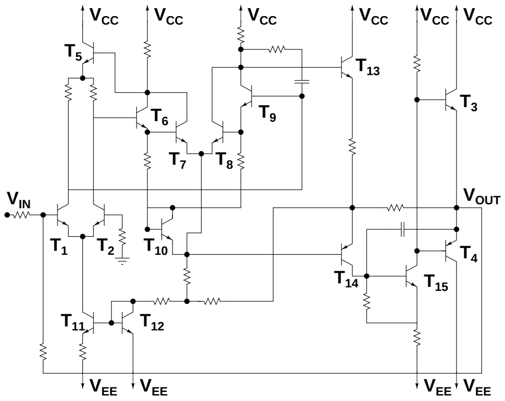

Figure (1.2): *Schematic of the $\mu A709$ Operational Amplifier simulated in [43]. All the transistors are modeled by a suitable set of PDEs. This permits a greater accuracy if compared to standard compact models but restricts the application to circuits composed of a few semiconductor devices.*

the two problems is usually solved in the linear case adopting some order reduction strategies to reduce the thermal part [18, 19, 53, 54] or some particular time-stepping techniques [62] to accelerate the simulation. The second issue, on the other hand, still constitutes an open problem in literature.

Other approaches involving thermal effects Approaches that do not enter in the preceding categories also exist in literature. For instance, in [107, 108] a method based on Green functions representation is proposed. In this case a linear parabolic PDE is employed to describe heat-diffusion, and rectangular shapes for the Chip and Package are assumed.

In [43] a distributed description of many electron devices is combined together with an RC network approach to simulate SiGe HBT circuits. This approach is proposed to fill the gap when compact models for modern or experimental devices are not readily available. In fact the usage of a distributed description for electron devices permits insight into the single device physical quantities and maintains a considerably high accuracy in the approximation. The price to pay is of course the tremendous computational cost required. To give an idea of the circuit size that could be treated in this way, we show the benchmark circuit studied in this paper in Figure 1.2.

1.3 Overview and setting of the proposed method

The method proposed in the following chapters is an attempt to extend the work done in [8, 10], where a model based on a lumped description of electrical devices and on a mixed 0D/1D description of linear heat-diffusion was proposed for SOI-CMOS technology. The adopted solution procedure consisted of a particular *relaxation* type

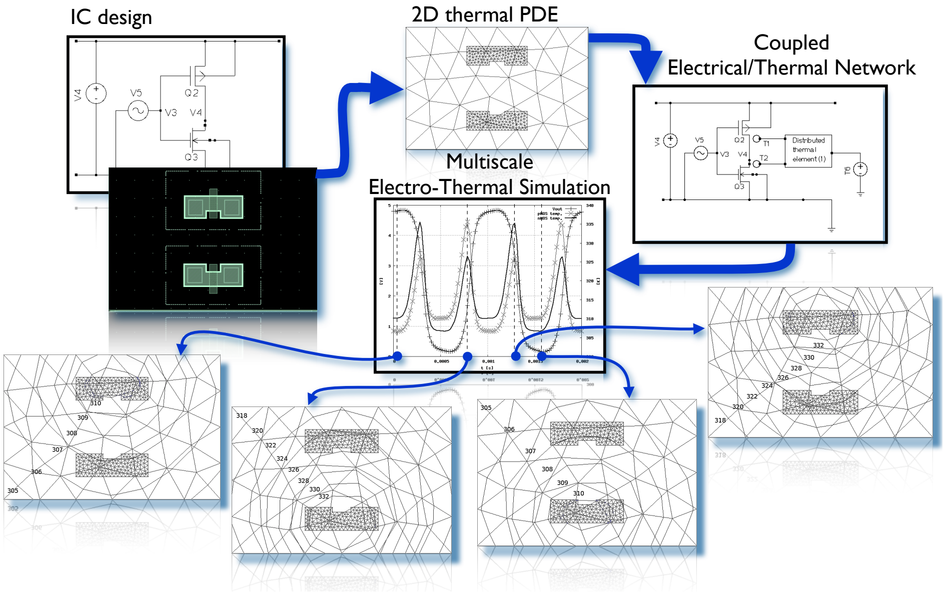
IC design
2D thermal PDE
Coupled
Electrical/Thermal Network
Multiscale
Electro-Thermal Simulation
V4
V5
V3
Q2
Q3
T1
T2
Distributed thermal element (1)
T6

Figure (1.3): *Automated design flow for the electro-thermal simulation of ICs. A thermal element model is automatically constructed from available circuit schematic and design layout, permitting the set-up and simulation of an electro-thermal network that accounts for heat diffusion. In the end information on the usual electrical variables, on the power dissipated by each thermally-active device and on the Chip/Package temperature field is obtained.*

method enabling a performance gain through the exploitation of the different time-scales involved in thermal and electric processes.

In this thesis a generalization to a 2D/3D description of possibly non-linear heat-diffusion is proposed. This thermal model shift makes the approach not bounded to a specific technology and permits to automate the extraction and simulation of the coupled ET system in an industrial design environment, feature lacking in [8, 10]. In fact, starting from available layout and/or package geometry information, a thermal element model is derived directly from PDEs describing heat-diffusion. By imposing suitable integral conditions this element is casted in a form analogous to that of usual electrical circuit elements, so that its use in a standard circuit simulator requires only the implementation of a new element evaluator, but no modification to the main structure of the solver.

To cope with multiscale issues a particular spatial discretization scheme (firstly introduced in [39]) was chosen. This method is based on the use of completely overlapping non-nested meshes and has two main advantages for the application at hand:

1. it allows to cover the whole thermal domain with a uniform triangulation without

having to excessively refine the mesh to capture small geometrical features,

2. it allows to generate a mesh for each circuit element only once and deploy it at different positions on the IC with a significant time improvement.

The latter feature may also give performance gain if an optimization of the relative device placement is to be performed. Because of the poor treatment of strong non-linearities found in literature the relaxation type solution procedure was dropped. In fact the adopted algorithm resembles more a *brute-force* approach, the only difference being that in this case no a-priori interpretation in terms of a circuit netlist is necessary for the discretized PDEs.

Finally, a sketch of the overall automated procedure is proposed in Figure 1.3. Each device in the electrical schematic that has been marked as *thermally-active* is extended with an additional temperature pin, while Chip/Package information is used to construct a circuit element whose purpose is to account for heat-diffusion at the system level. Though embedding a PDE in its constitutive relations, this element is devised to fit the structure of usual lumped devices. Therefore an electro-thermal netlist can be automatically set-up and simulated by means of standard circuit solvers. This permits to obtain information on the electrical and thermal quantities of interest and to compute them in a self-consistent way.

2

Electro-thermal models at the system level

Chapter 2 establishes the mathematical model used to describe ET effects on both SoCs and SiPs. The derivation of the underlying system of equations has been driven by the practical aim to fit already existing circuit simulator structures, especially the one based on Modified Nodal Analysis (MNA).

With this respect it is particularly important to maintain the possibility of an element-by-element assembly of the overall system. This characteristic of MNA stems directly from charge conservation laws at the network level and can be extended to ET systems exploiting the analogies in the physical description of electrical current-flow and heat power-flow (Section 2.1). Constitutive relations for the entities appearing in the system under examination are then needed to complete the derivation of a mathematical model. Therefore the standard treatment of purely electrical devices and thermally active devices is briefly reviewed in Section 2.2 (where an introduction on standard MNA is also given) and Section 2.3 respectively, while in Section 2.4 an exhaustive description of a novel thermal element model used to account for heat diffusion at the system level is provided. This element permits to describe thermal effects resorting to suitable PDEs casted on 2D/3D domains recovered from design information and is interfaced with the 0D device network via appropriate integral conditions. The overall system, constituted by a set of Partial Differential Algebraic Equations (PDAEs), is finally provided in Section 2.5 in a compact formulation stressing the structural similarities with standard MNA.

2.1 Conservation laws

A mathematical model is generally constituted by set of equations or other mathematical relations that are able to capture the interesting features of given physical phenomena in order to describe, foresee or control their development. In many cases such a model is constructed upon the right combination of conservation laws (expressing general physical principles) and constitutive relations which depend on the actual

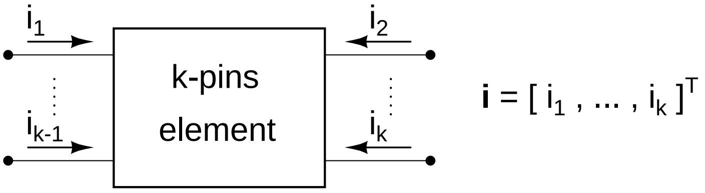

Figure (2.1): *Generic k-pins element. The components of the associated current vector are oriented in such a way that they leave the external pins and enter the element.*

nature of the system under examination [82].

Starting from the point of view of a purely electrical description of the circuit behavior, the physical principle that stands at the base of all the most important modeling paradigms is the balance of electrical currents, usually referred to as *Kirchhoff's current law* (KCL):

Statement 2.1 (KCL - Integral formulation)**.** *The rate of loss of charge ρ within a given volume Ω is equal to the current $\mathbf{J}_q$ flowing out of the surface enclosing it:*

$$-\int_{\Omega}\frac{\partial\rho}{\partial t}d\mathbf{x} = \int_{\partial\Omega}\mathbf{J}_q\mathbf{n}\; d\gamma = \int_{\Omega} div(\mathbf{J}_q)d\mathbf{x}. \tag{2.1}$$

Despite its generality equation (2.1) is not the best suited formulation of KCL for circuit analysis purpose, as its multidimensional character exceeds in details usual design requirements. A commonly assumed ansatz is in this case to neglect the spatial extension of physical devices and of their interconnections, providing the possibility to represent a physical circuit with a network (*schematic*) of discrete components (*elements*) connected at certain points (*nodes*). Each element is supposed to be possibly connected to $k \geq 2$ nodes (*k-pins element*), so that a k-dimensional current vector $\mathbf{i}$ can be associated with it.

In the following a conventional direction is fixed for the components of $\mathbf{i}$ in such a way that they leave the external pins and enter the element (as shown in Figure 2.1). Notice that due to Statement 2.1 these components are not independent, as their algebraic sum must be zero to ensure charge conservation, that is to say:

$$\mathbf{1}^T\mathbf{i} = 0\ , \tag{2.2}$$

where $\mathbf{1} \in \mathbb{R}^k$ is a vector with only unit entries. Readers interested in a thorough treatment of these assumptions and its implications are referred to [15]. For the purpose at hand it suffices to say that under this conceptual simplifications the usual nodal formulation of KCL can be recovered, which constitutes the core of many simulation algorithms:

Statement 2.2 (KCL - Nodal formulation)**.** *The algebraic sum of currents flowing away from any given node is zero.*

If a circuit schematic composed of M elements and $N+1$ nodes is being considered, it can be noticed that Statement 2.2 determines a set of $N+1$ relations. Anyhow, due to the fact that (2.2) holds for each element, only N of these relations result to be linearly independent and therefore a node is usually taken as reference (*ground node*) and omitted when deriving the set of balance equations to be used as a base for a mathematical model.

Numbering the nodes other than the ground node from 1 to N and assuming the m-th element of a circuit schematic to be a k-pins element then a $N \times k$ local incidence matrix A_m, defined as:

$$a_{ij} = \begin{cases} +1 & \text{if the } j\text{-th component of } \mathbf{i}_m \text{ leaves node } i, \\ 0 & \text{otherwise,} \end{cases} \tag{2.3}$$

can be associated with the m-th element itself. Statement 2.2 can thus be mathematically formalized as:

$$\sum_{m=1}^{M} A_m \mathbf{i}_m = 0. \tag{2.4}$$

At this point “only” the exact definitions of the system variables and the element constitutive relations are missing to complete the derivation of a closed system of equations describing the purely electrical behavior of a given circuit, as it will be shown in Section 2.2.

Notice that (2.4) is of utmost importance in practice as it permits the assembly of the system of balance equations via an element-by-element inspection. At the implementation level this consideration permits to keep the elemental constitutive relations separated from system assembly, with the considerable gain that if a new device model has to be added to an existing set this will not affect the overall program. Any attempt to extend a purely electrical description to thermal effects should therefore take this simple but essential structure into account, if it aims to be effectively usable in an industrial environment. To this end the method proposed in this thesis makes use of the well known analogy between electrical current-flow and heat power-flow [66] and exploits the same network approach to account for thermal effects at the 0D level. Each thermally active electrical element will therefore contribute its power flux to a node of the 0D thermal network. These power fluxes will be balanced by a suitable n-pins thermal element which embodies a 2D/3D description of heat-diffusion at the SoC/SiP level in its constitutive relations. In the end the same assembly structure as in (2.4) is retained.

Constitutive relations for standard and thermally active elements and for the thermal element should then be drawn, to complete the derivation of the coupled electro-thermal model: this is exactly the topic of the next sections. Notice that while the first two issues constitute a well known subject in literature, the particular derivation of the thermal network model represents an original contribution of this thesis.

Remark 2.1 (Incidence matrix concepts)**.** The concept of incidence matrix as presented in Section 2.1 slightly differs from the one usually employed in network theory.

Without entering into the details it should be stressed that the usual notion relies on the assumption for each k-pins element to be properly represented by an equivalent circuit (*companion model*) built upon 2-pins ideal devices. In this case, after the substitution of each circuit element with the corresponding companion model, a unique graph is derived from the initial schematic permitting the description of KCL in terms of *branch currents* and the exploitation, for analysis purposes, of all the mathematical tools provided by graph-theory (see Appendix A).

Nevertheless, this graph-based formalism has its main drawback in the fact that it does not allow for simple extensions when elements are not properly described by lumped networks. This may be the case, for instance, of mixed mode device simulation or of a distributed description of heat-diffusion. Furthermore, considering branches as basic entities, this formalism results to be inherently based on a *flattened netlist* (i.e. on the equivalent circuit obtained *after* the substitution of physical devices with their companion models) and loses therefore the assembly by element structure typical of actual realization of MNA. To overcome these limitations an *element-wise* formulation of MNA, based on the concept of incidence matrix as defined in (2.3), is introduced in this chapter. As it will be seen in the following this formulation naturally allows for a hierarchical description of the circuit, and permits thus to give a more applied perspective to the derivation of the thermal element model proposed in the thesis.

Example 2.1 (CMOS inverter - electrical balance equations)**.** To contextualize the abstract setting proposed in Section 2.1 a simple example based on a CMOS inverter circuit is proposed. The electrical schematic associated with this circuit is composed of 3 nodes (except ground) and 4 elements, as shown in Figure 2.2. Ground node has been numbered as 0. In this case the system of balance equations reads:

$$\begin{array}{lrcl} \text{(node 1)} & i_{V1} + i_{G2} + i_{G1} & = & 0, \\ \text{(node 2)} & i_{U1} + i_{S1} & = & 0, \\ \text{(node 3)} & i_{D1} + i_{D2} & = & 0. \end{array} \tag{2.5}$$

Notice that the balance of ground node, namely:

$$\text{(node 0)} \quad i_{V2} + i_{S2} + i_{U2} \quad = \quad 0, \tag{2.6}$$

can be recovered summing all the equations in (2.5) and taking into account that the algebraic sum of the components of each element current vector must be zero due to (2.2):

$$\begin{array}{rcl} i_{U1} + i_{U2} & = & 0, \\ i_{V1} + i_{V2} & = & 0, \\ i_{S1} + i_{G1} + i_{D1} & = & 0, \\ i_{S2} + i_{G2} + i_{D2} & = & 0. \end{array}$$

Defining the current vectors:

$$\mathbf{i}_U = \begin{bmatrix} i_{U1} \\ i_{U2} \end{bmatrix} , \ \mathbf{i}_V = \begin{bmatrix} i_{V1} \\ i_{V2} \end{bmatrix} , \ \mathbf{i}_{M1} = \begin{bmatrix} i_{G1} \\ i_{S1} \\ i_{D1} \end{bmatrix} , \ \mathbf{i}_{M2} = \begin{bmatrix} i_{G2} \\ i_{S2} \\ i_{D2} \end{bmatrix} , \tag{2.7}$$

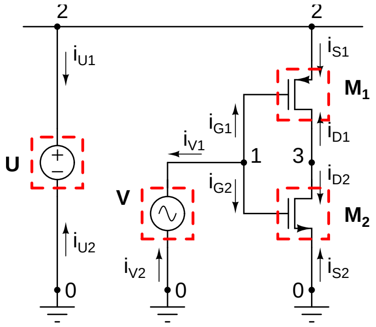

Figure (2.2): *CMOS inverter circuit electrical schematic, composed of 4 elements (dashed red frame) and 3 nodes plus ground.*

and the local incidence matrices:

$$A_U = \begin{bmatrix} 0 & 0 \\ 1 & 0 \\ 0 & 0 \end{bmatrix}, \; A_V = \begin{bmatrix} 1 & 0 \\ 0 & 0 \\ 0 & 0 \end{bmatrix}, \; A_{M1} = \begin{bmatrix} 1 & 0 & 0 \\ 0 & 1 & 0 \\ 0 & 0 & 1 \end{bmatrix}, \; A_{M2} = \begin{bmatrix} 1 & 0 & 0 \\ 0 & 0 & 0 \\ 0 & 0 & 1 \end{bmatrix}, \qquad (2.8)$$

it is possible to rewrite (2.5) in a form that suits (2.4):

$$A_U \mathbf{i}_U + A_V \mathbf{i}_V + A_{M1} \mathbf{i}_{M1} + A_{M2} \mathbf{i}_{M2} = 0. \qquad (2.9)$$

To derive a full system of equations from (2.9) it is at this point necessary to define an appropriate set of unknowns and constitutive relations for the electrical elements appearing in Figure 2.2. This will be precisely the topic of Section 2.2.

Example 2.2 (CMOS inverter - ET balance equations)**.** In Figure 2.3 an extension of the CMOS inverter schematic is proposed that accounts for a thermally active behavior of components $\mathbf{M}_1$ and $\mathbf{M}_2$. It can be readily seen that in this case an appropriate thermal network comes along with the electrical one. To derive a full set of balance equations, system (2.5) has to be completed with power balance at thermal network nodes:

$$\begin{array}{rrcl} \text{(node 4)} & P_{M1} + P_{T1} & = & 0, \\ \text{(node 5)} & P_{M2} + P_{T2} & = & 0, \\ \text{(node 6)} & P_{T3} + P_{E1} & = & 0. \end{array} \qquad (2.10)$$

Notice that the electrical and thermal networks are separated, as results obvious from the fact that they balance two different physical quantities. To stress this concept two different labels are used in Figure 2.3 for the electrical and thermal ground. It will be seen in the next sections that the coupling between the two networks is given by the constitutive relations of thermally active elements, which link currents in the electrical network to nodal quantities (*junction temperatures*) of the thermal network and vice versa. Considering the thermal ground as a part of the thermally active device models,

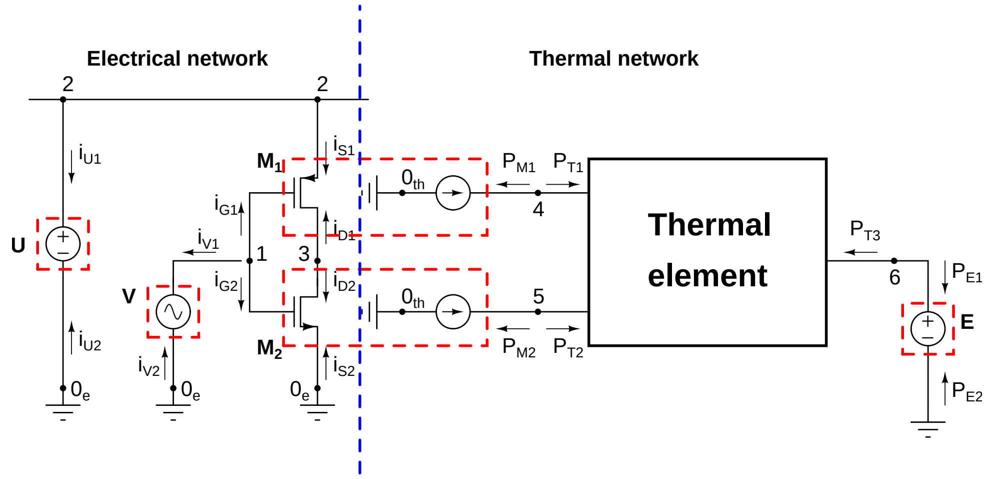

Figure (2.3): *CMOS inverter circuit electro-thermal schematic, composed of 5 elements (dashed red frame) plus a "thermal element". Node number 6 is used to set ambient temperature. Thermal and electrical parts of the network are separated by a dashed blue line.*

it is possible to introduce:

$$\begin{aligned} \mathbf{i}_U &= \begin{bmatrix} i_{U1} \\ i_{U2} \end{bmatrix} \quad , \quad \mathbf{i}_V = \begin{bmatrix} i_{V1} \\ i_{V2} \end{bmatrix} \quad , \quad \mathbf{i}_{M1} = \begin{bmatrix} i_{G1} \\ i_{S1} \\ i_{D1} \\ P_{M1} \end{bmatrix} , \\ \mathbf{i}_{M2} &= \begin{bmatrix} i_{G2} \\ i_{S2} \\ i_{D2} \\ P_{M2} \end{bmatrix} \quad , \quad \mathbf{i}_T = \begin{bmatrix} P_{T1} \\ P_{T2} \\ P_{T3} \end{bmatrix} \quad , \quad \mathbf{i}_E = \begin{bmatrix} P_{E1} \\ P_{E2} \end{bmatrix} , \end{aligned} \tag{2.11}$$

that together with the corresponding incidence matrices permit to recover formulation (2.4) also in the electro-thermal case:

$$A_U\mathbf{i}_U + A_V\mathbf{i}_V + A_{M1}\mathbf{i}_{M1} + A_{M2}\mathbf{i}_{M2} + A_T\mathbf{i}_T + A_E\mathbf{i}_E = 0. \tag{2.12}$$

Notice that, differently from Example 2.1, a full system of equations can be derived from (2.12) specifying not only the unknowns and constitutive relations related to purely electrical elements, but also the ones describing the extended electrical models (Section 2.3) and the thermal element (Section 2.4).

2.2 Standard device models and MNA

A constitutive relation for an electrical device is by definition an expression linking currents through an element with voltage drops across it. It is well known that through the usage of companion models for semiconductors, interconnects and complex devices [69, 73] the component typologies appearing in a circuit can be reduced to:

1. resistors,
2. capacitors,
3. current sources,
4. inductors,
5. voltage sources,

so that only the branch constitutive relations of this restricted set of 2-pins elements are needed to properly describe the electrical behavior of most part of ICs. Resistors, capacitors and current sources are *voltage controlled* elements, i.e. their currents can be expressed as a function of their voltage drops:

$$i_C = \dot{q}(v_C, t) \quad , \quad i_R = r(v_R, t) \quad , \quad i_I = i(v_I, \dot{\mathbf{q}}, \mathbf{i}_L, \mathbf{i}_V, t) \ , \tag{2.13}$$

while inductors and voltage sources are *current controlled* elements, i.e. their voltage drops can be expressed as a function of their currents:

$$v_L = \frac{d\phi}{dt}(i_L, t) \quad , \quad v_V = v(\mathbf{v}, \dot{\mathbf{q}}, \mathbf{i}_L, \mathbf{i}_V, t) \ . \tag{2.14}$$

In both (2.13) and (2.14) symbols in bold are used for sources, to indicate that they can possibly depend on quantities which refer to other elements (*controlled sources*). For more details about these basic components, the interested reader is referred to [15, 16]. Associating with each schematic node a quantity called *node potential* and assuming the potential of the ground node to be zero, it is possible to further develop each element voltage drop resorting to *Kirchhoff's voltage law* (KVL):

Statement 2.3 (KVL). *The algebraic sum of voltage drops around any loop in the circuit is zero.*

Although many modeling paradigms, like State Variable [27], Sparse Tableau [50] or Nodal Analysis [16], can be derived combining KCL, KVL and elemental constitutive relations, the focus in this thesis will be on Modified Nodal Analysis (MNA) [52] as it is nowadays an established industry standard. In its original formulation MNA keeps the node potential vector $\mathbf{e}$, the inductor current vector $\mathbf{i}_L$ and the voltage source current vector $\mathbf{i}_V$ as model variables, and derives a closed system of equations:

1. enforcing KCL at every node of the circuit graph,
2. expressing the current of each voltage controllable element in terms of node potentials,
3. complementing the system with current controllable elements constitutive relations (2.14).

It can be shown however that in this form MNA does not preserve charge and magnetic flux conservation when solved numerically. To handle this problem a charge-oriented formulation was proposed [48,49] where electric charges of capacitances $\mathbf{q}$ and magnetic fluxes of inductances $\boldsymbol{\phi}$ are added as explicit unknowns to the system.

A set of *differential algebraic equations* (DAEs) stems from both standard and charge-oriented MNA formulations: this will ask for some care in the choice of the time-discretization method when designing a numerical solution procedure [95]. Though a treatment of DAE properties and their implications it is out of the scope of the present chapter, a brief introduction to the topic is given in Appendix B together with further references.

Remark 2.2 (Standard DAE formulation of MNA system)**.** A restricted set of *global* incidence matrices (associated with each basic element category) can be constructed on the basis of the *flattened netlist* obtained after the substitution of each device appearing in the schematic with the corresponding companion model [32]. The DAE system stemming from MNA can thus be written in a notation that clearly underlines each elemental type contribution. In the most general case a charge-oriented MNA formulation gives then:

$$\begin{aligned}
A_C\frac{d\mathbf{q}}{dt} + A_R\mathbf{r}(A_R^T\mathbf{e}) + A_L\mathbf{i}_L + A_V\mathbf{i}_V + A_I\mathbf{i}(A^T\mathbf{e},\frac{d\mathbf{q}}{dt},\mathbf{i}_L,\mathbf{i}_V;t) &= 0,\\
\frac{d\boldsymbol{\phi}}{dt} - A_L^T\mathbf{e} &= 0,\\
A_V^T\mathbf{e} - \mathbf{v}(A^T\mathbf{e},\frac{d\mathbf{q}}{dt},\mathbf{i}_L,\mathbf{i}_V;t) &= 0,\\
\mathbf{q} - \mathbf{q}_C(A_C^T\mathbf{e}) &= 0,\\
\boldsymbol{\phi} - \boldsymbol{\phi}_L(\mathbf{i}_L) &= 0.
\end{aligned} \tag{2.15}$$

This graph-based notation is the best suited for analysis purpose, and therefore will be employed in the next chapter. It should be noticed, for the sake of completeness, that controlled sources cannot be prescribed arbitrarily in (2.15) but are instead subject to some constraints (see [29] for a deeper treatment of the subject) in order to limit the index of the overall system to be minor or equal than 2.

Example 2.3 (Shichman-Hodges MOS-FET model)**.** Consider the n-channel MOS-FET shown in Figure 2.4 on the left. Its four pins are respectively associated with *gate* (G), *drain* (D), *source* (S) and *bulk* (B) terminals. The corresponding Shichman-Hodges model [85] is given by the equivalent circuit shown in Figure 2.4 on the right.

Though being one of the most simple MOS-FET model usually provided with SPICE-like circuit simulators (see [34,93] for more sophisticated ones), it already introduces 4 inner nodes that do not appear in the original schematic. The current balance at these nodes is regarded in the usual DAE formulation of MNA (2.15) as being part of KCL, while in the proposed *element-wise* formulation it will be considered as part of the MOS-FET constitutive relations. It is precisely this latter feature that gives the *element-wise* notation the possibility to describe circuits on a hierarchical base.

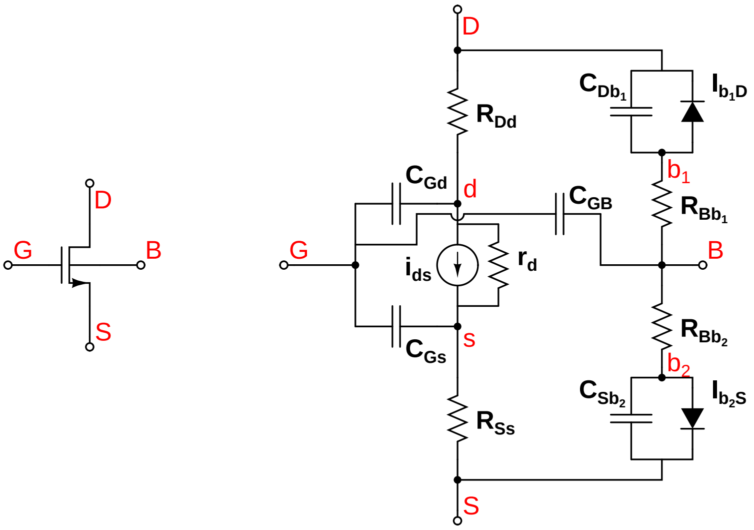

Figure (2.4): *On the left the symbol usually used in schematics to represent a* 4*-pins nMOS-FET, on the right the corresponding Shichman-Hodges model composed of* 5 *linear capacitors,* 5 *linear resistors,* 2 *non-linear resistors (diodes) and a voltage controlled current source. Notice the presence of* 4 *inner nodes.*

2.3 Extended electrical models

The extension of a standard device model to account for thermal effects requires:

1. the explicit introduction of *junction temperature* [1] dependence in the expressions defining electrical variables,
2. the derivation of a closed form expression to calculate dissipated power in the device.

An example of this approach can be found in [61] where a temperature dependent model for the source-drain current of a MOS-FET is derived, based on the *alpha-power law* [80], or in [71] where the *tanh law* introduced in [86] is extended to predict the temperature dependence of threshold voltage and carrier mobility in MOS transistors.

Notice that these approaches all require the implementation of a new element evaluator. An alternative approach widely used in practice relies on the fact that many complex device models implemented in industrial circuit simulators already take into account a parametric dependence of electrical quantities on junction temperatures. In many cases it is thus given the possibility to set-up a thermally-active device model

---

[1] As *node potentials* are associated with each node of the electrical network, similar quantities representing temperatures and called *junction temperatures* are associated with each node of the thermal network.

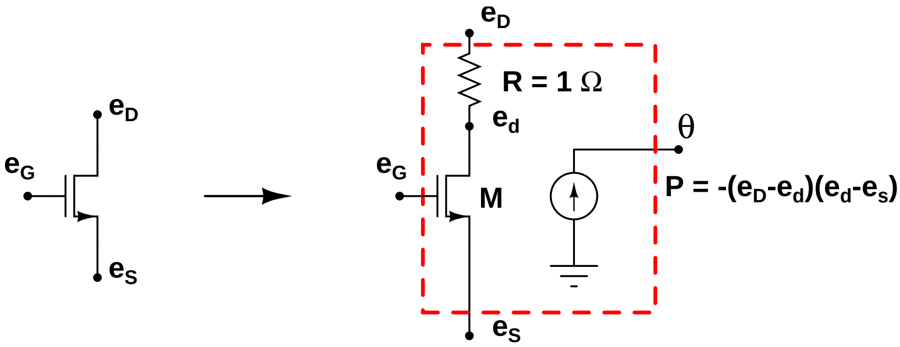

Figure (2.5): *Starting from the MOS-FET model shown on the left a thermally active element is built employing a* 1Ω *resistor to read the MOS drain current and using a voltage controlled current source as power generator. Notice that the particular choice of the resistance permits to read the current directly from the resistor voltage drop due to Ohm's law.*

combining already existing elements. An example is shown in Figure 2.5 where a n-channel MOS-FET, a 1Ω resistor and a voltage controlled current source are used to this end.

2.4 Thermal element model

As briefly introduced in Example 2.1, to extend a purely electrical description of a circuit to an electro-thermal one a suitable thermal element balancing power fluxes at junction temperature nodes is required. In the following it is shown how a multiscale model that fits such a purpose can be derived starting from information that is readily available during IC design phase, i.e. 2D or 3D layout geometry and possibly 3D package geometry. As sketched in Figure 2.6 this information is used to:

1. describe the overall physical region where to simulate thermal effects as an open, bounded domain $\Omega \subset \mathbb{R}^d$ $(d = 2, 3)$,
2. associate each thermally active device with a subset $\Omega_k \subset \Omega$ (related to its layout positioning) where its power flux is supposed to be dissipated.

Assuming the number of these subsets to be K, it is asked to each one to fulfill the following properties:

$$\begin{array}{rclrcll} \mathtt{int}(\Omega_k) & \neq & \emptyset & \forall k & = & 1,\dots,K, & \\ \bar{\Omega}_k & \subset & \Omega & \forall k & = & 1,\dots,K, & \\ \bar{\Omega}_k & \cap & \bar{\Omega}_j = \emptyset & \forall j,k & = & 1,\dots,K, & k \neq j. \end{array} \tag{2.16}$$

Furthermore it is supposed for either Ω and Ω_k $(k = 1,\dots,K)$ to have Lipschitz boundary. The unknowns considered in the thermal network model are the junction

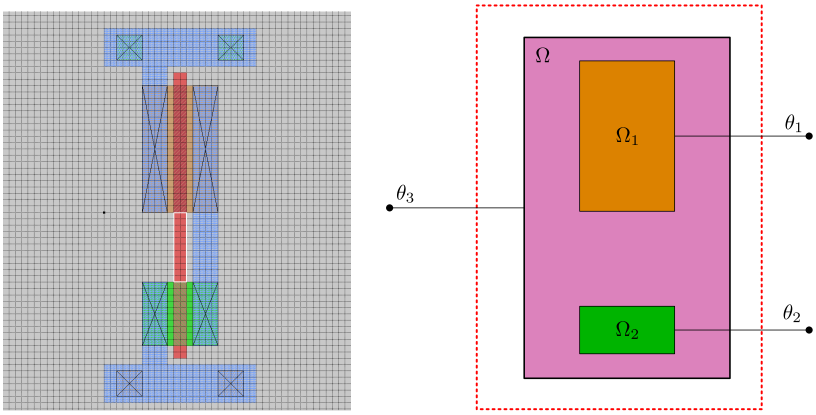

(a) Inverter layout (b) Extracted geometry

Figure (2.6): *Layout or package information from IC design is automatically converted into a geometrical description of the domains in which suitable PDEs describing heat diffusion at the system level are casted. Notice that while* θ_1 *and* θ_2 *refer to mean temperature values over* Ω_1 *and* Ω_2 *respectively,* θ_3 *represents ambient temperature.*

temperature vector:

$$\boldsymbol{\theta} = [\theta_1, \ldots, \theta_{K+1}]^T \ , \tag{2.17}$$

where the first K components are associated with each subset region while the last one represents ambient temperature, the power density vector:

$$\mathbf{p} = [p_1, \ldots, p_K]^T \ , \tag{2.18}$$

where each component represents the Joule power per unit area dissipated in each region and the distributed temperature field $T(\mathbf{x}, t)$ on Ω.

Interface to lumped network Assuming $(\cdot, \cdot)$ to denote the usual $\mathbb{L}^2(\Omega)$ scalar product:

$$\int_\Omega uv \; d\mathbf{x} = (u, v), \tag{2.19}$$

and $\mathbf{1}_{\Omega_k}$ to denote the indicator function of the set Ω_k, then the distributed temperature field $T(\mathbf{x}, t)$ is linked to junction temperature nodes through:

$$\frac{1}{|\Omega_k|}(T, \mathbf{1}_{\Omega_k}) = \theta_k \quad k = 1, \ldots, K, \tag{2.20}$$

i.e. θ_k represents the mean value over Ω_k of $T(\mathbf{x},t)$. [2] In the same way the power flux entering each node is related to the Joule power per unit area via:

$$(p_k, \mathbf{1}_{\Omega_k}) = p_k|\Omega_k| = P_k \quad k = 1,\ldots,K. \tag{2.21}$$

The total power P_k dissipated over Ω_k is thus equal, for every fixed time instant, to the product of a mean power density p_k times the area of each active region $|\Omega_k|$. Notice that the decisions to:

1. uniformly distribute dissipated power P_k inside Ω_k,
2. define θ_k as the mean temperature over Ω_k,

are somehow arbitrary. Any other shape for the power distribution inside Ω_k, as well as any other means to define junction temperatures starting from the distributed field $T(\mathbf{x},t)$ may have been adopted in principle. However these assumptions constitute a sound physical approximation at the macro-scale level, if it is considered that usually:

$$\operatorname{diam}(\Omega_k) \ll \operatorname{diam}(\Omega) \qquad k = 1,\ldots,K. \tag{2.22}$$

Finally, to respect (2.2), the power flux to ambient temperature node is defined to be:

$$P_{K+1} = -\sum_{k=1}^{K} p_k|\Omega_k|. \tag{2.23}$$

Heat diffusion on a 3D domain Heat diffusion on a 3D domain is supposed to be modeled in the most general case by the quasi-linear PDE:

$$c_V(T,\mathbf{x})\frac{\partial T(\mathbf{x},t)}{\partial t} + \mathcal{L}_3\,T(\mathbf{x},t) = \sum_{k=1}^{K} p_k(t)\,\mathbf{1}_{\Omega_k}(\mathbf{x}) \qquad \text{in } \Omega, \tag{2.24}$$

where:

$$\mathcal{L}_3\,T(\mathbf{x},t) := -\sum_{i,j=1}^{3} D_i\Big[\kappa_{ij}(T,\mathbf{x})D_jT(\mathbf{x},t)\Big], \tag{2.25}$$

In (2.24) the term $c_V(T,\mathbf{x})$ represents the distributed thermal capacitance of the material, while in (2.25) the terms $\kappa_{ij}(T,\mathbf{x})$ $(i,j = 1,\ldots,3)$ account for possibly anisotropic heat-diffusion. A common assumption, stemming from physical considerations, is that:

$$\kappa_{ij}(T,\mathbf{x}) = \kappa_{ji}(T,\mathbf{x}), \tag{2.26}$$

so that the associated tensor results to be symmetric.

This PDE has to be complemented by suitable boundary conditions, that are here assumed to be of Robin:

$$\frac{\partial\,T(\mathbf{x},t)}{\partial\,\mathbf{n}_{\mathcal{L}}} = R(T,\theta_{K+1}) \quad \text{on } \partial\Omega, \tag{2.27}$$

---

[2] Notice that as θ_{K+1} represents ambient temperature, it is given as initial datum and requires thus no constitutive relation to be fixed.

or Dirichlet type: [3]

$$T(\mathbf{x}, t) = \theta_{K+1} \quad \text{on } \partial\Omega. \tag{2.28}$$

In (2.27) the term $\dfrac{\partial\, T(\mathbf{x}, t)}{\partial\, \mathbf{n}_{\mathcal{L}}}$ denotes the conormal derivative of $T(\mathbf{x}, t)$ on $\partial\Omega$ and is defined as:

$$\frac{\partial\, T(\mathbf{x}, t)}{\partial\, \mathbf{n}_{\mathcal{L}}} := \sum_{i,j=1}^{3} n_i \kappa_{ij} D_j T(\mathbf{x}, t)\ ,$$

where n_i is the i-th component of the normal outward oriented unit vector on $\partial\Omega$.

Heat diffusion on a 2D domain In the case that only 2D layout information is available, or that package temperature field is not of interest, then heat diffusion can be modeled by a quasi-linear PDE similar to the one used in the 3D case:

$$\hat{c}_V(T, \mathbf{x}) \frac{\partial T(\mathbf{x}, t)}{\partial t} + \mathcal{L}_2\, T(\mathbf{x}, t) = \sum_{k=1}^{K} p_k(t)\, \mathbf{1}_{\Omega_k}(\mathbf{x}) \qquad \text{in } \Omega, \tag{2.29}$$

the only difference being that now the operator $\mathcal{L}_2$, defined as:

$$\mathcal{L}_2\, T(\mathbf{x}, t) := -\sum_{i,j=1}^{2} D_i \Big[\hat{\kappa}_{ij}(T, \mathbf{x}) D_j T(\mathbf{x}, t)\Big] + \hat{c}(T, \mathbf{x}) T(\mathbf{x}, t), \tag{2.30}$$

embodies a reaction term $\hat{c}(T, \mathbf{x})$ to model heat loss in the missing third direction. Suitable Robin or Dirichlet boundary conditions are used also in this case to close the model.

2.5 Coupled electro-thermal system

A closed system of equations modeling electro-thermal effects in ICs can be finally derived combining the conservation laws presented in Section 2.1 with the constitutive relations shown afterwards. Define to this end the vector of unknown nodal quantities as:

$$\mathbf{n} := \begin{bmatrix} \mathbf{e}^T & \boldsymbol{\theta}^T \end{bmatrix}^T\ . \tag{2.31}$$

Here $\mathbf{e}$ is a vector accounting for the n_e unknown node potentials while $\boldsymbol{\theta}$ represents the n_θ unknown junction temperatures. Assuming a 2D description of heat diffusion and Robin boundary conditions the full system of PDAEs reads, for instance: [4]

---

[3] Even Neumann boundary conditions may be enforced from a purely theoretical point of view. However their application is limited in practice and therefore they will not be considered in the following. Furthermore all the results presented in Chapter 3 can be straightforwardly extended to this case.

$$
\begin{array}{rcll}
\displaystyle\sum_{m=1}^{M-1} A_m\big[D_m\dot{\mathbf{r}}_m + \mathbf{J}_m(A_m^T\mathbf{n},\mathbf{r}_m;t)\big] + A_M\mathbf{J}_M(\mathbf{r}_M) & = & 0 & , \\
B_m\dot{\mathbf{r}}_m + \mathbf{Q}_m(A_m^T\mathbf{n},\mathbf{r}_m;t) & = & 0 & m=1,\dots,M-1, \\
\theta_k - \dfrac{1}{|\Omega_k|}(T,\mathbf{1}_{\Omega_k}) & = & 0 & k=1,\dots,n_\theta-1, \\
\hat{c}_V(T,\mathbf{x})\dfrac{\partial T(\mathbf{x},t)}{\partial t} + \mathcal{L}_2\,T(\mathbf{x},t) - \displaystyle\sum_{k=1}^{n_\theta-1} p_k(t)\,\mathbf{1}_{\Omega_k}(\mathbf{x}) & = & 0 & \text{in } \Omega, \\
\dfrac{\partial\,T(\mathbf{x},t)}{\partial\,\mathbf{n}_{\mathcal{L}}} - R(T,\theta_{n_\theta}) & = & 0 & \text{on } \partial\Omega.
\end{array}
\tag{2.32}
$$

In (2.32) the flux vector associated with standard and thermally active devices is expressed as:

$$
\mathbf{i}_m = D_m\dot{\mathbf{r}}_m + \mathbf{J}_m(A_m^T\mathbf{n},\mathbf{r}_m;t) \qquad m=1,\dots,M-1, \tag{2.33}
$$

where A_m is the incidence matrix defined in Section 2.1 while $\mathbf{r}_m$ is the set of the remaining variables appearing in the equations defining the fluxes relative to the m-th element (for this reason it is sometimes referred to as the set of the m-th element *internal variables*). Assuming the m-th element to be a k-pins element and $\mathbf{r}_m$ to be a vector of I_m components with:

$$
I_m \in \mathbb{N}_0\ ,\ m=1,\dots,M-1, \tag{2.34}
$$

then D_m is an appropriate $k \times I_m$ matrix while:

$$
\mathbf{J}_m\ :\ \mathbb{R}^k \times \mathbb{R}^{I_m} \to \mathbb{R}^k\,. \tag{2.35}
$$

Notice that the assumption that only time derivatives of internal variables appear and that terms involving such derivatives are linear does not impose restrictions on the applicability of the model, as it fits perfectly with charge-oriented MNA formulation. The set of I_m additional relations[5] associated with each generic k-pins element are expressed in (2.32) as:

$$
B_m\dot{\mathbf{r}}_m + \mathbf{Q}_m(A_m^T\mathbf{n},\mathbf{r}_m;t) = 0 \qquad m=1,\dots,M-1, \tag{2.36}
$$

where B_m is a suitable $I_m \times I_m$ matrix while:

$$
\mathbf{Q}_m\ :\ \mathbb{R}^k \times \mathbb{R}^{I_m} \to \mathbb{R}^{I_m}\,. \tag{2.37}
$$

---

[4] In the following an electro-thermal network composed of M elements is assumed. Furthermore the M-th element is considered to be the distributed thermal element.

[5] Notice that it is assumed, with a slight abuse of notation, that I_m could be possibly zero. Furthermore the reader should be warned that a particular care has to be taken with current controlled sources: as the controlling current is defined in another element constitutive relations, no additional equations are required in this case to close the system.

Concerning the thermal element, denoted as the M-th element of the network, θ_{n_θ} is assumed to represent ambient temperature while $\mathbf{r}_M$ and $\mathbf{J}_M$ are defined as:

$$\begin{aligned}
\mathbf{r}_M &= \begin{bmatrix} p_1 & \dots & p_{n_\theta - 1} & T(\mathbf{x}, t) \end{bmatrix}^T , \\
\mathbf{J}_M(\mathbf{r}_M) &= \begin{bmatrix} p_1|\Omega_1| & \dots & p_{n_\theta-1}|\Omega_{n_\theta-1}| & -\sum_{k=1}^{n_\theta-1} p_k|\Omega_k| \end{bmatrix}^T .
\end{aligned} \tag{2.38}$$

It will be shown in Part III that after space discretization the structure of the thermal element will fit (2.33-2.36). This will allow to write the semi-discretized counterpart of (2.32) in the extremely compact form:

$$\begin{aligned}
\sum_{m=1}^{M} A_m \left[D_m \dot{\mathbf{r}}_m + \mathbf{J}_m(A_m^T \mathbf{n}, \mathbf{r}_m; t) \right] &= 0 \\
B_m \dot{\mathbf{r}}_m + \mathbf{Q}_m(A_m^T \mathbf{n}, \mathbf{r}_m; t) &= 0 \qquad m = 1, \dots, M,
\end{aligned} \tag{2.39}$$

making thus evident that MNA and system (2.39) share the same structure (and with it the possibility to assemble the overall system on the base of a by element inspection). As a last remark it should be noticed that a compact notation similar to (2.39) can be devised for the continuous system (2.32) resorting to abstract DAEs [91]. Anyhow this topic is out of the scope of the present work.

Example 2.4 (CMOS inverter - charge oriented MNA with element-wise formulation)**.** In the following it is shown how to derive the full system of equations stemming from the charge-oriented MNA description of the CMOS inverter depicted in Figure 2.3. Consider then the electro-thermal circuit schematic and assume that a thermally extended version (see Section 2.3) of the simple Shichman-Hodges model [85] is used for both the MOS-FETs. For the sake of simplicity the bulk terminals of the transistors are assumed to be connected to the ground node, so that the *element-wise* formulation starts from the system of balance equations (2.5,2.10). The vector of nodal variables reads:

$$\mathbf{n} = \begin{bmatrix} e_1 & e_2 & e_3 & \theta_4 & \theta_5 & \theta_6 \end{bmatrix}^T , \tag{2.40}$$

where e_1, e_2 and e_3 are respectively the node potentials associated with the electrical nodes 1, 2 and 3, while θ_4, θ_5 and θ_6 are the junction temperatures associated with nodes 4, 5 and 6.

The set-up for a generic voltage source is depicted in Figure 2.7. It can be readily seen that one internal variable is employed (namely the branch current j), and thus the additional constitutive relation:

$$\mathbf{Q}([e_+, e_-]^T; t) = e_+ - e_- - V(t) = 0 , \tag{2.41}$$

is needed to close the system. In (2.41) e_+ and e_- indicate the generic node potentials of the considered two-pins element while $V(t)$ is the known voltage waveform of the source.

A similar set-up is presented in Figure 2.8 for the n-channel MOS-FET. In this case 9 internal variables are required to completely describe the element: these are constituted by the four internal nodes e_d, e_s, e_{b_1}, e_{b_2} and by the 5 charges associated with each capacitor (q_{Gd},q_{Gs},q_{GB},q_{Db_1},q_{Sb_2}). The current balances at the internal nodes are part of the nMOS-FET constitutive relations, as they stem from the choice to model the transistor with the Shichman Hodges equivalent circuit. Notice that no other k-pins element is allowed to be connected to these nodes, as they constitute only an internal representation of the MOS-FET. This latter feature is often employed in practice to enhance simulation performance exploiting a Schur-complement based technique on these inner equations, as shown in [33]. Of course a similar representation can be derived for the p-channel MOS-FET. Finally, the thermal element will be described as outlined in Section 2.4.

At this point each flux vector appearing in (2.5,2.10) is expressed in a form that suits (2.33), while the additional constitutive relations of the corresponding element are provided in a form resembling (2.36). It is thus possible to follow the procedure depicted in Section 2.5 and derive a closed system of:

- 3 balance equations at the electrical nodes 1-3:

$$\begin{aligned}
j^{[\mathbf{V}]} + \dot{q}_{Gd}^{[\mathbf{M}_1]} + \dot{q}_{Gs}^{[\mathbf{M}_1]} + \dot{q}_{GB}^{[\mathbf{M}_1]} + \dot{q}_{Gd}^{[\mathbf{M}_2]} + \dot{q}_{Gs}^{[\mathbf{M}_2]} + \dot{q}_{GB}^{[\mathbf{M}_2]} &= 0 \, , \\
j^{[\mathbf{U}]} + \dot{q}_{Sb2}^{[\mathbf{M}_1]} + \frac{e_2 - e_s^{[\mathbf{M}_1]}}{R_{Ss}^{[\mathbf{M}_1]}} + I_{b_2 S}^{[\mathbf{M}_1]}(e_2, \theta_4, e_{b_2}^{[\mathbf{M}_1]}) &= 0 \, , \\
\dot{q}_{Db1}^{[\mathbf{M}_1]} + \frac{e_3 - e_d^{[\mathbf{M}_1]}}{R_{Dd}^{[\mathbf{M}_1]}} + I_{b_1 D}^{[\mathbf{M}_1]}(e_3, \theta_4, e_{b_1}^{[\mathbf{M}_1]}) + \dot{q}_{Db1}^{[\mathbf{M}_2]} + \frac{e_3 - e_d^{[\mathbf{M}_2]}}{R_{Dd}^{[\mathbf{M}_2]}} - I_{b_1 D}^{[\mathbf{M}_2]}(e_3, \theta_5, e_{b_1}^{[\mathbf{M}_2]}) &= 0 \, ,
\end{aligned}$$

- 3 balance equations at the thermal nodes 4-6:

$$\begin{aligned}
|\Omega_1| p_1 - (e_d^{[\mathbf{M}_1]} - e_s^{[\mathbf{M}_1]}) i_{ds}^{[\mathbf{M}_1]}(e_1, \theta_4, e_d^{[\mathbf{M}_1]}, e_s^{[\mathbf{M}_1]}) &= 0 \, , \\
|\Omega_2| p_2 - (e_d^{[\mathbf{M}_2]} - e_s^{[\mathbf{M}_2]}) i_{ds}^{[\mathbf{M}_2]}(e_1, \theta_5, e_d^{[\mathbf{M}_2]}, e_s^{[\mathbf{M}_2]}) &= 0 \, , \\
-|\Omega_1| p_1 - |\Omega_2| p_2 + j^{[\mathbf{E}]} &= 0 \, ,
\end{aligned}$$

- 1 constitutive relation for the input voltage source V:

  $$e_1 - v(t) = 0 \, ,$$

  where $v(t)$ is a given voltage waveform,

- 1 constitutive relation for the feed voltage source U:

  $$e_2 - V_{DD} = 0 \, ,$$

  where V_{DD} is the given feed voltage,

- 9 constitutive relations for the p-channel MOS-FET M_1:

$$\begin{aligned}
-\dot{q}_{Gd}^{[\mathbf{M}_1]} - \frac{e_3 - e_d^{[\mathbf{M}_1]}}{R_{Dd}^{[\mathbf{M}_1]}} + i_{ds}^{[\mathbf{M}_1]}(e_1, \theta_4, e_d^{[\mathbf{M}_1]}, e_s^{[\mathbf{M}_1]}) + \frac{e_d^{[\mathbf{M}_1]} - e_s^{[\mathbf{M}_1]}}{r_d^{[\mathbf{M}_1]}} &= 0 \, , \\
-\dot{q}_{Gs}^{[\mathbf{M}_1]} - \frac{e_2 - e_s^{[\mathbf{M}_1]}}{R_{Ss}^{[\mathbf{M}_1]}} - i_{ds}^{[\mathbf{M}_1]}(e_1, \theta_4, e_d^{[\mathbf{M}_1]}, e_s^{[\mathbf{M}_1]}) - \frac{e_d^{[\mathbf{M}_1]} - e_s^{[\mathbf{M}_1]}}{r_d^{[\mathbf{M}_1]}} &= 0 \, , \\
-\dot{q}_{Db1}^{[\mathbf{M}_1]} - I_{b_1 D}^{[\mathbf{M}_1]}(e_3, \theta_4, e_{b_1}^{[\mathbf{M}_1]}) + \frac{e_{b_1}^{[\mathbf{M}_1]}}{R_{Bb_1}^{[\mathbf{M}_1]}} &= 0 \, , \\
-\dot{q}_{Sb2}^{[\mathbf{M}_1]} - I_{b_2 S}^{[\mathbf{M}_1]}(e_2, \theta_4, e_{b_2}^{[\mathbf{M}_1]}) + \frac{e_{b_2}^{[\mathbf{M}_1]}}{R_{Bb_2}^{[\mathbf{M}_1]}} &= 0 \, , \\
q_{Gd}^{[\mathbf{M}_1]} - C_{Gd}^{[\mathbf{M}_1]}(e_1 - e_d^{[\mathbf{M}_1]}) &= 0 \, , \\
q_{Gs}^{[\mathbf{M}_1]} - C_{Gs}^{[\mathbf{M}_1]}(e_1 - e_s^{[\mathbf{M}_1]}) &= 0 \, , \\
q_{GB}^{[\mathbf{M}_1]} - C_{GB}^{[\mathbf{M}_1]}(e_1) &= 0 \, , \\
q_{Db_1}^{[\mathbf{M}_1]} - C_{Db_1}^{[\mathbf{M}_1]}(e_3 - e_{b_1}^{[\mathbf{M}_1]}) &= 0 \, , \\
q_{Sb_2}^{[\mathbf{M}_1]} - C_{Sb_2}^{[\mathbf{M}_1]}(e_2 - e_{b_2}^{[\mathbf{M}_1]}) &= 0 \, ,
\end{aligned}$$

- 9 constitutive relations for the n-channel MOS-FET M_2:

$$\begin{aligned}
-\dot{q}_{Gd}^{[\mathbf{M}_2]} - \frac{e_3 - e_d^{[\mathbf{M}_2]}}{R_{Dd}^{[\mathbf{M}_2]}} + i_{ds}^{[\mathbf{M}_2]}(e_1, \theta_5, e_d^{[\mathbf{M}_2]}, e_s^{[\mathbf{M}_2]}) + \frac{e_d^{[\mathbf{M}_2]} - e_s^{[\mathbf{M}_2]}}{r_d^{[\mathbf{M}_2]}} &= 0 \, , \\
-\dot{q}_{Gs}^{[\mathbf{M}_2]} + \frac{e_s^{[\mathbf{M}_2]}}{R_{Ss}^{[\mathbf{M}_2]}} - i_{ds}^{[\mathbf{M}_2]}(e_1, \theta_5, e_d^{[\mathbf{M}_2]}, e_s^{[\mathbf{M}_2]}) - \frac{e_d^{[\mathbf{M}_2]} - e_s^{[\mathbf{M}_2]}}{r_d^{[\mathbf{M}_2]}} &= 0 \, , \\
-\dot{q}_{Db1}^{[\mathbf{M}_2]} + I_{b_1 D}^{[\mathbf{M}_2]}(e_3, \theta_5, e_{b_1}^{[\mathbf{M}_2]}) + \frac{e_{b_1}^{[\mathbf{M}_2]}}{R_{Bb_1}^{[\mathbf{M}_2]}} &= 0 \, , \\
-\dot{q}_{Sb2}^{[\mathbf{M}_2]} + I_{b_2 S}^{[\mathbf{M}_2]}(0, \theta_5, e_{b_2}^{[\mathbf{M}_2]}) + \frac{e_{b_2}^{[\mathbf{M}_2]}}{R_{Bb_2}^{[\mathbf{M}_2]}} &= 0 \, , \\
q_{Gd}^{[\mathbf{M}_2]} - C_{Gd}^{[\mathbf{M}_2]}(e_1 - e_d^{[\mathbf{M}_2]}) &= 0 \, , \\
q_{Gs}^{[\mathbf{M}_2]} - C_{Gs}^{[\mathbf{M}_2]}(e_1 - e_s^{[\mathbf{M}_2]}) &= 0 \, , \\
q_{GB}^{[\mathbf{M}_2]} - C_{GB}^{[\mathbf{M}_2]}(e_1) &= 0 \, , \\
q_{Db_1}^{[\mathbf{M}_2]} - C_{Db_1}^{[\mathbf{M}_2]}(e_3 - e_{b_1}^{[\mathbf{M}_2]}) &= 0 \, , \\
q_{Sb_2}^{[\mathbf{M}_2]} + C_{Sb_2}^{[\mathbf{M}_2]}(e_{b_2}^{[\mathbf{M}_2]}) &= 0 \, ,
\end{aligned}$$

- 1 constitutive relation for the voltage source E:

$$\theta_6 - T_{EE} \quad = \quad 0 \, ,$$

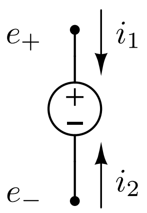

$$\mathbf{r} = \begin{bmatrix} j \end{bmatrix} \qquad I = 1$$

$$\mathbf{i} = \begin{bmatrix} i_1 \\ i_2 \end{bmatrix} = \mathbf{J}(\mathbf{r}) = \begin{bmatrix} +j \\ -j \end{bmatrix}$$

$$\mathbf{Q}\left(\begin{bmatrix} e_+ & e_- \end{bmatrix}^T ; t\right) = e_+ - e_- - V(t) = 0$$

Figure (2.7): *Voltage source set-up in the element-wise notation. Notice that in this case one internal variable is needed to properly describe the element, and thus one additional constitutive relation is given to close the set of MNA equations.*

where T_{EE} represents a constant ambient temperature,

- 3 constitutive relations for the thermal element:

$$\begin{aligned} |\Omega_1|\theta_4 - (T, \mathbf{1}_{\Omega_1}) &= 0 \,, \\ |\Omega_2|\theta_5 - (T, \mathbf{1}_{\Omega_2}) &= 0 \,, \\ \hat{c}_V(T,\mathbf{x})\frac{\partial T(\mathbf{x},t)}{\partial t} + \mathcal{L}_2\, T(\mathbf{x},t) - \sum_{k=1}^{2} p_k(t)\, \mathbf{1}_{\Omega_k}(\mathbf{x}) &= 0 \,, \end{aligned}$$

  where the PDE has to be supplemented with suitable boundary conditions, depending on θ_6 (see Section 2.4).

All these equations describe the electro-thermal behavior of the CMOS inverter circuit. The corresponding system variables are the 6 nodal variables $\mathbf{n}$, the branch currents $j^{[\mathbf{U}]}$,$j^{[\mathbf{V}]}$ and $j^{[\mathbf{E}]}$ associated with the voltage sources, the 8 inner node potentials plus the 10 capacitor charges contributed by the two MOS-FETs and finally the Joule power densities p_1, p_2 and the distributed temperature field T stemming from the thermal element model.

Chapter summary In this chapter the model used to describe ET effects was established. A non-standard *element-wise* formulation, fitting the customary circuit simulator structures, was devised and used to derive a suitable thermal element accounting for heat diffusion at the system level. A PDAE system, that will be analyzed in Part II and numerically approximated in Part III, stemmed from the model.

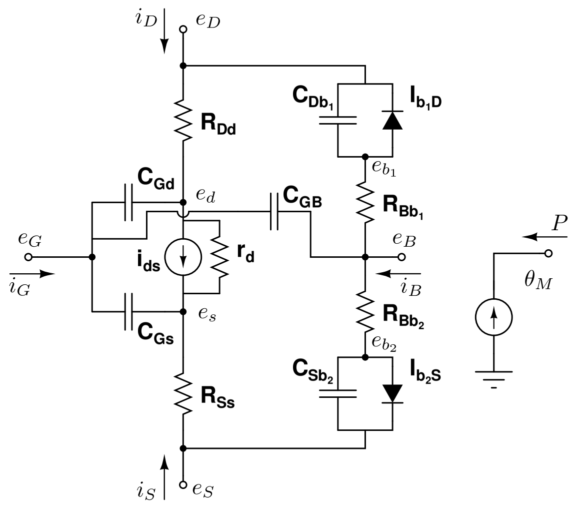
i_D
e_D
$\mathbf{R_{Dd}}$
$\mathbf{C_{Db_1}}$
$\mathbf{I_{b_1D}}$
e_{b_1}
$\mathbf{C_{Gd}}$
e_d
$\mathbf{C_{GB}}$
$\mathbf{R_{Bb_1}}$
e_G
i_G
$\mathbf{i_{ds}}$
$\mathbf{r_d}$
e_B
i_B
P
θ_M
e_s
$\mathbf{C_{Gs}}$
$\mathbf{R_{Bb_2}}$
e_{b_2}
$\mathbf{C_{Sb_2}}$
$\mathbf{I_{b_2S}}$
$\mathbf{R_{Ss}}$
i_S
e_S

$$\mathbf{e} = \begin{bmatrix} e_G & e_D & e_S & e_B & \theta_M \end{bmatrix}^T \qquad I = 9$$

$$\mathbf{r} = \begin{bmatrix} e_d & e_s & e_{b1} & e_{b2} & q_{Gd} & q_{Gs} & q_{GB} & q_{Db1} & q_{Sb2} \end{bmatrix}^T$$

$$B\dot{\mathbf{r}} + \mathbf{Q}(\mathbf{e}, \mathbf{r}) = \begin{bmatrix} -\dot{q}_{Gd} - \dfrac{e_D - e_d}{R_{Dd}} + i_{ds}(e_G, \theta_M, e_d, e_s) + \dfrac{e_d - e_s}{r_d} \\ -\dot{q}_{Gs} - \dfrac{e_S - e_s}{R_{Ss}} - i_{ds}(e_G, \theta_M, e_d, e_s) - \dfrac{e_d - e_s}{r_d} \\ -\dot{q}_{Db1} + I_{b_1D}(e_D, \theta_M, e_{b_1}) - \dfrac{e_B - e_{b_1}}{R_{Bb_1}} \\ -\dot{q}_{Sb2} + I_{b_2S}(e_S, \theta_M, e_{b_2}) - \dfrac{e_B - e_{b_2}}{R_{Bb_2}} \\ q_{Gd} - C_{Gd}(e_G - e_d) \\ q_{Gs} - C_{Gs}(e_G - e_s) \\ q_{GB} - C_{GB}(e_G - e_B) \\ q_{Db_1} - C_{Db_1}(e_D - e_{b_1}) \\ q_{Sb_2} - C_{Sb_2}(e_S - e_{b_2}) \end{bmatrix} = 0$$

$$\mathbf{i} = \begin{bmatrix} i_G \\ i_D \\ i_S \\ i_B \\ P \end{bmatrix} = D\dot{\mathbf{r}} + \mathbf{J}(\mathbf{e}, \mathbf{r}) = \begin{bmatrix} \dot{q}_{Gd} + \dot{q}_{Gs} + \dot{q}_{GB} \\ \dot{q}_{Db1} + \dfrac{e_D - e_d}{R_{Dd}} - I_{b_1D}(e_D, \theta_M, e_{b_1}) \\ \dot{q}_{Sb2} + \dfrac{e_S - e_s}{R_{Ss}} - I_{b_2S}(e_S, \theta_M, e_{b_2}) \\ -\dot{q}_{GB} + \dfrac{e_B - e_{b_1}}{R_{Bb_1}} + \dfrac{e_B - e_{b_2}}{R_{Bb_2}} \\ -(e_d - e_s) i_{ds}(e_G, \theta_M, e_d, e_s) \end{bmatrix}$$

Figure (2.8): *Set-up of the extended n-channel MOS-FET using the Shichman Hodges model in the element-wise notation. In this case* 9 *internal variables are present, and thus* 9 *additional constitutive relations are given to close the set of MNA equations.* $I_{b_1D}(e_D, \theta_M, e_{b_1})$, $I_{b_2S}(e_S, \theta_M, e_{b_2})$ *and* $i_{ds}(e_G, \theta_M, e_d, e_s)$ *are given functions modeling respectively the leakage currents through the diodes, and the current of the voltage controlled current source appearing in the equivalent circuit.*

Part II

Analysis

3

Analysis of a coupled electro-thermal system

This chapter addresses the well posedness of the electro-thermal model established in Chapter 2 under particular assumptions on the overall system. The aim is to provide a first step towards the analysis of the completely non-linear model arising from real applications, as well as to furnish a sound theoretical basis to the solution approaches proposed later in the thesis (Chapter 5).

To this end in Section 3.1 a rigorous description of the thermal element that will be addressed throughout the whole chapter is given. Thermal diffusion is supposed to be modelled by a linear PDE casted in a weak formulation on a 2D or 3D domain. Then in Section 3.2 the thermal element is investigated when driven by external independent sources, fixing either the Joule power per unit area or the average temperature in a region. It will be shown that in the first case the analysis leads back to standard PDE theory, while in the second case theorems proving the well posedness of the system will be given. Finally in Section 3.3 the existence and uniqueness of the solution to a coupled problem is investigated. The main point will be here to prove that given a well-posed electrical network with a functional dependence on temperature, then the extension to an electro-thermal one remains well-posed under mild assumptions.

3.1 Assumptions on the heat diffusion operator

Let $\Omega \subset \mathbb{R}^d$ $(d = 2, 3)$ and $\{\Omega_k\}$ $(k = 1, \ldots, K)$ be defined as in Section 2.4. Throughout the whole chapter heat diffusion is supposed to be described by the linear operator:

$$\mathcal{L}\, T(\mathbf{x}) := -\sum_{i,j=1}^{d} D_i \Big[\kappa_{ij}(\mathbf{x}) D_j T(\mathbf{x})\Big] + c(\mathbf{x}) T(\mathbf{x}), \tag{3.1}$$

where $\kappa_{ij}(\mathbf{x}), c(\mathbf{x}) \in \mathbb{L}^\infty(\Omega)$ and:

$$\begin{array}{rcll} c(\mathbf{x}) & \geq & 0 & \text{a.e. in } \Omega\ , \\ \kappa_{ij}(\mathbf{x}) & = & \kappa_{ji}(\mathbf{x}) & i, j = 1, \ldots, d\ . \end{array}$$

Furthermore it is assumed for $\mathcal{L}$ to be uniformly elliptic in Ω, i.e. $\exists\ \tau > 0$ such that:

$$\sum_{i,j=1}^{d} \kappa_{ij}(\mathbf{x})\xi_j\xi_i \geq \tau\,|\boldsymbol{\xi}|^2\,, \tag{3.2}$$

for each $\boldsymbol{\xi} \in \mathbb{R}^d$ and almost every $\mathbf{x} \in \Omega$. According to Section 2.4 the PDE employed to describe thermal effects on a distributed domain results to be:

$$\begin{aligned} \frac{d}{dt}\,T(\mathbf{x},t) + \mathcal{L}\ T(\mathbf{x},t) \quad &= \quad \sum_{k=1}^{K} p_k(t)\,\mathbf{1}_{\Omega_k} \qquad \text{in } \Omega, \\ T(\mathbf{x},t) + \alpha\frac{\partial\, T(\mathbf{x},t)}{\partial\,\mathbf{n}_{\mathcal{L}}} \quad &= \quad \theta_{K+1} \qquad\qquad \text{on } \partial\Omega, \end{aligned} \tag{3.3}$$

where θ_{K+1} represents the environment temperature while $\alpha \geq 0$ is a real parameter. Notice that α permits to choose between Dirichlet boundary condition ($\alpha = 0$) and Robin boundary condition ($\alpha > 0$). Associating $\mathcal{L}$ with the following bilinear form:

$$a(T,v) := \int_{\Omega} \big(\sum_{i,j=1}^{d} \kappa_{ij}(\mathbf{x})\ D_jT\ D_iv\big)\ d\mathbf{x} + \int_{\Omega} c(\mathbf{x})\ T\ v\ d\mathbf{x}, \tag{3.4}$$

a weak formulation of (3.3) can be provided. Formally speaking this weak formulation is obtained multiplying the first equation in (3.3) by a suitable test function v, integrating over Ω, applying Green formula and substituting appropriately the boundary term. In the case of Robin boundary conditions the weak formulation reads, for instance:

$$\frac{d}{dt}(T,v) + a(T,v) + \frac{1}{\alpha}(T-\theta_{K+1},v)_{\partial\Omega} = \sum_{k=1}^{n} p_k(\mathbf{1}_{\Omega_k},v), \tag{3.5}$$

where $(\cdot,\cdot)$ and $(\cdot,\cdot)_{\partial\Omega}$ denote respectively $\mathbb{L}^2(\Omega)$ and $\mathbb{L}^2(\partial\Omega)$ scalar products:

$$\begin{aligned} (u,v) \quad &:= \quad \int_{\Omega} u\ v\, d\mathbf{x}, \\ (u,v)_{\partial\Omega} \quad &:= \quad \int_{\partial\Omega} u\ v\, d\mathbf{x}. \end{aligned}$$

Notice that, as $c(\mathbf{x}) \geq 0$ a.e. in Ω, the bilinear form:

$$a(\cdot,\cdot) : \mathbb{H}^1(\Omega) \times \mathbb{H}^1(\Omega) \to \mathbb{R}, \tag{3.6}$$

results to be continuous and coercive in Ω:

$$\begin{aligned} \exists\ \gamma > 0: \quad |a(u,v)| \quad &\leq \quad \gamma\|u\|_{\mathbb{H}^1}\ \|v\|_{\mathbb{H}^1} \qquad \forall u,v \in \mathbb{H}^1(\Omega), \\ \exists\ \eta > 0: \quad a(u,u) \quad &\geq \quad \eta\|u\|^2_{\mathbb{H}^1} \qquad\qquad\ \ \forall u,v \in \mathbb{H}^1(\Omega). \end{aligned} \tag{3.7}$$

Less stringent assumptions could be made in order to ensure coerciveness (see e.g. [30]). The reader interested in further details concerning PDE theory can refer to Appendix C and the references therein.

3.2 Well posedness of the thermal element model

The aim of this section is to analyze the well posedness of the thermal element model when externally controlled by independent sources. This analysis is conducted first on steady state problems, where the elliptic counterpart of (3.3) has to be taken into account [3], and extended then to the transient case. Consistently with the construction of the thermal element presented in Section 2.4 the cases of Robin or Dirichlet boundary conditions are taken into account. Notice furthermore that the boundary conditions are here and in Section 3.3 generalized to:

$$T(\mathbf{x},t) + \alpha \frac{\partial T(\mathbf{x},t)}{\partial \mathbf{n}_{\mathcal{L}}} = g(\mathbf{x},t), \tag{3.8}$$

where $g(\mathbf{x},t)$ is an appropriate function of space and (possibly) time.

3.2.1 Elliptic case

The elliptic case results to be of major importance in the application, as shown in [3]. In particular the existence and uniqueness of a solution when heat fluxes or average temperatures are prescribed provides a theoretical validation of an implementation of the thermal element in conductance and admittance form respectively [15].

Prescribed heat fluxes To start with, the case where independent current sources prescribe the Joule power per unit area produced in a region of the thermal element is considered. It is not difficult to see that, due to the particular structure of the thermal element, this case leads directly to standard PDE theory. The well posedness of the system is then a consequence of *Lax-Milgram lemma* [60], reported below for completeness:

Theorem 3.1 (Lax-Milgram lemma)**.** *Define:*

1. *V to be a real Hilbert space, endowed with the norm $\|\cdot\|$,*
2. *$\mathcal{A} : V \times V \to \mathbb{R}$ to be a bilinear form, continuous and coercive on V,*
3. *$\mathcal{F} : V \to \mathbb{R}$ to be a linear and continuous functional.*

Then there exists unique $u \in V$ solution of:

$$\mathcal{A}(u,v) = \mathcal{F}(v) \qquad \forall v \in V. \tag{3.9}$$

To apply Theorem 3.1 an appropriate functional $\mathcal{F}$ and bilinear form $\mathcal{A}$ have to be defined. In the case of Robin boundary conditions, and assuming $g(\mathbf{x}) \in \mathbb{L}^2(\partial\Omega)$, this results to be for instance:

$$\begin{aligned} \mathcal{A} &: \mathbb{H}^1(\Omega) \times \mathbb{H}^1(\Omega) \to \mathbb{R}, \\ \mathcal{F} &: \mathbb{H}^1(\Omega) \to \mathbb{R}, \end{aligned} \tag{3.10}$$

where the bilinear form and the linear functional are defined as:

$$\begin{aligned} \mathcal{A}(u,v) &:= a(u,v) + \frac{1}{\alpha}(u,v)_{\partial\Omega}, \\ \mathcal{F}(v) &:= \sum_{k=1}^{K} p_k(\mathbf{1}_{\Omega_k}, v) + \frac{1}{\alpha}(g,v)_{\partial\Omega}. \end{aligned} \tag{3.11}$$

For a deeper treatment of the subject the interested reader is referred to [30, 79].

Prescribed average temperatures The second case considered is the one where independent voltage sources impose the average temperature in a region of the thermal element. Regarding this situation the following theorem holds for the case of Robin boundary conditions:

Theorem 3.2 (Robin boundary conditions)**.** *Define* $\hat{\alpha} = 1/\alpha$*. Given:*

1. $\theta_k \in \mathbb{R}$ *(*$k = 1, \dots, K$*),*
2. $g \in \mathbb{L}^2(\partial\Omega)$*,*

there exist unique:

1. $T \in \mathbb{H}^1(\Omega)$*,*
2. $p_k \in \mathbb{R}$ *(*$k = 1, \dots, K$*),*

such that:

$$a(T,v) + (\hat{\alpha}T, v)_{\partial\Omega} = \sum_{k=1}^{K} p_k(\mathbf{1}_{\Omega_k}, v) + (\hat{\alpha}g, v)_{\partial\Omega} \qquad \forall v \in \mathbb{H}^1(\Omega), \tag{3.12a}$$

$$(T, \mathbf{1}_{\Omega_k}) = \theta_k|\Omega_k| \qquad k = 1, \dots, K. \tag{3.12b}$$

Proof. Since the differential operator (3.12a) is linear the general solution, for any choice of p_k, can be represented as [30]:

$$T(\mathbf{x}) = T_*(\mathbf{x}) + \sum_{k=1}^{K} p_k T_k(\mathbf{x}), \tag{3.13}$$

with $T_*(\mathbf{x})$ solution of the problem:

$$a(T_*, v) + (\hat{\alpha}T_*, v)_{\partial\Omega} = (\hat{\alpha}g, v)_{\partial\Omega} \qquad \forall v \in \mathbb{H}^1(\Omega), \tag{3.14}$$

and $T_k(\mathbf{x})$ solution of the problem:

$$a(T_k, v) + (\hat{\alpha}T_k, v)_{\partial\Omega} = (\mathbf{1}_{\Omega_k}, v) \qquad \forall v \in \mathbb{H}^1(\Omega). \tag{3.15}$$

Substitute (3.13) into (3.12b):

$$(T, \mathbf{1}_{\Omega_k}) = (T_* + \sum_{j=1}^{K} p_j T_j, \mathbf{1}_{\Omega_k}) = (T_*, \mathbf{1}_{\Omega_k}) + \sum_{j=1}^{K} p_j (T_j, \mathbf{1}_{\Omega_k}) \overset{!}{=} \theta_k |\Omega_k|, \tag{3.16}$$

with $(k = 1, \ldots, K)$. The conditions for p_k in (3.12b) can now be written as a linear algebraic system:

$$\sum_{j=1}^{K} (T_j, \mathbf{1}_{\Omega_k}) p_j \overset{!}{=} \theta_k |\Omega_k| - (T_*, \mathbf{1}_{\Omega_k}) \quad k = 1, \ldots, K. \tag{3.17}$$

This system is uniquely solvable if and only if the matrix $\mathrm{B} = \left[(T_j, \mathbf{1}_{\Omega_k})\right]$ is non-singular, that is to say $\det(\mathrm{B}) \neq 0$. Noting that:

$$(T_j, \mathbf{1}_{\Omega_k}) = (\mathbf{1}_{\Omega_k}, T_j) = a(T_k, T_j) + (\hat{\alpha} T_k, T_j)_{\partial\Omega} = \mathcal{A}(T_k, T_j), \tag{3.18}$$

an equivalent condition on the matrix $\mathrm{A} = \left[\mathcal{A}(T_k, T_j)\right]$ is derived:

$$\det(\mathrm{A}) \neq 0. \tag{3.19}$$

By using the (extended) Cauchy-Schwarz inequality (see [26], Chapter 5) it results A positive-semidefinite and therefore $\det(\mathrm{A}) \geq 0$. Furthermore the equality holds true if and only if there exist $\lambda_k \in \mathbb{R}$ $(k = 1, \ldots, K)$ not all equal to zero, such that:

$$\sum_{k=1}^{K} \lambda_k T_k(\mathbf{x}) = 0. \tag{3.20}$$

In conclusion to prove existence and uniqueness it is sufficient to prove that (3.20) implies $\lambda_k = 0$ for all $k = 1, \ldots, K$. This fact follows from the equality:

$$0 \equiv \sum_{k=1}^{K} \lambda_k \mathcal{A}(T_k, v) = \sum_{k=1}^{K} \lambda_k (\mathbf{1}_{\Omega_k}, v) \quad \forall v \in \mathbb{H}^1(\Omega). \tag{3.21}$$

Then for any $k = 1, \ldots, K$ it is possible to choose v such that $\mathrm{supp}(v) \subset \Omega_k$ and get $\lambda_k = 0$. Notice that this last consideration implies $\det(\mathrm{A}) > 0$ and A positive definite. ☐

The case of Dirichlet boundary conditions differs from the previous one in some technical details (see Appendix C and the reference therein for a deeper treatment). Here it is possible to prove the following:

Theorem 3.3 (Dirichlet boundary conditions)**.** *Given:*

1. $\theta_k \in \mathbb{R}$ *$(k = 1, \ldots, K)$,*
2. $g \in \mathbb{H}^{1/2}(\partial\Omega)$,

there exist unique:

1. $\tilde{T} \in \mathbb{H}^1_0(\Omega)$,
2. $p_k \in \mathbb{R}$ *(*$k = 1, \dots, K$*),*

such that:

$$a(\tilde{T}, v) = (\sum_{k=1}^{K} p_k \, \mathbf{1}_{\Omega_k}, v) - a(\tilde{g}, v), \qquad \forall v \in \mathbb{H}^1_0(\Omega), \tag{3.22a}$$

$$(\tilde{T} + \tilde{g}, \mathbf{1}_{\Omega_k}) = \theta_k |\Omega_k|, \qquad k = 1, \dots, K. \tag{3.22b}$$

where $\tilde{g} \in \mathbb{H}^1(\Omega)$ *is an arbitrary extension of* $g \in \mathbb{H}^{1/2}(\partial\Omega)$*.*

Proof. Even in the case of Dirichlet boundary conditions a general representation of the solution reads:

$$\tilde{T}(\mathbf{x}) = \tilde{T}_*(\mathbf{x}) + \sum_{k=1}^{K} p_k \tilde{T}_k(\mathbf{x}) \ , \tag{3.23}$$

where $\tilde{T}_*(\mathbf{x}) \in \mathbb{H}^1_0(\Omega)$ is the solution of:

$$a(\tilde{T}_*, v) = -a(\tilde{g}, v) \qquad \forall v \in \mathbb{H}^1_0(\Omega) \ , \tag{3.24}$$

while $\tilde{T}_k(\mathbf{x}) \in \mathbb{H}^1_0(\Omega)$ is the solution of:

$$a(\tilde{T}_k, v) = (\mathbf{1}_{\Omega_k}, v) \qquad \forall v \in \mathbb{H}^1_0(\Omega) \ . \tag{3.25}$$

As before, a linear algebraic system for p_k can be derived:

$$\sum_{j=1}^{K} (\tilde{T}_j, \mathbf{1}_{\Omega_k}) p_j \overset{!}{=} \theta_k |\Omega_k| - (\tilde{g} + \tilde{T}_*, \mathbf{1}_{\Omega_k}) \quad k = 1, \dots, K. \tag{3.26}$$

From this point on the same strategy as in Theorem 3.2 can be adopted, the only difference being that in this case:

$$\mathrm{A} = \big[a(\tilde{T}_k, \tilde{T}_j)\big]. \tag{3.27}$$

□

Linear constraints between average temperatures and power fluxes Finally , as a generalization of the previous theorems, the case where non-ideal sources are connected to the thermal element pins is considered.

Theorem 3.4 (Robin boundary conditions)**.** *Define* $\hat{\alpha} = 1/\alpha$*. Given:*

1. $g \in \mathbb{L}^2(\partial\Omega)$,

2. *$a_k, c_k \geq 0$, $b_k > 0$,*

there exist unique:

1. *$T \in \mathbb{H}^1(\Omega)$,*
2. *$p_k, \theta_k \in \mathbb{R}$ $(k = 1, \ldots, K)$,*

such that:

$$a(T, v) + (\hat{\alpha} T, v)_{\partial\Omega} = \sum_{k=1}^{K} p_k(\mathbf{1}_{\Omega_k}, v) + (\hat{\alpha} g, v)_{\partial\Omega} \qquad \forall v \in \mathbb{H}^1(\Omega), \tag{3.28a}$$

$$(T, \mathbf{1}_{\Omega_k}) = \theta_k |\Omega_k| \qquad k = 1, \ldots, K, \tag{3.28b}$$

$$a_k p_k + b_k \theta_k = c_k \qquad k = 1, \ldots, K. \tag{3.28c}$$

Proof. The same decomposition employed in Theorem 3.2 can be used also in this case. The only difference is that (3.28c) gives a system for p_k and θ_k, with matrix:

$$\begin{bmatrix} B & -\mathrm{diag}(\boldsymbol{\Omega}) \\ \mathrm{diag}(\mathbf{a}) & \mathrm{diag}(\mathbf{b}) \end{bmatrix}, \tag{3.29}$$

where:

$$\begin{aligned} \mathbf{a} &= (a_1, \ldots, a_K), \\ \mathbf{b} &= (b_1, \ldots, b_K), \\ \boldsymbol{\Omega} &= (|\Omega_1|, \ldots, |\Omega_K|). \end{aligned} \tag{3.30}$$

This is a block matrix, where the two lower blocks commute. Then, by using results from [87] and recalling that the matrix B is positive definite, it holds:

$$\begin{aligned} \det \begin{bmatrix} B & -\mathrm{diag}(\boldsymbol{\Omega}) \\ \mathrm{diag}(\mathbf{a}) & \mathrm{diag}(\mathbf{b}) \end{bmatrix} &= \det \left[\mathrm{B}\ \mathrm{diag}(\mathbf{b}) + \mathrm{diag}(\mathbf{a})\mathrm{diag}(\boldsymbol{\Omega}) \right] \\ &= \det \left[\mathrm{B} + \mathrm{diag}(\mathbf{a})\mathrm{diag}(\boldsymbol{\Omega})\mathrm{diag}(\mathbf{b})^{-1} \right] \det \left[\mathrm{diag}(\mathbf{b}) \right] > 0, \end{aligned}$$

since the matrix:

$$\left[\mathrm{B} + \mathrm{diag}(\mathbf{a})\mathrm{diag}(\boldsymbol{\Omega})\mathrm{diag}(\mathbf{b})^{-1} \right],$$

is positive definite. ☐

Following the same line of reasoning it is also possible to prove the following:

Theorem 3.5 (Dirichlet boundary conditions)**.** *Given:*

1. *$g \in \mathbb{H}^{1/2}(\partial\Omega)$,*
2. *$a_k, c_k \geq 0$, $b_k > 0$,*

there exist unique:

1. $\tilde{T} \in \mathbb{H}_0^1(\Omega)$,
2. $p_k, \theta_k \in \mathbb{R}$ *(*$k = 1, \dots, K$*),*

such that:

$$a(\tilde{T}, v) = (\sum_{k=1}^{K} p_k \, \mathbf{1}_{\Omega_k}, v) - a(\tilde{g}, v) \qquad \forall v \in \mathbb{H}_0^1(\Omega), \tag{3.31a}$$

$$(\tilde{T} + \tilde{g}, \mathbf{1}_{\Omega_k}) = \theta_k |\Omega_k| \qquad k = 1, \dots, K, \tag{3.31b}$$

$$a_k p_k + b_k \theta_k = c_k \qquad k = 1, \dots, K. \tag{3.31c}$$

where $\tilde{g} \in \mathbb{H}^1(\Omega)$ *is an arbitrary extension of* $g \in \mathbb{H}^{1/2}(\partial\Omega)$*.*

3.2.2 Parabolic case

After having treated the elliptic case, its parabolic counterpart is taken into account. This will ensure the well posedness of the thermal element model before a suitable time discretization has been performed.

Prescribed heat fluxes Even in the parabolic case the assignment of the Joule power per unit area dissipated in a region leads back to standard PDE theorems. The case of Robin boundary conditions can be treated as follows:

Theorem 3.6 (Robin boundary conditions)**.** *Define* $\hat{\alpha} = 1/\alpha$*. Given:*

1. $p_k \in \mathbb{C}^0[0, \mathrm{t}_1] \quad k = 1, \dots, K$,
2. $T_0 \in \mathbb{L}^2(\Omega)$,
3. $g \in \mathbb{C}^0\left([0, \mathrm{t}_1], \mathbb{L}^2(\partial\Omega)\right)$,

there exists unique:

1. $T \in \mathbb{C}^0\left([0, \mathrm{t}_1], \mathbb{L}^2(\Omega)\right) \cap \mathbb{L}^2\left((0, \mathrm{t}_1), \mathbb{H}^1(\Omega)\right)$,

such that:

$$\begin{aligned} \frac{d}{dt}(T, v) + a(T, v) + (\hat{\alpha} T, v)_{\partial\Omega} &= \sum_{k=1}^{K} p_k (\mathbf{1}_{\Omega_k}, v) + (\hat{\alpha} g, v)_{\partial\Omega} \qquad \forall v \in \mathbb{H}^1(\Omega), \\ T(\mathbf{x}, 0) &= T_0(\mathbf{x}). \end{aligned} \tag{3.32}$$

The corresponding statement concerning Dirichlet boundary conditions reads:

Theorem 3.7 (Dirichlet boundary conditions)**.** *Given:*

1. $p_k \in \mathbb{C}^0[0,\mathrm{t}_1] \quad k = 1,\ldots,K$,
2. $T_0 \in \mathbb{L}^2(\Omega)$,
3. $g \in \mathbb{C}^0\big([0,\mathrm{t}_1],\mathbb{H}^{1/2}(\partial\Omega)\big)$,

there exists unique:

1. $\tilde{T} \in \mathbb{C}^0\left([0,\mathrm{t}_1],\mathbb{L}^2(\Omega)\right) \cap \mathbb{L}^2\left((0,\mathrm{t}_1),\mathbb{H}^1_0(\Omega)\right)$,

such that:

$$\begin{aligned} \frac{d}{dt}(\tilde{T},v) + a(\tilde{T},v) &= \sum_{k=1}^{K} p_k(\mathbf{1}_{\Omega_k},v) - a(\tilde{g},v) \qquad \forall v \in \mathbb{H}^1_0(\Omega), \\ \tilde{T}(\mathbf{x},0) &= T_0(\mathbf{x}) - \tilde{g}(\mathbf{x},0). \end{aligned} \tag{3.33}$$

with $\tilde{g} \in \mathbb{C}^0\left([0,\mathrm{t}_1],\mathbb{H}^1(\Omega)\right)$ *arbitrary extension of* $g \in \mathbb{C}^0\big([0,\mathrm{t}_1],\mathbb{H}^{1/2}(\partial\Omega)\big)$.

Readers interested in the proof of the previous statements are referred to [13,75,79].

Prescribed mean temperatures To prove the well posedness of the thermal element in the case of assigned mean temperatures the following lemmas are needed.

Lemma 3.1. *Define:*

$$\begin{aligned} U &:= \left\{u \in \mathbb{L}^2(\Omega) \ \textit{s.t.}\ (u,\mathbf{1}_{\Omega_k}) = 0,\ \forall k = 1,\ldots,K\right\}, \\ V &:= \left\{u \in \mathbb{H}^1(\Omega) \ \textit{s.t.}\ (u,\mathbf{1}_{\Omega_k}) = 0,\ \forall k = 1,\ldots,K\right\}. \end{aligned}$$

Then:

1. *U is a closed subspace of* $\mathbb{L}^2(\Omega)$
2. *V is a closed subspace of* $\mathbb{H}^1(\Omega)$

Proof. The first assertion is trivial to prove, as:

$$\mathbb{L}^2(\Omega) = U \oplus \mathrm{span}(\mathbf{1}_{\Omega_1},\ldots,\mathbf{1}_{\Omega_K}). \tag{3.34}$$

To prove the second assertion a Cauchy sequence $\{u_j\} \in (V,\|\cdot\|_{\mathbb{H}^1})$ is considered. It holds that:

$$u_j \to u^* \in \mathbb{H}^1(\Omega), \tag{3.35}$$

since $\mathbb{H}^1(\Omega)$ is a Banach space. Furthermore:

$$\begin{aligned} |(u^*,\mathbf{1}_{\Omega_k})| \le |(u^*-u_j,\mathbf{1}_{\Omega_k})| + |(u_j,\mathbf{1}_{\Omega_k})| &\le \int_{\Omega_k} |u^*-u_j| d\mathbf{x} \\ = \int_{\Omega_k} 1\cdot|u^*-u_j| d\mathbf{x} \le \left[\int_{\Omega_k} 1^2 d\mathbf{x}\right]^{1/2} &\left[\int_{\Omega_k} |u^*-u_j|^2 d\mathbf{x}\right]^{1/2} \\ \le \sqrt{|\Omega_k|}\ \|u^*-u_j\|_{\mathbb{L}^2(\Omega)} \le \sqrt{|\Omega_k|}\ \|u^*-u_j\|_{\mathbb{H}^1(\Omega)} \to 0. \end{aligned}$$

Then it follows that $u^* \in V$ and Lemma 3.1 is proved. □

Lemma 3.2. *$\mathbb{H}^1(\Omega)$ can be decomposed into the direct sum:*

$$\mathbb{H}^1(\Omega) = V \oplus W, \tag{3.36}$$

where V is defined in Lemma 3.1 and W is a K-dimensional space.

Proof. To prove this lemma a particular space W is constructed. Then any other space satisfying (3.36) must have the same dimension. Let $\{\phi_k\}$ denote a set of basis function for $\mathbb{H}^1(\Omega)$. These functions are chosen such that:

$$\begin{aligned} \operatorname{supp}(\phi_j) &\subset \Omega_j \quad j = 1, \dots, K, \\ (\phi_j, \mathbf{1}_{\Omega_j}) &\neq 0 \qquad j = 1, \dots, K. \end{aligned} \tag{3.37}$$

It is possible to define then:

$$W := \operatorname{span}_{k=1,\dots,K}(\phi_k). \tag{3.38}$$

Notice that every $u \in \mathbb{H}^1(\Omega)$ can be uniquely represented by:

$$u = \sum_{k=1}^{\infty} \gamma_k \ \phi_k. \tag{3.39}$$

Define the two operators:

$$\begin{aligned} P_V(u) &: \mathbb{H}^1(\Omega) \to V, \\ P_W(u) &: \mathbb{H}^1(\Omega) \to W, \end{aligned} \tag{3.40}$$

as:

$$\begin{aligned} P_V(u) &:= \sum_{k=1}^{K} \hat{\gamma}_k \phi_k + \sum_{k=K+1}^{\infty} \gamma_k \phi_k, \\ P_W(u) &:= \sum_{k=1}^{K} [\gamma_k - \hat{\gamma}_k] \phi_k. \end{aligned} \tag{3.41}$$

where the coefficients $\hat{\gamma}_k$ are given by:

$$\hat{\gamma}_k := -\frac{\displaystyle\int_{\Omega_k} \sum_{j=K+1}^{\infty} \gamma_j \phi_j d\mathbf{x}}{\displaystyle\int_{\Omega_k} \phi_k d\mathbf{x}}. \tag{3.42}$$

It holds by construction that:

$$\begin{aligned} P_V(u) &= v \in V \\ P_W(u) &= w \in W \end{aligned} \qquad \forall u \in \mathbb{H}^1(\Omega), \tag{3.43}$$

and:

$$\begin{aligned} P_V(v) &= v \qquad \forall v \in V, \\ P_W(w) &= w \qquad \forall w \in W. \end{aligned} \tag{3.44}$$

Combining (3.43) and (3.44) it follows:

$$\left.\begin{aligned} P_V^2(u) &= P_V(u) \\ P_W^2(u) &= P_W(u) \end{aligned}\right. \qquad \forall u \in \mathbb{H}^1(\Omega). \tag{3.45}$$

Then P_V and P_W are (oblique) projection operators and every $u \in \mathbb{H}^1(\Omega)$ admits the unique representation:

$$u = P_V(u) + P_W(u), \tag{3.46}$$

and thus the lemma is proved. ☐

With Lemma 3.2 it is established that $\mathbb{H}^1(\Omega)$ can be decomposed into the direct sum of V and a K-dimensional space. The actual choice of the space W is not important in view of Theorem 3.8. Notice that:

$$\dim(V_\perp) = K,$$

can be deduced as a particular application of Lemma 3.2.

Theorem 3.8 (Robin boundary conditions)**.** *Define* $\hat{\alpha} = 1/\alpha$*. Given:*

1. $T_0 \in \mathbb{L}^2(\Omega)$,
2. $\theta_k \in \mathbb{C}^0[0, \mathrm{t}_1]$ *and* $\theta_k(0)$ *consistent with* T_0 *(*$k = 1, \dots, K$*),*
3. $g \in \mathbb{C}^0\big([0, \mathrm{t}_1], \mathbb{L}^2(\partial\Omega)\big)$,

there exist unique:

1. $T \in \mathbb{C}^0\big([0, \mathrm{t}_1]; \mathbb{L}^2(\Omega)\big) \cap \mathbb{L}^2\big((0, \mathrm{t}_1); \mathbb{H}^1(\Omega)\big)$,
2. $p_k \in \mathbb{C}^0[0, \mathrm{t}_1]$ *(*$k = 1, \dots, K$*),*

such that:

$$\frac{d}{dt}(T, v) + a(T, v) + (\hat{\alpha} T, v)_{\partial\Omega} = \sum_{k=1}^{K} p_k(\mathbf{1}_{\Omega_k}, v) + (\hat{\alpha} g, v)_{\partial\Omega} \qquad \forall v \in \mathbb{H}^1(\Omega), \tag{3.47a}$$

$$T(\mathbf{x}, 0) = T_0(\mathbf{x}), \tag{3.47b}$$

$$(T, \mathbf{1}_{\Omega_k}) = \theta_k(t)|\Omega_k| \qquad k = 1, \dots, K. \tag{3.47c}$$

Proof. In the following the well-posedness of system (3.47) will be proved exploiting its linearity to divide it into three subproblems that are tackled successively. The well-posedness of the first one, accounting for non-zero mean temperatures, will be proved resorting to Theorem 3.2. Then to prove existence and uniqueness of a solution for the remaining two subproblems, Lemma 3.1 and Lemma 3.2 are employed. Assume then:

$$T(\mathbf{x},t) = \tilde{T}(\mathbf{x},t) + \hat{T}(\mathbf{x},t) \ , \tag{3.48}$$

where $\tilde{T}(\mathbf{x},t)$ is solution of:

$$a(\tilde{T}(t),v) + (\hat{\alpha}\tilde{T}(t),v)_{\partial\Omega} = \sum_{k=1}^{K} \tilde{p}_k(t)(\mathbf{1}_{\Omega_k},v) + (\hat{\alpha}g,v)_{\partial\Omega} \qquad \forall v \in \mathbb{H}^1(\Omega), \tag{3.49a}$$

$$(\tilde{T}(t),\mathbf{1}_{\Omega_k}) = \theta_k(t)|\Omega_k| \qquad k = 1,\ldots,K. \tag{3.49b}$$

This problem admits a unique solution:

1. $\tilde{T} \in \mathbb{C}^0\big([0,\mathrm{t}_1];\mathbb{H}^1(\Omega)\big)$,
2. $\tilde{p}_k \in \mathbb{C}^0[0,\mathrm{t}_1]$,

due to Theorem 3.2. In fact the continuity of $\tilde{p}_k$ $(k = 1,\ldots,K)$ stems from (3.17), as:

- T^* is continuous with respect to time due to the assumptions on g and to the well-posedness of the elliptic problem (3.14),
- θ_k $(k = 1,\ldots,K)$ are continuous by hypothesis,
- $\mathrm{A} = \big[\mathcal{A}(T_k,T_j)\big]$ does not depend on time.

The continuity of $\tilde{T}$ is then a consequence of (3.13). Substituting (3.48) into (3.47) the following problem is obtained:

$$\begin{aligned} \frac{d}{dt}(\tilde{T}+\hat{T},v) + a(\hat{T},v) + (\hat{\alpha}\hat{T},v)_{\partial\Omega} &= \sum_{k=1}^{K}\left[p_k(t) - \tilde{p}_k(t)\right](\mathbf{1}_{\Omega_k},v) \quad \forall v \in \mathbb{H}^1(\Omega), \\ \hat{T}(\mathbf{x},0) &= T_0(\mathbf{x}) - \tilde{T}(\mathbf{x},0), \\ (\hat{T},\mathbf{1}_{\Omega_k}) &= 0 \qquad\qquad k = 1,\ldots,K. \end{aligned} \tag{3.50}$$

where the unknowns are:

1. $\hat{T} \in \mathbb{C}^0\big([0,\mathrm{t}_1];\mathbb{L}^2(\Omega)\big) \cap \mathbb{L}^2\big((0,\mathrm{t}_1);\mathbb{H}^1(\Omega)\big)$,
2. $p_k \in \mathbb{C}^0[0,\mathrm{t}_1]$.

Resorting to Lemma 3.1 and Lemma 3.2 it is possible to move the zero mean conditions inside the space in which $\hat{T}$ is sought. Equation (3.50) can thus be written in the equivalent form:

$$\begin{aligned} \frac{d}{dt}(\tilde{T}+\hat{T},v)+a(\hat{T},v)+(\hat{\alpha}\hat{T},v)_{\partial\Omega} &= \sum_{k=1}^{K}\left[p_k(t)-\tilde{p}_k(t)\right](\mathbf{1}_{\Omega_k},v) \quad \forall v\in\mathbb{H}^1(\Omega), \\ \hat{T}(\mathbf{x},0) &= T_0(\mathbf{x})-\tilde{T}(\mathbf{x},0), \end{aligned} \tag{3.51}$$

where the unknowns now result to be:

1. $\hat{T}\in\mathbb{C}^0\big([0,\mathrm{t}_1];U\big)\cap\mathbb{L}^2\big((0,\mathrm{t}_1);V\big)$,
2. $p_k\in\mathbb{C}^0[0,\mathrm{t}_1]$.

Recalling that:

$$\mathbb{H}^1(\Omega)=V\oplus W, \tag{3.52}$$

it is feasible to start testing (3.51) upon $v\in V$. In this case an abstract evolutionary problem involving only $\hat{T}$ is found:

$$\frac{d}{dt}(\hat{T},v)+a(\hat{T},v)+(\hat{\alpha}\hat{T},v)_{\partial\Omega}=-\frac{d}{dt}(\tilde{T},v), \quad \forall v\in V. \tag{3.53}$$

Notice that the time derivative at right hand side in (3.53) is to be intended in a weak sense (see for instance [74, Chapter 11, pag.368]), that is to say:

$$-\int_0^t(\frac{d}{d\tau}\tilde{T}(\tau),v)\psi(\tau)d\tau:=\int_0^t(\tilde{T},v)\frac{d}{d\tau}\psi(\tau)d\tau-(\tilde{T}(0),v)\psi(0)+(\tilde{T}(t),v)\psi(t)\ ,$$

for a suitable test function $\psi(t)$. Since (V,U,V^{-1}) constitute a *Gelfand triple* this problem is uniquely solvable for:

1. $\hat{T}\in\mathbb{C}^0\big([0,\mathrm{t}_1];U\big)\cap\mathbb{L}^2\big((0,\mathrm{t}_1);V\big)$,

and furthermore:

$$\frac{\partial\hat{T}}{\partial t}\in\mathbb{L}^2\big((0,\mathrm{t}_1);V^{-1}\big)\ .$$

The interested reader is referred to [106, Theorem 23.A] for an extensive treatment of the subject. Finally it remains to test upon $v\in W$:

$$\frac{d}{dt}(T,v)+a(T,v)+(\hat{\alpha}T,v)_{\partial\Omega}=\sum_{k=1}^{K}p_k(t)(\mathbf{1}_{\Omega_k},v)+(\hat{\alpha}g,v)_{\partial\Omega}, \quad \forall v\in W, \tag{3.54}$$

where now $T(\mathbf{x},t)$ is known. As W is K-dimensional (see Lemma 3.2) this problem admits a unique solution and therefore the theorem is proved. □

The statement corresponding to Theorem 3.8 but accounting for Dirichlet boundary conditions is given next. Of course the proof can be obtained following the same line of reasoning used in Theorem 3.8.

Theorem 3.9 (Dirichlet boundary conditions)**.** *Given:*

1. $T_0 \in \mathbb{L}^2(\Omega)$,
2. $\theta_k \in \mathbb{C}^0[0, \mathrm{t}_1]$ *and* $\theta_k(0)$ *consistent with* T_0 $(k = 1, \ldots, K)$,
3. $g \in \mathbb{C}^0\big([0, \mathrm{t}_1], \mathbb{H}^{1/2}(\partial\Omega)\big)$,

there exist unique:

1. $\tilde{T} \in \mathbb{C}^0\big([0, \mathrm{t}_1]; \mathbb{L}^2(\Omega)\big) \cap \mathbb{L}^2\big((0, \mathrm{t}_1); \mathbb{H}^1_0(\Omega)\big)$,
2. $p_k \in \mathbb{C}^0[0, \mathrm{t}_1]$ $(k = 1, \ldots, K)$,

such that:

$$\frac{d}{dt}(\tilde{T}, v) + a(\tilde{T}, v) = \sum_{k=1}^{K} p_k(\mathbf{1}_{\Omega_k}, v) - a(\tilde{g}, v)_{\partial\Omega} \qquad \forall v \in \mathbb{H}^1_0(\Omega), \tag{3.55a}$$

$$T(\mathbf{x}, 0) = T_0(\mathbf{x}), \tag{3.55b}$$

$$(T, \mathbf{1}_{\Omega_k}) = \theta_k(t)|\Omega_k| \qquad k = 1, \ldots, K, \tag{3.55c}$$

with $\tilde{g} \in \mathbb{C}^0\left([0, \mathrm{t}_1], \mathbb{H}^1(\Omega)\right)$ *arbitrary extension of* $g \in \mathbb{C}^0\big([0, \mathrm{t}_1], \mathbb{H}^{1/2}(\partial\Omega)\big)$.

3.3 Well posedness of the coupled system

To conclude Chapter 3 the well posedness of an initial value problem on a given time interval $[0, \mathrm{t}_1]$ is discussed. The system taken into consideration is composed of standard and thermally active electrical elements connected to a linear thermal network. Define then:

$$\mathbf{p} := [p_1(t), \ldots, p_K(t)]^T \ , \tag{3.56}$$

to be the vector of the K Joule power densities, and:

$$\boldsymbol{\theta} := [\theta_1(t), \ldots, \theta_K(t)]^T \ , \tag{3.57}$$

to be the vector of the corresponding K junction temperatures. [1] Employing the DAE formulation briefly introduced in Section 2.2 the electrical part of the system can be formalized as:

---

[1] As already anticipated in Section 3.2, the boundary conditions for the PDE describing heat diffusion are for analysis purpose prescribed in a more general manner than the one introduced in Chapter 2. Thus (3.57) does not include any component referring to the environment temperature.

$$\begin{aligned}
A_C\frac{d\mathbf{q}}{dt}+A_R\mathbf{r}(A_R^T\mathbf{e},\boldsymbol{\theta})+A_L\mathbf{i}_L+A_V\mathbf{i}_V+A_I\mathbf{i}(A_C^T\mathbf{e},\boldsymbol{\theta}) &= 0,\\
\frac{d\boldsymbol{\phi}}{dt}-A_L^T\mathbf{e} &= 0,\\
A_V^T\mathbf{e}-\mathbf{V}(t) &= 0,\\
\mathbf{q}-\mathbf{q}_C(A_C^T\mathbf{e}) &= 0,\\
\boldsymbol{\phi}-\boldsymbol{\phi}_L(\mathbf{i}_L) &= 0,
\end{aligned}\tag{3.58}$$

where an additional dependence on junction temperatures is assumed for resistors and controlled current sources. The electrical part has then to be complemented by the balance of Joule power at the thermal network nodes:

$$|\Omega_k|p_k-W_k(\boldsymbol{\theta},\mathbf{e}) = 0 \quad k=1,\dots,K,\tag{3.59}$$

by the thermal element interface conditions:

$$|\Omega_k|\theta_k-(T,\mathbf{1}_{\Omega_k}) = 0 \quad k=1,\dots,K,\tag{3.60}$$

and by the PDE describing heat diffusion at the system level:

$$\frac{d}{dt}(T,v)+a(T,v)+\hat{\alpha}(T,v)_{\partial\Omega}-\sum_{k=1}^{K}p_k(\mathbf{1}_{\Omega_k},v)-\hat{\alpha}(g,v)_{\partial\Omega}=0 \quad \forall v\in\mathbb{H}^1(\Omega).\tag{3.61}$$

In (3.59) the functions $W_k(\boldsymbol{\theta},\mathbf{e})$ $(k=1,\dots,K)$ account for the Joule power dissipated by the thermally active electrical elements, and in practice they will be implicitly constructed by the stamping procedure described in Chapter 5. Finally, even though Robin boundary conditions are assumed for (3.61), all the analysis carried out in the following can be easily generalized to the case of Dirichlet boundary conditions, as done in Section 3.2.

Assumptions on the electrical part The electrical part (3.58) is supposed in the following to be index-1 for any given:

$$\boldsymbol{\theta}\in\mathbb{C}^0[0,\mathrm{t}_1]\ .$$

Defining Q_C to be the orthogonal projector onto the kernel of A_C^T and $P_C := I-Q_C$ to be its complement, then sufficient conditions to fulfill the index-1 requirement are [29]:

1. $\ker(A_C,A_R,A_V)^T=\{0\}$, $\ker Q_C^TA_V=\{0\}$,
2. $\mathbf{i}(A_C^T\mathbf{e},\boldsymbol{\theta})$ uniformly continuous in $\boldsymbol{\theta}$ and Lipschitz continuous in $A_C^T\mathbf{e}$,
3. $\mathbf{V}(\cdot)$ continuous,

4. $\boldsymbol{\phi}_L(\cdot)$ and $\mathbf{q}_C(\cdot)$ differentiable functions of their arguments,
5. $\dfrac{\partial \mathbf{q}_C(A_C^T\mathbf{e})}{\partial(A_C^T\mathbf{e})}$, $\dfrac{\partial \boldsymbol{\phi}_L(\mathbf{i}_L)}{\partial(\mathbf{i}_L)}$ positive definite,
6. $\mathbf{r}(A_R^T\mathbf{e}, \boldsymbol{\theta})$ uniformly continuous in $\boldsymbol{\theta}$ and differentiable in $A_R^T\mathbf{e}$,
7. $\dfrac{\partial \mathbf{r}(A_R^T\mathbf{e}, \boldsymbol{\theta})}{\partial(A_R^T\mathbf{e})}$ positive definite and uniformly continuous in $\boldsymbol{\theta}$.

Notice that the extension of (3.58) to account for more general controlled sources requires particular care if the index-1 hypothesis is to be preserved, see for instance [29].

Under these assumptions the existence and uniqueness of a global solution to an initial value problem with consistent initial conditions on $[0, \mathrm{t}_1]$ follows from standard results [45, Theorem 15]. Furthermore, for each component of the solution in the time interval $[0, \mathrm{t}_1]$ a bound of the form:

$$|x(t)| \leq |d_A(\boldsymbol{\theta}(t))| + \int_0^t |d_D(\boldsymbol{\theta}(\tau))| d\tau \ , \tag{3.62}$$

holds, where $d_A(\cdot)$ and $d_D(\cdot)$ are continuous functions. Notice that the form of (3.62) is due to the index-1 condition, thanks to which the time-derivatives of $\boldsymbol{\theta}(t)$ do not appear in the bound. In this case also the following a-priori bound (uniform in $\boldsymbol{\theta} \in \mathcal{G}$) can be shown to hold:

$$|x(t)| \leq \max_{\boldsymbol{\theta} \in \mathcal{G}} |d_A(\boldsymbol{\theta})| + |t| \max_{\boldsymbol{\theta} \in \mathcal{G}} |d_D(\boldsymbol{\theta})| \ , \tag{3.63}$$

where $\mathcal{G}$ is a closed set, such that:

$$\mathcal{F} := \left\{ \mathbf{s} \in \mathbb{R}^K : |\mathbf{s}| \leq \max_{t \in [0, \mathrm{t}_1]} |\boldsymbol{\theta}(t)| \right\} \subseteq \mathcal{G} \subseteq \mathbb{R}^K \ . \tag{3.64}$$

Assumptions on the thermal part The assumptions made on the thermal part of the system are:

1. $g(\mathbf{x}, t) \in \mathbb{C}^0\left([0, \mathrm{t}_1], \mathbb{L}^2(\partial\Omega)\right)$,
2. $W_k(\cdot, \cdot)$ continuous function of its arguments ($k = 1, \ldots, K$),

Consistent initial conditions for the coupled problem To provide system (3.58-3.61) with consistent initial conditions it is possible to prescribe arbitrarily:

1. $T(\mathbf{x}, 0) := T_0(\mathbf{x}) \in \mathbb{L}^2(\Omega)$,
2. $P_C\mathbf{e}(0)$,
3. $\mathbf{i}_L(0)$.

Then:

1. $\boldsymbol{\theta}(0)$ is obtained from (3.60),
2. $Q_C\mathbf{e}(0)$, $\mathbf{i}_V(0)$, $\boldsymbol{\phi}(0)$, $\mathbf{q}(0)$ are computed from the algebraic constraints of (3.58), once $\boldsymbol{\theta}(0)$ is known,
3. $\mathbf{p}(0)$ is finally determined from (3.59).

Existence and uniqueness The existence and uniqueness of a solution to (3.58-3.61) in a given time interval $t \in [0, \mathrm{t}_1]$ is investigated in the next:

Theorem 3.10. *Consider system (3.58-3.61) with the further hypothesis that:*

1. *there exist* $C_{\mathbf{W}} > 0$ *such that* $|W_k(\boldsymbol{\theta}, \mathbf{e})| \leq C_{\mathbf{W}}$ *for* $k = 1, \ldots, K$.

Suppose furthermore that the assumptions outlined in the previous paragraphs on the electrical and thermal part of the network are fulfilled. Then, given consistent initial conditions, there exist a unique solution to an initial value problem on a given time interval $[0, \mathrm{t}_1]$ *and:*

1. $P_C\mathbf{e}$, $\mathbf{i}_L$, $\mathbf{q}$ *and* $\boldsymbol{\phi}$ *are differentiable,*
2. $Q_C\mathbf{e}$, $\mathbf{i}_V$, $\boldsymbol{\theta}$ *and* $\mathbf{p}$ *are continuous,*
3. *the regularity of the PDE solution is at least:*

   $$T \in \mathbb{L}^2\left((0, \mathrm{t}_1), \mathbb{H}^1(\Omega)\right) \cap \mathbb{C}^0\left([0, \mathrm{t}_1], \mathbb{L}^2(\Omega)\right) \ , \tag{3.65}$$

   while:

   $$\frac{\partial T}{\partial t} \in \mathbb{L}^2\left((0, \mathrm{t}_1), \mathbb{H}^{-1}(\Omega)\right) \ , \tag{3.66}$$

4. *the energy estimate:*

   $$\|T(\mathbf{x}, t)\|^2_{\mathbb{L}^2(\Omega)} + \eta \int_0^t \|T(\mathbf{x}, \tau)\|^2_{\mathbb{H}^1(\Omega)} d\tau \leq \|T_0(\mathbf{x})\|^2_{\mathbb{L}^2(\Omega)} + \frac{1}{\eta} \int_0^t S^2 d\tau \ , \tag{3.67}$$

   holds for each $t \in [0, \mathrm{t}_1]$ *where:*

   $$S = S(C_{\mathbf{W}}, \hat{\alpha}, \Omega_k, g) := C_{\mathbf{W}} \sum_{k=1}^{K} \sqrt{|\Omega_k|} + \hat{\alpha} \, \|g(t)\|_{\mathbb{L}^2(\partial\Omega)} \ . \tag{3.68}$$

Proof. In the following the so-called Faedo-Galerkin method is exploited to construct a sequence of DAE systems that approximate the PDAE system (3.58-3.61). The line followed stems directly from the one usually employed to prove the well posedness of parabolic PDEs casted in a weak formulation (see [75, Chapter 11, Theorem 11.1.1]).

That being said, since $\mathbb{H}^1(\Omega)$ is a separable Hilbert space it admits a complete orthonormal basis $\{\phi_j\}_{j \geq 1}$. Define then:

$$V^N := \mathrm{span}\{\phi_1, \ldots, \phi_N\} \ . \tag{3.69}$$

Substitute the PDE appearing in (3.58-3.61) with the approximate problem:

$$\frac{d}{dt}(T^N,v)+a(T^N,v)+\hat{\alpha}(T^N,v)_{\partial\Omega}-\sum_{k=1}^{K}p_k^N(\mathbf{1}_{\Omega_k},v)-\hat{\alpha}(g,v)_{\partial\Omega}=0 \quad \forall v\in V^N, \tag{3.70}$$

where $N \geq K$ in order to fullfill the constraints imposed by (3.60). Writing:

$$T^N(\mathbf{x},t) := \sum_{s=1}^{N} c_s^N(t)\phi_s(\mathbf{x}) \ , \tag{3.71}$$

then (3.70) results to be equivalent to:

$$M\frac{d\mathbf{c}^N}{dt}+A\mathbf{c}^N-B\mathbf{p}^N-\mathbf{F}^N(t)=0 \ . \tag{3.72}$$

where the stiffness and mass matrices are defined as:

$$\begin{aligned} M &\in \mathbb{R}^{N\times N} \quad \text{with} \quad \left[M_{ij}\right] := [(\phi_i,\phi_j)] \ , \\ A &\in \mathbb{R}^{N\times N} \quad \text{with} \quad [A_{ij}] := [a(\phi_j,\phi_i)+\hat{\alpha}(\phi_j,\phi_i)_{\partial\Omega}] \ , \\ B &\in \mathbb{R}^{N\times K} \quad \text{with} \quad [B_{ij}] := [(\mathbf{1}_{\Omega_k},\phi_i)] \ , \end{aligned} \tag{3.73}$$

while the known vector $\mathbf{F}^N$ reads:

$$\mathbf{F}^N \in \left[\mathbb{C}^0[0,\mathrm{t}_1]\right]^N \quad \text{with} \quad [F_i^N] := [\hat{\alpha}(g,\phi_i)_{\partial\Omega}] \ . \tag{3.74}$$

Finally the unknown vectors in (3.72) are:

$$\begin{aligned} \mathbf{p}^N(t) &:= [p_1^N(t),\dots,p_K^N(t)]^T \ , \\ \mathbf{c}^N(t) &:= [c_1^N(t),\dots,c_N^N(t)]^T \ . \end{aligned} \tag{3.75}$$

Similarly it is possible to substitute (3.71) in (3.60) and obtain the equivalent system:

$$\boldsymbol{\Omega}\boldsymbol{\theta}^N - B^T\mathbf{c}^N = 0 \ , \tag{3.76}$$

where:

$$\boldsymbol{\Omega} \in \mathbb{R}^{K\times K} \quad \text{with} \quad \boldsymbol{\Omega} := \mathrm{diag}(|\Omega_1|,\dots,|\Omega_K|) \ , \tag{3.77}$$

and:

$$\boldsymbol{\theta}^N(t) := [\theta_1^N(t),\dots,\theta_K^N(t)]^T \ . \tag{3.78}$$

Reformulating (3.59) in matrix notation:

$$\boldsymbol{\Omega}\mathbf{p}^N - \mathbf{W}(\boldsymbol{\theta}^N,\mathbf{e}^N) = 0 \ , \tag{3.79}$$

with:

$$\boldsymbol{W}(\boldsymbol{\theta}^N,\mathbf{e}^N) := [W_1(\boldsymbol{\theta}^N,\mathbf{e}^N),\dots,W_K(\boldsymbol{\theta}^N,\mathbf{e}^N)]^T \ , \tag{3.80}$$

it is possible to write the DAE system approximating (3.58-3.61) as:

$$\begin{aligned}
A_C\frac{d\mathbf{q}^N}{dt} + A_R\mathbf{r}(A_R^T\mathbf{e}^N,\boldsymbol{\theta}^N) + A_L\mathbf{i}_L^N + A_V\mathbf{i}_V^N + A_I\mathbf{i}(A_C^T\mathbf{e}^N,\boldsymbol{\theta}^N) &= 0\ ,\\
\frac{d\boldsymbol{\phi}^N}{dt} - A_L^T\mathbf{e}^N &= 0\ ,\\
A_V^T\mathbf{e}^N - \mathbf{V}(t) &= 0\ ,\\
\mathbf{q}^N - \mathbf{q}_C(A_C^T\mathbf{e}^N) &= 0\ ,\\
\boldsymbol{\phi}^N - \boldsymbol{\phi}_L(\mathbf{i}_L^N) &= 0\ ,\\
\boldsymbol{\Omega}\mathbf{p}^N - \mathbf{W}(\boldsymbol{\theta}^N,\mathbf{e}^N) &= 0\ ,\\
\boldsymbol{\Omega}\boldsymbol{\theta}^N - B^T\mathbf{c}^N &= 0\ ,\\
M\frac{d\mathbf{c}^N}{dt} + A\mathbf{c}^N - B\mathbf{p}^N - \mathbf{F}^N(t) &= 0\ .
\end{aligned} \tag{3.81}$$

Notice that M can be inverted as it is positive definite. Thus (3.72) defines an explicit differential equation for the variable $\mathbf{c}^N$:

$$\frac{d\mathbf{c}^N}{dt} = -M^{-1}\left[A\mathbf{c}^N - B\mathbf{p}^N - \mathbf{F}^N(t)\right]\ . \tag{3.82}$$

From (3.76) it holds:

$$\boldsymbol{\theta}^N \quad = \quad \boldsymbol{\Omega}^{-1}B^T\mathbf{c}^N\ , \tag{3.83}$$

due to the regularity of $\boldsymbol{\Omega}$. Differentiating (3.83) and taking into account (3.82) the following explicit differential equation is obtained for $\boldsymbol{\theta}^N$:

$$\frac{d\boldsymbol{\theta}^N}{dt} = \boldsymbol{\Omega}^{-1}B^T\frac{d\mathbf{c}^N}{dt} = -\boldsymbol{\Omega}^{-1}B^TM^{-1}\left[A\mathbf{c}^N - B\mathbf{p}^N - \mathbf{F}^N(t)\right]\ . \tag{3.84}$$

Substituting (3.83) into (3.58) reads:

$$\begin{aligned}
A_C\frac{d\mathbf{q}}{dt} + A_R\hat{\mathbf{r}}(A_R^T\mathbf{e},\mathbf{c}^N) + A_L\mathbf{i}_L + A_V\mathbf{i}_V + A_I\hat{\mathbf{i}}(A_C^T\mathbf{e},\mathbf{c}^N) &= 0,\\
\frac{d\boldsymbol{\phi}}{dt} - A_L^T\mathbf{e} &= 0,\\
A_V^T\mathbf{e} - \mathbf{V}(t) &= 0,\\
\mathbf{q} - \mathbf{q}_C(A_C^T\mathbf{e}) &= 0,\\
\boldsymbol{\phi} - \boldsymbol{\phi}_L(\mathbf{i}_L) &= 0,
\end{aligned} \tag{3.85}$$

where:

$$\begin{aligned}
\hat{\mathbf{r}}(A_R^T\mathbf{e},\mathbf{c}^N) &:= \mathbf{r}(A_R^T\mathbf{e},\boldsymbol{\Omega}^{-1}B^T\mathbf{c}^N)\ ,\\
\hat{\mathbf{i}}(A_C^T\mathbf{e},\mathbf{c}^N) &:= \mathbf{i}(A_C^T\mathbf{e},\boldsymbol{\Omega}^{-1}B^T\mathbf{c}^N)\ .
\end{aligned}$$

The assumptions on the electrical part of the system ensure that only one differentiation of (3.85) is needed to derive, through appropriate algebraic manipulations, a set of explicit differential equations for the variables $\mathbf{e}$, $\mathbf{q}$, $\boldsymbol{\phi}$, $\mathbf{i}_L$ and $\mathbf{i}_V$. Finally from (3.79) it stems:

$$\mathbf{p}^N = \boldsymbol{\Omega}^{-1}\mathbf{W}(\boldsymbol{\theta}^N, \mathbf{e}^N) \ .$$

Even here only one differentiation is necessary to derive an explicit differential equation for $\mathbf{p}^N$. The index of system (3.81) results then to be one.

Defining the orthogonal projection:

$$P_N : \mathbb{L}^2(\Omega) \to V^N \ , \tag{3.86}$$

it is possible to derive a set of consistent initial conditions for (3.81). In fact, it just suffices to define the initial conditions for the approximate problem (3.70) as:

$$T_0^N := P_N(T_0) \ , \tag{3.87}$$

and proceed as done in the original PDAE system. Notice that the initial condition for system (3.72) equivalent to (3.87) is given by the solution of the linear system:

$$(M\mathbf{c}^N(0))_j = (T_0, \phi_j) \qquad j = 1, \ldots, N \ . \tag{3.88}$$

As consistent initial conditions have been obtained, then (3.81) admits a unique global solution [45].

To proceed with the Faedo-Galerkin method it is necessary at this point to recover, for all the variables in (3.81), upper bounds in $\mathbb{L}^2(0, \mathrm{t}_1)$ that are independent of N. These bounds will be employed afterwards to pass to the weak-limit $N \to \infty$ and determine then a solution to the initial PDAE system. Due to the hypothesis made on the boundedness of $|W_k(\cdot, \cdot)|$ it is convenient to start from the thermal part of the network, noticing that:

$$\begin{aligned} p_k^N &\in \mathbb{C}^0[0, \mathrm{t}_1] \subset \mathbb{L}^2(0, \mathrm{t}_1) \quad k = 1, \ldots, K, \\ c_k^N &\in \mathbb{C}^1[0, \mathrm{t}_1] \subset \mathbb{H}^1(0, \mathrm{t}_1) \quad k = 1, \ldots, K, \end{aligned}$$

hold, from which it follows naturally:

$$T^N \in \mathbb{H}^1\left((0, \mathrm{t}_1), \mathbb{H}^1(\Omega)\right) \ . \tag{3.89}$$

Choosing T^N as a test function in (3.70) gives:

$$\left(\frac{d}{dt}T^N, T^N\right) + a(T^N, T^N) + \hat{\alpha}(T^N, T^N)_{\partial\Omega} = \sum_{k=1}^{K} p_k^N(\mathbf{1}_{\Omega_k}, T^N) + \hat{\alpha}(g, T^N)_{\partial\Omega} \ . \tag{3.90}$$

Exploiting the coercivity of the bilinear form it is possible to obtain:

$$\frac{1}{2}\frac{d}{dt}\left\|T^N\right\|^2_{\mathbb{L}^2(\Omega)} + \eta\left\|T^N\right\|^2_{\mathbb{H}^1(\Omega)} \leq \left(\frac{d}{dt}T^N, T^N\right) + a(T^N, T^N) + \hat{\alpha}(T^N, T^N)_{\partial\Omega} \ , \tag{3.91}$$

while from the continuity of the right hand side in (3.90) and the hypothesis on the boundedness of $|W_k(\mathbf{e},\boldsymbol{\theta})|$ $(k=1,\dots,K)$ follows:

$$\sum_{k=1}^{K} p_k^N(\mathbf{1}_{\Omega_k},T^N)+\hat{\alpha}(g,T^N)_{\partial\Omega} \leq \left(C_{\mathbf{W}}\sum_{k=1}^{K}\sqrt{|\Omega_k|}+\hat{\alpha}\,\|g(t)\|_{\mathbb{L}^2(\partial\Omega)}\right)\left\|T^N(t)\right\|_{\mathbb{L}^2(\Omega)} \ . \tag{3.92}$$

Defining:

$$S(C_{\mathbf{W}},\hat{\alpha},\Omega_k,g) := C_{\mathbf{W}}\sum_{k=1}^{K}\sqrt{|\Omega_k|}+\hat{\alpha}\,\|g(t)\|_{\mathbb{L}^2(\partial\Omega)} \tag{3.93}$$

and combining (3.91) with (3.92) it is possible to obtain:

$$\frac{1}{2}\frac{d}{dt}\left\|T^N(t)\right\|^2_{\mathbb{L}^2(\Omega)}+\eta\left\|T^N(t)\right\|^2_{\mathbb{H}^1(\Omega)} \leq S(C_{\mathbf{W}},\hat{\alpha},\Omega_k,g)\left\|T^N(t)\right\|_{\mathbb{L}^2(\Omega)} \ . \tag{3.94}$$

Integrating over $(0,t)$ with $t\in(0,\mathrm{t}_1)$, employing Young's inequality and taking into account that:

$$\|T_0^N\|_{\mathbb{L}^2(\Omega)} \leq \|T_0\|_{\mathbb{L}^2(\Omega)} \ , \tag{3.95}$$

as T_0^N is a projection of T_0 onto a finite dimensional space, it follows then:

$$\left\|T^N(t)\right\|^2_{\mathbb{L}^2(\Omega)}+\eta\int_0^t\left\|T^N(\tau)\right\|^2_{\mathbb{H}^1(\Omega)}d\tau \leq \|T_0\|^2_{\mathbb{L}^2(\Omega)}+\frac{1}{\eta}\int_0^t S^2 d\tau \ . \tag{3.96}$$

The sequence T^N is thus bounded in $\mathbb{L}^2\left((0,\mathrm{t}_1),\mathbb{H}^1(\Omega)\right)\cap\mathbb{L}^\infty\left((0,\mathrm{t}_1),\mathbb{L}^2(\Omega)\right)$ and from (3.59) it is trivial to infer that also $\mathbf{p}^N$ is bounded in the $\mathbb{L}^2(0,\mathrm{t}_1)$ sense. From (3.60) it is possible to obtain, after some algebra:

$$|\theta_k^N(t)|^2 \leq \frac{1}{|\Omega_k|^2}\|T^N(t)\|^2_{\mathbb{L}^2(\Omega)} \quad k=1,\dots,K,$$

and derive an upper bound in $\mathbb{L}^2(0,\mathrm{t}_1)$ for $\boldsymbol{\theta}^N$ by means of (3.96):

$$|\theta_k^N(t)|^2 \leq \frac{1}{|\Omega_k|^2}\left[\|T_0\|^2_{\mathbb{L}^2(\Omega)}+\frac{1}{\eta}\int_0^{\mathrm{t}_1}S^2d\tau\right] \quad k=1,\dots,K. \tag{3.97}$$

Also this bound does not depend on N. It is now possible to define:

$$C_{\boldsymbol{\theta}} := \max_{k=1,\dots,K}\left(\frac{1}{|\Omega_k|^2}\left[\|T_0\|^2_{\mathbb{L}^2(\Omega)}+\frac{1}{\eta}\int_0^{\mathrm{t}_1}S^2d\tau\right]\right) ,$$

and then:

$$\mathcal{G} := \left\{\mathbf{s}\in\mathbb{R}^K : |s| \leq \sqrt{C_{\boldsymbol{\theta}}}\right\} \ .$$

As $\mathcal{G}$ does not depend on N and fulfills condition (3.64) then the bound on the variables of the electrical part is derived from (3.63). Notice that this is possible in this framework due to the index-1 hypothesis made on (3.58). Finally, due to the continuity of the non-linear functions in (3.81) also the terms:

$$\begin{array}{rclcrclc} \mathbf{r}^N & := & \mathbf{r}(A_R^T\mathbf{e}^N, \boldsymbol{\theta}^N) & , & \mathbf{i}^N & := & \mathbf{i}(A_C^T\mathbf{e}^N, \boldsymbol{\theta}^N) & , \\ \mathbf{q}_C^N & := & \mathbf{q}_C(A_C^T\mathbf{e}^N) & , & \boldsymbol{\phi}_L^N & := & \boldsymbol{\phi}_L(\mathbf{i}_L^N) & , \\ \mathbf{W}^N & := & \mathbf{W}(\boldsymbol{\theta}^N, \mathbf{e}^N) & , & & & & \end{array}$$

are bounded in the $\mathbb{L}^2(0, \mathrm{t}_1)$ norm by a constant that is independent of N. At this point upper bounds for every entity in (3.81) have been determined. Hence it is possible to select a subsequence (still denoted with the N super-script) in which (see e.g. [60]):

- T^N converges in the weak* topology of $\mathbb{L}^\infty\left((0, \mathrm{t}_1), \mathbb{L}^2(\Omega)\right)$,
- T^N converges weakly in $\mathbb{L}^2\left((0, \mathrm{t}_1), \mathbb{H}^1(\Omega)\right)$,
- $\mathbf{e}^N$, $\mathbf{i}_L^N$, $\mathbf{q}^N$, $\boldsymbol{\phi}^N$, $\mathbf{i}_V^N$, $\mathbf{p}^N$ and $\boldsymbol{\theta}^N$ converge weakly in the $\mathbb{L}^2(0, \mathrm{t}_1)$ sense,
- $\mathbf{r}^N$, $\mathbf{i}^N$, $\mathbf{q}_C^N$, $\boldsymbol{\phi}_L^N$ and $\mathbf{W}^N$ converge weakly in the $\mathbb{L}^2(0, \mathrm{t}_1)$ sense.

Anyhow, to exploit weak convergence properties in order to construct a solution to the original PDAE system it is still necessary to prove that:

$$\begin{array}{rclcrclc} \mathbf{r}^N & \rightharpoonup & \mathbf{r}(A_R^T\mathbf{e}, \boldsymbol{\theta}) & , & \mathbf{i}^N & \rightharpoonup & \mathbf{i}(A_C^T\mathbf{e}, \boldsymbol{\theta}) & , \\ \mathbf{q}_C^N & \rightharpoonup & \mathbf{q}_C(A_C^T\mathbf{e}) & , & \boldsymbol{\phi}_L^N & \rightharpoonup & \boldsymbol{\phi}_L(\mathbf{i}_L) & , \\ \mathbf{W}^N & \rightharpoonup & \mathbf{W}(\boldsymbol{\theta}, \mathbf{e}) & , & & & & \end{array}$$

when:

$$\mathbf{e}^N \rightharpoonup \mathbf{e} \quad , \quad \mathbf{i}_L^N \rightharpoonup \mathbf{i}_L \quad , \quad \boldsymbol{\theta}^N \rightharpoonup \boldsymbol{\theta} \quad .$$

This will be shown in the following taking advantage of regularity results that hold for the PDE part of this system. Indeed it will turn out that the convergence of the DAE part of (3.58-3.61) is to be intended at least pointwise.

Let us start then multiplying the first term at the left hand side in (3.70) by:

$$\Psi \in \mathbb{C}^1([0, \mathrm{t}_1]) \ , \ \Psi(\mathrm{t}_1) = 0 \ ,$$

and integrating by parts ($j = 1, \ldots, N$):

$$\int_0^{\mathrm{t}_1} \left(\frac{dT^N}{dt}(\tau), \phi_j \right) \Psi(\tau) d\tau = - \int_0^{\mathrm{t}_1} \left(T^N(\tau), \phi_j \right) \frac{d\Psi}{dt}(\tau) d\tau - (T_0^N, \phi_j)\Psi(0) \ . \quad (3.98)$$

Passing to the limit in (3.70), choosing an arbitrary $N_0 \geq K$ and recalling that T_0^N

converges in $\mathbb{L}^2(\Omega)$ to T_0 while p_k^N converges in $\mathbb{L}^2(0,\mathrm{t}_1)$ to p_k, it is finally obtained:

$$\begin{aligned} -\int_0^{\mathrm{t}_1}(T(\tau),\phi_j)\,\frac{d\Psi}{dt}(\tau)d\tau &- (T_0,\phi_j)\Psi(0)+\int_0^{\mathrm{t}_1}a(T,\phi_j)\Psi(\tau)d\tau \\ +\int_0^{\mathrm{t}_1}\hat{\alpha}(T(\tau),\phi_j)_{\partial\Omega}\Psi(\tau)d\tau &= \int_0^{\mathrm{t}_1}\sum_{k=1}^{K}p_k(\mathbf{1}_{\Omega_k},\phi_j)\Psi(\tau)d\tau \\ +\int_0^{\mathrm{t}_1}\hat{\alpha}(g,\phi_j)_{\partial\Omega}\Psi(\tau)d\tau & \qquad j=1,\ldots,N_0. \end{aligned} \tag{3.99}$$

Since the linear combinations of ϕ_j are dense in $\mathbb{H}^1(\Omega)$, then (3.99) can be written equivalently testing on each $v\in\mathbb{H}^1(\Omega)$. Thus, following the reasoning in [75, Chapter11, pag.368]:

$$T(\mathbf{x},t)\in\mathbb{L}^2\left((0,\mathrm{t}_1),\mathbb{H}^1(\Omega)\right)\cap\mathbb{L}^\infty\left((0,\mathrm{t}_1),\mathbb{L}^2(\Omega)\right)\ , \tag{3.100}$$

fullfills (3.61) with p_k $(k=1,\ldots,K)$ as source terms. From (3.100) it follows also:

$$T(\mathbf{x},t)\in\mathbb{L}^2\left((0,\mathrm{t}_1),\mathbb{H}^1(\Omega)\right)\cap\mathbb{H}^1\left((0,\mathrm{t}_1),\mathbb{H}^{-1}(\Omega)\right)\ , \tag{3.101}$$

and using the arguments in [75, Chapter 11, pag.369] and [68, pag.23]:

$$T\in\mathbb{C}^0\left([0,\mathrm{t}_1],\mathbb{L}^2(\Omega)\right)\quad,\quad\frac{\partial T}{\partial t}\in\mathbb{L}^2\left((0,\mathrm{t}_1),\mathbb{H}^{-1}(\Omega)\right)\ . \tag{3.102}$$

Define:

$$\Delta T^N(t):=T^N(t)-T(t)\quad,\quad\Delta p_k^N(t):=p_k^N(t)-p_k(t)\ .$$

Subtracting (3.61) from (3.70) and choosing $\Delta T^N(t)$ as a test function reads:

$$\frac{1}{2}\frac{d}{dt}\|\Delta T^N\|^2_{\mathbb{L}^2(\Omega)}+a(\Delta T^N,\Delta T^N)+\hat{\alpha}\|\Delta T^N\|^2_{\mathbb{L}^2(\partial\Omega)}=\sum_{k=1}^{K}\Delta p_k^N(\mathbf{1}_{\Omega_k},\Delta T^N)\ .$$

Integrating over $(0,t)$ and exploiting the coercivity of the bilinear form it is then possible to obtain the following inequality:

$$\left\|\Delta T^N(t)\right\|^2_{\mathbb{L}^2(\Omega)}\le\Delta K^N(t)\xrightarrow{N\to\infty}0\ , \tag{3.103}$$

with:

$$\Delta K^N(t):=\left\|\Delta T^N(0)\right\|^2_{\mathbb{L}^2(\Omega)}+2\sum_{k=1}^{K}\left[\int_0^t\Delta p_k^N(\tau)(\mathbf{1}_{\Omega_k},\Delta T^N(\tau))d\tau\right]\ .$$

As both sides of (3.103) are continuous, this inequality holds also in the form:

$$\max_{t\in[0,\mathrm{t}_1]}\left\|\Delta T^N(t)\right\|^2_{\mathbb{L}^2(\Omega)}\le\max_{t\in[0,\mathrm{t}_1]}\Delta K^N(t)\xrightarrow{N\to\infty}0\ .$$

Introducing $\Delta\theta_k^N := \theta_k^N(t) - \theta_k(t)$ and noticing that:

$$\max_{t\in[0,\mathrm{t}_1]} |\Delta\theta_k^N(t)|^2 \leq \frac{1}{|\Omega_k|^2} \max_{t\in[0,\mathrm{t}_1]} \left\|\Delta T^N(t)\right\|^2_{\mathbb{L}^2(\Omega)} \qquad k = 1, \ldots, K,$$

it follows that the convergence of $\boldsymbol{\theta}^N$ to $\boldsymbol{\theta}$ is not only weak, but uniform. Then, due to the stability properties of (3.58) the electrical variables also converge to their limit uniformly and not only weakly. In particular it can be inferred that:

- $P_C\mathbf{e}$, $\mathbf{i}_L$, $\mathbf{q}$ and $\boldsymbol{\phi}$ are differentiable,
- $Q_C\mathbf{e}$ and $\mathbf{i}_V$ are continuous.

As at this point $\mathbf{e}$ and $\boldsymbol{\theta}$ are known to be continuous, then it follows that $\mathbf{W}^N$ converges to $\mathbf{W}$ pointwise and thus $\mathbf{p}$ is also continuous.

Finally it remains to show that $T(\mathbf{x}, 0) = T_0(\mathbf{x})$ in order to prove that the constructed solution actually solves the initial value problem prescribed in the beginning. Multiplying (3.61) by:

$$\Psi \in \mathbb{C}^1([0, \mathrm{t}_1]) \ , \ \Psi(\mathrm{t}_1) = 0 \ ,$$

and integrating by parts it follows:

$$\begin{aligned} -\int_0^{\mathrm{t}_1} (T(\tau), v) \frac{d\Psi}{dt}(\tau) d\tau &- (T(0), v)\Psi(0) + \int_0^{\mathrm{t}_1} a(T, v)\Psi(\tau) d\tau \\ +\int_0^{\mathrm{t}_1} \hat{\alpha}(T(\tau), v)_{\partial\Omega}\Psi(\tau) d\tau &= \int_0^{\mathrm{t}_1} \sum_{k=1}^{K} p_k(\mathbf{1}_{\Omega_k}, v)\Psi(\tau) d\tau \\ +\int_0^{\mathrm{t}_1} \hat{\alpha}(g, v)_{\partial\Omega}\Psi(\tau) d\tau & \qquad \forall v \in \mathbb{H}^1(\Omega), \end{aligned} \tag{3.104}$$

thus, taking $\Psi(0) = 1$:

$$(T(0) - T_0, v) = 0 \quad \forall v \in \mathbb{H}^1(\Omega) \ . \tag{3.105}$$

This implies $T(\mathbf{x}, 0) = T_0(\mathbf{x})$, and proves the existence and uniqueness of a solution to a prescribed initial value problem for system (3.58-3.61).

□

Chapter summary In this chapter the well-posedness of the thermal element model established in Part I has been addressed. The results on the elliptic problem validate a possible implementation of the thermal element in admittance or conductance form, while the ones on the parabolic problem ensure the well-posedness of the model before a suitable time discretization has been adopted. Finally existence and uniqueness of a solution to the whole PDAE system has been proved in the case of an index 1 electrical network. This provides a sound theoretical basis to the solution approach that will be presented in Part III.

Part III

Numerical Discretization

4

Patched mesh method

As seen in Chapter 1 thermal effects at the system level occur at largely different space scales. Thus, in order to be effectively employed, the thermal element presented in Chapter 2 requires to be space-discretized by a method that efficiently handles the treatment of multiscale issues.

In the current chapter an approach of such a kind, included among the Galerkin-type approximations and regardable as a "patched" finite element method, is introduced. In Section 4.1 the definition of an appropriate patched space is therefore given, together with some interpolation estimates. Then in Section 4.2 the approximation of a model diffusion-reaction PDE is treated. Even though for the sake of simplicity a case with only one patch domain is used, all the major merits and flaws of the method are clearly underlined. Furthermore a direct and iterative procedure to the solution of the discrete problem as well as their algebraic structure are presented. Finally, the interested reader will find in Appendix D an extension of this patched method devised to resolve layers in the case of reaction-dominant PDEs. [1] Though belonging to the class of Shishkin-mesh approach, this extension overcomes the difficulty of generating a structured conforming mesh for general domain geometries employing instead overlapping grids. A model 1D problem is used to introduce the novel method and analyze it in details and then a sound extension to 2D case and complex geometries is provided together with an illustrative example.

4.1 Patched space definition and interpolation estimates

The aim of this section is to introduce a particular finite element space that allows for the discretization of diffusion-reaction PDEs on unstructured, overlapping, non-nested grids and provide then a generalization of the usual a-priori estimates. As it will be seen in Chapter 5 this will be the method of choice to space-discretize the PDE appearing in the constitutive relations of the thermal element presented in Chapter 2. Notice that the *patched finite element space* was firstly proposed by Wagner et al. in [40, 41, 76, 77, 96] and is in this thesis generalized to account for an arbitrary hierarchical structure of the patched domains. The aim of this extension is to follow closely the current trend towards the hierarchical design of ICs [83], associating each *functional unity* with a grid that gets coarser or finer depending on the "depth level" of the functional unity itself in the design hierarchy.

---

[1] The choice to present this extension in an appendix chapter stems from the fact that, though theoretically usable to space discretize the thermal element defined in Chapter 2, no numerical example employing this method will be presented in Part IV.

Triangulation, triangular finite element spaces, projection operators To begin with, some basic notions that constitute the core of the patches of finite element approach are gathered in the following. The first one, i.e. the definition of a triangulation over a polygonal domain, is peculiar to every finite element method:

Definition 4.1 (Triangulation)**.** *Assume* $\Omega \subset \mathbb{R}^d$ *(*$d = 2, 3$*) to be a polygonal domain and* $h \in \mathbb{R}^+$*. Then* $\mathcal{T}_\mathrm{h} = \{K_1, K_2, \ldots\}$ *is said to be a triangulation of* $\bar{\Omega}$ *if:*

$$\bar{\Omega} = \bigcup_{K \in \mathcal{T}_\mathrm{h}} K, \tag{4.1}$$

and furthermore each $K \in \mathcal{T}_\mathrm{h}$ *satisfies the following properties:*

1. K *is a triangle (*$d = 2$*) or a tetrahedron (*$d = 3$*) with* $\mathtt{int}(K) \neq \emptyset$*,*
2. $\mathtt{int}(K_i) \cap \mathtt{int}(K_j) = \emptyset$*,* $\forall K_i \neq K_j \in \mathcal{T}_\mathrm{h}$*,*
3. *If* $S = K_i \cap K_j \neq \emptyset$*, then* S *is a common face, side or vertex of* K_i *and* K_j*,*
4. $\mathtt{diam}(K) < h$*,* $\forall K \in \mathcal{T}_\mathrm{h}$*.*

Definition 4.2 (Regular triangulation)**.** *Define:*

$$h_K := \mathtt{diam}(K) \quad , \quad \rho_K := \sup \mathtt{diam}(S_K), \tag{4.2}$$

where S_K *is a ball contained in* K*. Then a family of triangulations* $\{\mathcal{T}_\mathrm{h}\}_{h>0}$*, is called regular if* $\exists\ \varepsilon \geq 1$ *such that:*

$$\max_{K \in \mathcal{T}_\mathrm{h}} \frac{h_K}{\rho_K} \leq \varepsilon \qquad \forall h > 0. \tag{4.3}$$

Starting from the triangulation $\mathcal{T}_\mathrm{h}$ it is then possible to determine a class of *finite dimensional* spaces (usually referred to as *triangular finite element spaces*) which result in a piecewise-polynomial approximation of $\mathbb{H}^1(\Omega)$ and $\mathbb{H}^1_0(\Omega)$:

$$\begin{aligned} X_h^s(\Omega) &:= \left\{ w_h \in \mathbb{C}^0(\bar{\Omega}),\ \text{such that } w_h|_K \in \mathbb{P}_s\ \forall K \in \mathcal{T}_\mathrm{h} \right\} &\subset\ \mathbb{H}^1(\Omega), \\ Z_h^s(\Omega) &:= \{ w_h \in X_h^s(\Omega),\ \text{such that } w_h|_{\partial\Omega} = 0 \} &\subset\ \mathbb{H}^1_0(\Omega), \end{aligned} \tag{4.4}$$

where $\mathbb{P}_s$ denotes the space of polynomials of degree less than or equal to $s \geq 1$. The reader interested in a broad treatment of this subject is referred to [110], where finite element classes other than triangular are also introduced. Finally it can be noticed that, as $X^s_h(\Omega)$ is a closed subspace of $\mathbb{H}^1(\Omega)$ and $\mathbb{L}^2(\Omega)$, it is possible to define the following orthogonal projection operators [75, Chapter 3]:

$$\begin{aligned} P^s_{0,h} &: \mathbb{L}^2(\Omega) \rightarrow X^s_h(\Omega), \\ P^s_{1,h} &: \mathbb{H}^1(\Omega) \rightarrow X^s_h(\Omega). \end{aligned} \tag{4.5}$$

Patched space definition Making use of the concept of triangulation and of the definitions (4.4) of triangular finite element, it is now possible to rigorously define a *patched finite element space*. As already anticipated, this space is constructed upon a set of overlapping, possibly non-nested triangulations. It is therefore necessary to properly define the set of polygonal domains from which these triangulations are stemming.

Definition 4.3 (Set of hierarchical families of domains)**.** *Assume* $\Omega \subset \mathbb{R}^d$ *(*$d = 2, 3$*) to be a polygonal domain. Consider the following families of polygonal domains:*

$$\begin{aligned} \Upsilon_0 &= \{\Omega^0_1\}\ , \\ \Upsilon_1 &= \{\Omega^1_1, \dots, \Omega^1_{N_1}\}\ , \\ &\dots \\ \Upsilon_m &= \{\Omega^m_1, \dots, \Omega^m_{N_m}\}\ , \\ &\dots \\ \Upsilon_M &= \{\Omega^M_1, \dots, \Omega^M_{N_M}\}\ . \end{aligned} \tag{4.6}$$

The overall set:

$$\Xi := \{\Upsilon_0, \Upsilon_1, \dots, \Upsilon_m, \dots, \Upsilon_M\}\ , \tag{4.7}$$

is defined to be the set of hierarchical families of domains. In (4.7)*:*

$$m \in (0, \dots, M), \tag{4.8}$$

is the index identifying each family, while $(M + 1)$ *is the number of families. The following properties are required:*

1. *For* $m = 0$ *it must be* $N_0 = 1$ *and* $\Omega^0_1 \equiv \Omega$.
2. *For* $m = 0, \dots, M$ *then:*

$$\texttt{int}(\Omega^m_k) \neq \emptyset \quad k = 1, \dots, N_m\ . \tag{4.9}$$

3. *For* $m = 1, \dots, M$ *then:*

$$\bar{\Omega}^m_k \cap \bar{\Omega}^m_j = \emptyset \quad \forall k \neq j \in (1, \dots, N_m)\ . \tag{4.10}$$

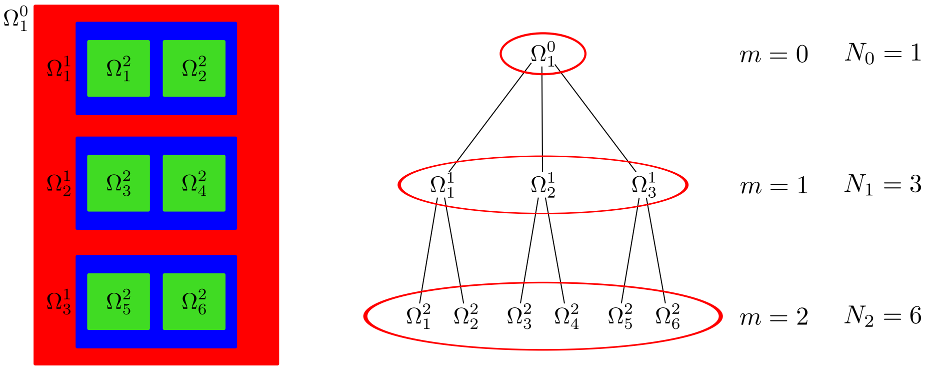
Ω_1^0
Ω_1^1
Ω_1^2
Ω_2^2
Ω_2^1
Ω_3^2
Ω_4^2
Ω_3^1
Ω_5^2
Ω_6^2
Ω_1^0
$m = 0$
$N_0 = 1$
Ω_1^1
Ω_2^1
Ω_3^1
$m = 1$
$N_1 = 3$
Ω_1^2
Ω_2^2
Ω_3^2
Ω_4^2
Ω_5^2
Ω_6^2
$m = 2$
$N_2 = 6$

Figure (4.1): *Example of a possible set of hierarchical domains (left) and of the associated tree structure (right). The three families of domains are circled in red. Notice that the domains are all rectangles and overlap with each other.*

4. For $m = 1, \ldots, M$ then:

$$\exists!\ j \quad : \quad \bar{\Omega}_k^m \subset \texttt{int}(\Omega_j^{m-1}) \quad \forall k \in (1, \ldots, N_m)\ . \tag{4.11}$$

The polygonal domains Ω_k^m introduced in Definition 4.3 are feasible to be organized in a hierarchical tree structure, as shown in Figure 4.1. With this respect the index m represents a sort of *depth* index. Roughly speaking this index is often associated in the application to an increasing demand of accuracy so that the greater the index m is, the more are the details required in the subsets $\Omega_k^m \subset \Omega$. Notice that due to (4.10) the closure of the domains inside the same family are required not to intersect with each other, while (4.11) states that the closure of each element of a given family should be a subset of one (and only one) element of the family coming before in the hierarchy. Furthermore from (4.11) it can be inferred that:

$$\bigcup_{m=1}^{M} \left(\bigcup_{k=1}^{N_m} \Omega_k^m \right) \neq \Omega\ . \tag{4.12}$$

Examples of possible structures violating these hypothesis are given in Figure 4.2. A space of patched finite element is then defined combining Definition 4.3 with the concepts introduced before.

Definition 4.4 (Patched finite element space)**.** *Consider Ξ as in Definition 4.3. Associate with each polygonal domain Ω_k^m a regular triangulation $\mathcal{T}_{\mathrm{h}}(m,k)$. The space of patched finite element is then defined as:*

$$V := X_h^s(\Omega_1^0)\ + \bigcup_{m=1}^{M} \left(\bigcup_{k=1}^{N_m} Y_h^s(\Omega_k^m) \right), \tag{4.13}$$

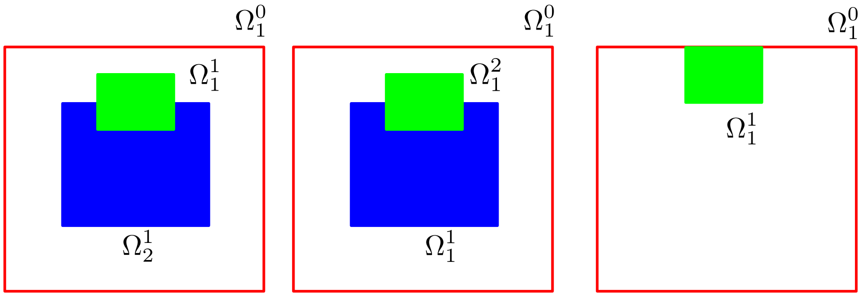

Figure (4.2): *Example of possible domains violating the hypothesis of Definition 4.3. On the left Ω_1^1 intersects with Ω_2^1, thus violating* (4.10)*, while in the center* (4.11) *is violated as $\Omega_1^2 \nsubseteq \Omega_1^1$. Finally on the right Ω_1^1 is not permitted to share part of its boundary with Ω_1^0 due to* (4.11)*.*

where:

$$Y_h^s(\Omega_k^m) := \left\{ w_h \in \mathbb{C}^0(\bar{\Omega}) : w_h|_{\Omega_k^m} \in Z_h^s(\Omega_k^m) \ , \ supp(w_h) \subseteq \Omega_k^m \right\} \ . \tag{4.14}$$

Definition 4.4 is slightly more general than the ones usually found in literature (e.g. in [77]), often restricted to a single level of patch domains ($M = 1$). Notice furthermore that the usual finite element space $X_h^s(\Omega)$ can be recovered setting $M = 0$. As a last remark, it should be stressed that the characteristic lengths h of the triangulations $\mathcal{T}_\mathrm{h}(m,k)$ and the polynomial degrees s of the corresponding finite element spaces depend on the indices m and k, that is to say:

$$h = h(m,k) \quad , \quad s = s(m,k) \ . \tag{4.15}$$

Nevertheless, to ease the notation, this dependence was hidden in (4.13). Finally an extension of the usual interpolation estimates to the case of hierarchical patches is given in the next:

Lemma 4.1 (Interpolation estimates)**.** *Consider a function $u \in \mathbb{H}^q(\Omega)$ with:*

$$q := \max_{m,k}(s) + 1 \ , \tag{4.16}$$

defined as:

$$u := \sum_{m=0}^{M} \left(\sum_{k=1}^{N_m} \tilde{u}_k^m \right) \ , \tag{4.17}$$

where $\tilde{u}_1^0 \in \mathbb{H}^q(\Omega_1^0)$, while $\tilde{u}_k^m|_{\Omega_k^m} \in \mathbb{H}_0^q(\Omega_k^m)$ and $supp(\tilde{u}_k^m) \subseteq \Omega_k^m$ for $m \geq 1$. Defining *the operators:* [2]

$$\begin{aligned} P_0(u) &:= \sum_{m=0}^{M}\left(\sum_{k=1}^{N_m} P^s_{0,h}\tilde{u}^m_k\right), \\ P_1(u) &:= \sum_{m=0}^{M}\left(\sum_{k=1}^{N_m} P^s_{1,h}\tilde{u}^m_k\right). \end{aligned} \tag{4.18}$$

then the following estimates hold:

$$\begin{aligned} \|u - P_0(u)\|_{\mathbb{L}^2(\Omega)} &\leq C\sum_{m=0}^{M}\left(\sum_{k=1}^{N_m} h^{s+1}(k,m)\,|\tilde{u}^m_k|_{\mathbb{H}^q(\Omega^m_k)}\right), \\ \|u - P_1(u)\|_{\mathbb{H}^1(\Omega)} &\leq C\sum_{m=0}^{M}\left(\sum_{k=1}^{N_m} h^{s}(k,m)\,|\tilde{u}^m_k|_{\mathbb{H}^q(\Omega^m_k)}\right), \end{aligned} \tag{4.19}$$

where $|\cdot|_{\mathbb{H}^q(\Omega^m_k)}$ *denotes the seminorm of* $\mathbb{H}^q(\Omega^m_k)$*.*

Proof. By construction it follows:

$$\begin{aligned} \|u - P_0(u)\|_{\mathbb{L}^2(\Omega)} &= \left\|\sum_{m=0}^{M}\left(\sum_{k=1}^{N_m}\tilde{u}^m_k\right) - \sum_{m=0}^{M}\left(\sum_{k=1}^{N_m} P^s_{0,h}\tilde{u}^m_k\right)\right\|_{\mathbb{L}^2(\Omega)} \\ &= \left\|\sum_{m=0}^{M}\left(\sum_{k=1}^{N_m}\tilde{u}^m_k - P^s_{0,h}\tilde{u}^m_k\right)\right\|_{\mathbb{L}^2(\Omega)} \\ &\leq \sum_{m=0}^{M}\left(\sum_{k=1}^{N_m}\|\tilde{u}^m_k - P^s_{0,h}\tilde{u}^m_k\|_{\mathbb{L}^2(\Omega)}\right) \\ &\leq C\sum_{m=0}^{M}\left(\sum_{k=1}^{N_m} h^{s+1}(k,m)\,|\tilde{u}^m_k|_{\mathbb{H}^q(\Omega^m_k)}\right), \end{aligned} \tag{4.20}$$

the last line stemming from standard interpolation results [75, Chapter 3]. Similar considerations hold true for $\|u - P_1(u)\|_{\mathbb{H}^1(\Omega)}$. □

4.2 Approximation of diffusion-reaction equations

In the following section an elliptic diffusion-reaction model problem will be approximated on a patched finite element space. For the sake of simplicity a case involving only one patch domain is considered. Pros and cons of the method as well as its abstract collocation and algebraic formulation are commented in details.

---

[2] To ease the notation $P^s_{0,h}\tilde{u}^m_k$ is intended as $P^s_{0,h}(\tilde{u}^m_k|_{\Omega^m_k})$

Elliptic model problem and abstract discrete formulation Consider the two families of domains:

$$\Upsilon_0 := \{\Omega_1^0 \equiv \Omega\} \quad , \quad \Upsilon_1 := \{\Omega_1^1\} \quad , \tag{4.21}$$

and the set Ξ as in Definition 4.3. Furthermore define an elliptic diffusion-reaction operator $\mathcal{L}$ and the associated conormal derivative as in Section 3.1. Then the model problem considered next reads:

$$\begin{cases} \mathcal{L}\, u(\mathbf{x}) &=& f_1(\mathbf{x}) + f_2(\mathbf{x}) & \text{in } \Omega_1^0 \equiv \Omega, \\ \dfrac{\partial u(\mathbf{x})}{\partial\, \mathbf{n}_{\mathcal{L}}} &=& \hat{\alpha}\big(u(\mathbf{x}) - g(\mathbf{x})\big) & \text{on } \partial\Omega_1^0 \equiv \partial\Omega, \end{cases} \tag{4.22}$$

where $\hat{\alpha}$ is a given constant and:

$$f_1, f_2 \in \mathbb{L}^2(\Omega_1^0) \quad , \quad \operatorname{supp}(f_2) \subseteq \Omega_1^1 \quad , \quad g \in \mathbb{L}^2(\partial\Omega_1^0) \quad . \tag{4.23}$$

Passing to the associated weak formulation, problem (4.22) asks for finding $u \in \mathbb{H}^1(\Omega_1^0)$ such that:

$$a(u,v) + \hat{\alpha}(u,v)_{\partial\Omega_1^0} = (f_1 + f_2, v) + \hat{\alpha}(g,v)_{\partial\Omega_1^0} \qquad \forall v \in \mathbb{H}^1(\Omega_1^0), \tag{4.24}$$

where the scalar products and bilinear form are defined in Section 3.1. Consider the patched finite element space:

$$V = X_H^s(\Omega_1^0) + Y_h^s(\Omega_1^1). \tag{4.25}$$

A *Galerkin* type approximation of (4.24) is obtained casting the problem on a finite dimensional subspace of $\mathbb{H}^1(\Omega_1^0)$ [75, Chapter 5]. In the case at hand this approximation asks for finding $u_{Hh} \in V$ such that:

$$a(u_{Hh}, v_{Hh}) + \hat{\alpha}(u_{Hh}, v_{Hh})_{\partial\Omega_1^0} = (f_1 + f_2, v_{Hh}) + \hat{\alpha}(g, v_{Hh})_{\partial\Omega_1^0} \qquad \forall v_{Hh} \in V. \tag{4.26}$$

Notice that the existence and uniqueness of a solution to this problem are directly inferred from Theorem 3.1. Furthermore the following a-priori estimate, known as *Céa lemma*, holds:

$$\|u - u_{Hh}\| \leq \frac{\gamma}{\eta} \inf_{v \in V} \|u - v\|, \tag{4.27}$$

where γ and η are respectively the continuity and coercivity constants of the bilinear form $a(\cdot,\cdot)$. Combining (4.27) with the interpolation estimates of the previous section it is possible to prove the convergence of the patches of finite element method and, under suitable assumptions, give an a-priori error estimates. This procedure was already performed in [96, Proposition 1.1] for the model problem considered in this section, involving a single patch.

In order to generalize it to account for the hierarchical structure devised in Definition 4.4 it will be necessary to resort to a partition of Ω into a set of non-overlapping subdomains. This partition can be easily obtained on the base of Definition 4.3 introducing the set of indices that identify the subsets of a generic element Ω_k^m:

$$\Delta_k^m := \begin{cases} \{j \in \{1, \dots, N_{m+1}\} \mid \Omega_j^{m+1} \subset \Omega_k^m\} & m = 0, \dots, M-1, \\ \emptyset & m = M. \end{cases} \tag{4.28}$$

Notice that it may happen Δ_k^m to be equal to the empty set even if $m \neq M$. Given Δ_k^m it is possible to define:

$$\Theta_k^m := \begin{cases} \bigcup_{j \in \Delta_k^m} \Omega_j^{m+1} & \text{if } \Delta_k^m \neq \emptyset \ , \\ \emptyset & \text{otherwise} \ , \end{cases} \tag{4.29}$$

to be the union of the subdomains contained in Ω_k^m and:

$$\Psi_k^m := \begin{cases} \Omega_k^m \setminus \bar{\Theta}_k^m & \text{if } \Theta_k^m \neq \emptyset \ , \\ \Omega_k^m & \text{otherwise} \ , \end{cases} \tag{4.30}$$

to be the complementary of Θ_k^m with respect to Ω_k^m. Notice that:

$$\{\Psi_k^m \ , \ m = 0, \dots, M \ ; k = 1, \dots, N_m\} \ ,$$

constitutes the searched partition of Ω. In the following:

$$\Gamma_k^m := \bar{\Theta}_k^m \cap \bar{\Psi}_k^m, \tag{4.31}$$

will denote the "internal" boundary of Ψ_k^m. Given these definitions it is then possible to provide the following:

Theorem 4.1 (A-priori error estimate)**.** *Denote* $u \in \mathbb{H}_0^1(\Omega)$ *to be the solution of the problem:*

$$a(u, v) = (f, v) \quad \forall v \in \mathbb{H}_0^1(\Omega), \tag{4.32}$$

where the bilinear form a *and the function* f *satisfy the requirements of Theorem 3.1. Consider* u_h *to be the corresponding approximation obtained on the patched space defined in* (4.13)*. Under these assumptions the patches of finite element method is convergent. If moreover the exact solution* $u \in \mathbb{H}^q(\Omega)$ *with:*

$$q := \max_{m,k}(s) + 1 \ , \tag{4.33}$$

then the following error estimate holds:

$$\|u - u_h\|_{\mathbb{H}^1(\Omega)} \leq C \sum_{m=0}^{M} \left(\sum_{k=1}^{N_m} h^s(k, m) \, \|u\|_{\mathbb{H}^q(\Psi_k^m)} \right) \ , \tag{4.34}$$

where the constant C *is independent of* u *and of the mesh characteristic lengths* $h(k, m)$*.*

Proof. Consider the partition of Ω defined in (4.30). As Γ_k^m is Lipschitz, Stein extension theorem [1] ensures the existence of a *bounded* extension operator:

$$E_k^m \; : \; \mathbb{H}^q(\Psi_k^m) \to \; \mathbb{H}^q(\Omega_k^m) \; , \tag{4.35}$$

for all $v \in \mathbb{H}^q(\Psi_k^m)$. Notice that $E_k^m(v)|_{\Gamma_k^m} = v|_{\Gamma_k^m}$ in the sense of traces. It is then possible to recursively define for each:

$$\begin{array}{rcl} m & = & 0, \dots, M, \\ k & = & 1, \dots, N_m, \end{array}$$

the function $\tilde{u}_k^m$ with $\operatorname{supp}(\tilde{u}_k^m) \subseteq \Omega_k^m$ as $\tilde{u}_k^m|_{\Omega_k^m} := E_k^m(\hat{u}_k^m|_{\Psi_k^m})$ if:

$$\left\| E_k^m(\hat{u}_k^m|_{\Psi_k^m}) \right\|_{\mathbb{H}^q(\Psi_j^n)} \leq \|\hat{u}_k^m\|_{\mathbb{H}^q(\Psi_j^n)} \qquad \begin{array}{rcl} \forall n & > & m \; , \\ \forall j & \text{in} & \text{the subtrees of } \Omega_k^m, \end{array} \tag{4.36}$$

and $\tilde{u}_k^m|_{\Omega_k^m} := \hat{u}_k^m|_{\Omega_k^m}$ otherwise, where:

$$\hat{u}_k^m := \begin{cases} u & \text{if } m = 0 \; , \\ u - \displaystyle\sum_{n<m} \left(\sum_{j=1}^{N_n} \tilde{u}_j^n \right) & \text{if } m \geq 1 \; . \end{cases} \tag{4.37}$$

It follows then by construction that:

$$u = \sum_{m=0}^{M} \left(\sum_{k=1}^{N_m} \tilde{u}_k^m \right) \; . \tag{4.38}$$

The (possibly non-unique) decomposition defined in (4.38) fullfills the requirements of Lemma 4.1 since $\tilde{u}_1^0 \in \mathbb{H}^q(\Omega_1^0)$ and $\tilde{u}_k^m|_{\Omega_k^m} \in \mathbb{H}_0^q(\Omega_k^m)$ for $m \geq 1$. Furthermore, it follows from the definition of $\tilde{u}_k^m$ and from the boundedness of E_k^m that:

$$\|\tilde{u}_k^m\|_{\mathbb{H}^q(\Omega_k^m)} \quad \leq \quad C \, \|u\|_{\mathbb{H}^q(\Psi_k^m)} \;\; , \tag{4.39}$$

where C is a generic constant independent of u. Introduce $\tilde{u}_h \in V$ to be the function defined as:

$$\tilde{u}_h := \sum_{m=0}^{M} \left(\sum_{k=1}^{N_m} P_{1,h}^s(\tilde{u}_k^m) \right) \; , \tag{4.40}$$

and set $v_h := u_h - \tilde{u}_h$. By the definition of *Galerkin method* it follows that:

$$a(u, v_h) = a(u_h, v_h) \; , \tag{4.41}$$

and combining (4.41) with the definition of $v_h \in V$ leads to:

$$a(v_h, v_h) = a(u - \tilde{u}_h, v_h) \; . \tag{4.42}$$

Employing the Cauchy -Schwarz inequality it is thus possible to state:

$$\|u_h - \tilde{u}_h\|_{\mathbb{H}^1(\Omega)} \leq \|u - \tilde{u}_h\|_{\mathbb{H}^1(\Omega)} \ , \tag{4.43}$$

deriving then the following relation:

$$\|u - u_h\|_{\mathbb{H}^1(\Omega)} \leq \|u - \tilde{u}_h\|_{\mathbb{H}^1(\Omega)} + \|u_h - \tilde{u}_h\|_{\mathbb{H}^1(\Omega)} \leq 2\,\|u - \tilde{u}_h\|_{\mathbb{H}^1(\Omega)} \ , \tag{4.44}$$

by an application of the triangle inequality. At this point it is possible to apply Lemma 4.1 to the right hand side of (4.44) obtaining:

$$\|u - u_h\|_{\mathbb{H}^1(\Omega)} \leq C \sum_{m=0}^{M} \left(\sum_{k=1}^{N_m} h^s(k,m)\, |\tilde{u}_k^m|_{\mathbb{H}^q(\Omega_k^m)} \right) . \tag{4.45}$$

Finally, substituting (4.39) into (4.45) gives:

$$\|u - u_h\|_{\mathbb{H}^1(\Omega)} \leq C \sum_{m=0}^{M} \left(\sum_{k=1}^{N_m} h^s(k,m)\, \|u\|_{\mathbb{H}^q(\Psi_k^m)} \right) . \tag{4.46}$$

□

Notice that the assumption to take into account in Theorem 4.1 a problem casted on $\mathbb{H}_0^1(\Omega)$ results not to be restrictive. In fact the error estimate can be extended to boundary conditions other than homogeneous Dirichlet ones employing standard functional analysis techniques [75, Chapter 6].

Returning to our model problem, the task to derive a closed system of algebraic equations from (4.26) requires a set of basis function for the finite dimensional space V to be constructed. Unfortunately this is generally far from being trivial. The difficulty lies in the fact that the sum appearing in Definition 4.4 may not be a direct sum: therefore in the case at hand it is not possible to construct a basis set for V merging the usual sets of basis function of $X_H^s(\Omega_1^0)$ and $Y_h^s(\Omega_1^1)$ as their elements may be linearly dependent. A thorough explanation of this topic can be found in [96], where some means to measure an abstract angle between the two spaces are also provided. In practice solving (4.26) having only a basis for $X_H^s(\Omega_1^0)$ and $Y_h^s(\Omega_1^1)$ requires either:

1. a particular care in the mesh generation phase, ensuring the sum appearing in Definition 4.4 to be direct and therefore allowing the construction of a basis set for V,
2. the employment of a subspace iterative technique [77] to solve the discrete problem alternatively on $X_H^s(\Omega_1^0)$ and $Y_h^s(\Omega_1^1)$ until convergence has been achieved.

Mixed integrals In both the direct and iterative approach a delicate matter is constituted by the numerical evaluation of the *mixed integrals*, i.e. of integrals where an element of each basis set appear. Denoting with:

$$N_H = \dim\bigl(X_H^s(\Omega_1^0)\bigr) \quad , \quad N_h = \dim\bigl(Y_h^s(\Omega_1^1)\bigr) \quad , \tag{4.47}$$

then any function $v_{Hh} \in V$ admits in fact the (possibly non-unique) representation:

$$v_{Hh} = v_H + v_h = \sum_{j=1}^{N_H} V_j \Phi_j + \sum_{j=1}^{N_h} v_j \phi_j, \tag{4.48}$$

where $\{\Phi_j\}_{j=1,\dots,N_H}$ is the set of basis function associated with $X_H^k(\Omega_1^0)$, while $\{\phi_j\}_{j=1,\dots,N_h}$ is the one associated with $Y_h^k(\Omega_1^1)$. Considering then the evaluation of the following expressions:

$$\begin{aligned} a(v_{Hh}, \Phi_i) &= \sum_{j=1}^{N_H} V_j a(\Phi_j, \Phi_i) + \sum_{j=1}^{N_h} v_j \boxed{a(\phi_j, \Phi_i)} \quad , \\ a(v_{Hh}, \phi_i) &= \sum_{j=1}^{N_H} V_j \boxed{a(\Phi_j, \phi_i)} + \sum_{j=1}^{N_h} v_j a(\phi_j, \phi_i) \quad , \end{aligned} \tag{4.49}$$

it becomes evident that the boxed terms cannot be evaluated a-priori via a closed formula, as they depend on the relative displacement between the two meshes. To numerically evaluate these terms it is thus assumed in the following that the basis functions $\{\Phi_j\}$ associated with the coarser grid can be expressed in the bilinear form as their interpolation upon the finer grid:

$$\Phi_j \approx \sum_{k=1}^{N_h} R_{jk} \phi_k. \tag{4.50}$$

In this way (4.49) is reduced to:

$$\begin{aligned} a(v_{Hh}, \Phi_i) &= \sum_{j=1}^{N_H} V_j a(\Phi_j, \Phi_i) + \sum_{j=1}^{N_h} v_j \sum_{k=1}^{N_h} R_{ik} a(\phi_j, \phi_k) \quad , \\ a(v_{Hh}, \phi_i) &= \sum_{j=1}^{N_H} V_j \sum_{k=1}^{N_h} R_{jk} a(\phi_k, \phi_i) + \sum_{j=1}^{N_h} v_j a(\phi_j, \phi_i) \quad , \end{aligned} \tag{4.51}$$

which is an expression where no mixed terms appear. Notice that (4.50) is an arbitrary assumption and other means of approximation are possible: for instance in [96] a different approach is proposed that makes use of a third finer structured grid to evaluate mixed terms.

Direct solution procedure If the computational meshes are generated in a way that prevents the elements of different basis sets from being linearly dependent, then a direct approach to the solution of the Galerkin problem is possible. [3] In this case representation (4.48) happens to be unique, so that (4.26) results to be equivalent to:

---

[3] In practice this will be always the case when fine meshes are generated independently and not as a refinement of the coarser ones.

$$\begin{aligned} a(u_{Hh},\Phi_i)+\hat{\alpha}(u_{Hh},\Phi_i)_{\partial\Omega_1^0} &= (f_1+f_2,\Phi_i)+\hat{\alpha}(g,\Phi_i)_{\partial\Omega_1^0} \quad && i=1,\dots,N_H,\\ a(u_{Hh},\phi_j) &= (f_1+f_2,\phi_j) && j=1,\dots,N_h. \end{aligned} \tag{4.52}$$

Notice that the boundary term has been removed when testing on $Y_h^s(\Omega_1^1)$ basis functions as the domain Ω_1^1 is defined not to share any external boundary with Ω_1^0 (see Definition 4.3). Introducing thus the finite element matrices:

$$\begin{aligned} A_C &\in \mathbb{R}^{N_H\times N_H} \quad \text{with} \quad A_C = \left[a_{ij}^C\right] = \left[a(\Phi_j,\Phi_i)\right]\,,\\ M_C &\in \mathbb{R}^{N_H\times N_H} \quad \text{with} \quad M_C = \left[m_{ij}^C\right] = \left[(\Phi_j,\Phi_i)_{\partial\Omega_1^0}\right]\,,\\ A_P &\in \mathbb{R}^{N_h\times N_h} \quad \text{with} \quad A_P = \left[a_{ij}^P\right] = \left[a(\phi_j,\phi_i)\right]\,, \end{aligned} \tag{4.53}$$

as well as the interpolation matrix:

$$R \in \mathbb{R}^{N_H\times N_h} \quad \text{with} \quad R = \left[R_{ij}\right]\,, \tag{4.54}$$

and the vectors:

$$\begin{aligned} \mathbf{u}_C &= \left[U_1,\dots,U_{N_H}\right]\,,\\ \mathbf{u}_P &= \left[u_1,\dots,u_{N_h}\right]\,, \end{aligned} \tag{4.55}$$

it is possible to write the algebraic counterpart of (4.52) as:

$$\begin{bmatrix} (A_C+\hat{\alpha}M_C) & RA_P\\ A_PR^T & A_P \end{bmatrix} \begin{bmatrix} \mathbf{u}_C\\ \mathbf{u}_P \end{bmatrix} = \begin{bmatrix} \mathbf{b}_C\\ \mathbf{b}_P \end{bmatrix}, \tag{4.56}$$

where $\mathbf{b}_C$ and $\mathbf{b}_P$ represent the right hand sides appearing in the first and second line of (4.52) respectively.

Iterative solution procedure An iterative approach, comprised in the theoretical framework of *successive subspace corrections* studied by Xu, Zikatanov and Huang [55, 101–103] and aiming at the solution of (4.26) when the linear independence of the basis sets $\{\Phi_j\}$ and $\{\phi_j\}$ is not ensured, was firstly proposed in [39]. Though a detailed discussion of this algorithm is out of the scope of the present chapter, it is worth to point the interested reader to [39, 96] where the spectral analysis of the iteration operator is given together with some considerations regarding the choice of the optimal relaxation parameter and its effect on the solution method efficiency. Notice that in the particular case where the sum in (4.13) is direct, then the iterative method presented above reduces to a solution via the *successive over-relaxation* (SOR) method [74, Chapter 4] of the linear system (4.56).

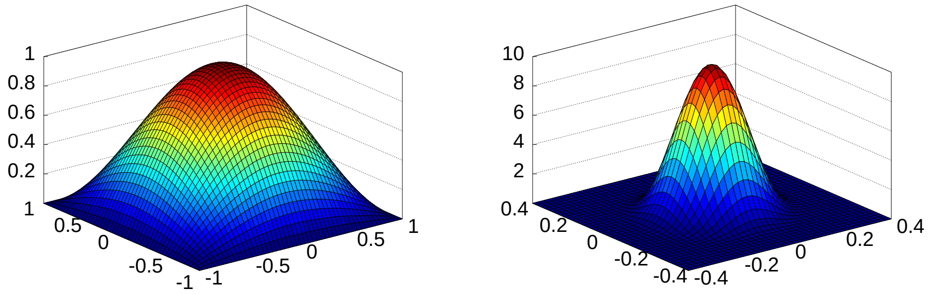

(a) Solution: u_0 (b) Solution: u_1

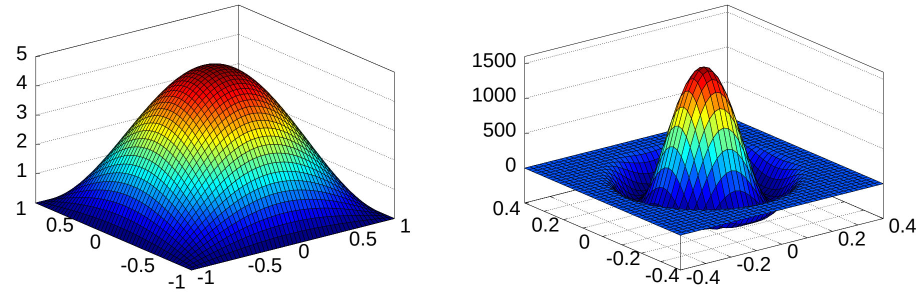

(c) Right hand side: f_0 (d) Right hand side: f_1

Figure (4.3): *Smooth and rapidly varying components of the solution and right hand side appearing in Example 4.1. Notice the different scaling of the axis.*

Example 4.1. Consider the problem [96, Chapter 1]:

$$\left\{\begin{array}{rcll} -\Delta u & = & f_0 + f_1 & \text{in } \Omega := (-1,1)^2, \\ u & = & 0 & \text{on } \partial\Omega\ . \end{array}\right. \tag{4.57}$$

The terms f_0 and f_1 appearing in the right hand side are constructed in such a way that the analytical solution of (4.57) results to be:

$$u = u_0 + u_1, \tag{4.58}$$

where:

$$\begin{array}{rcl} u_0 & := & \cos\left(\dfrac{\pi}{2}x\right)\cos\left(\dfrac{\pi}{2}y\right), \\ u_1 & := & \eta\,\chi(R)\exp\left(\epsilon_f^2\right)\exp\left(-\dfrac{1}{|\epsilon_f^2 - R^2|}\right). \end{array} \tag{4.59}$$

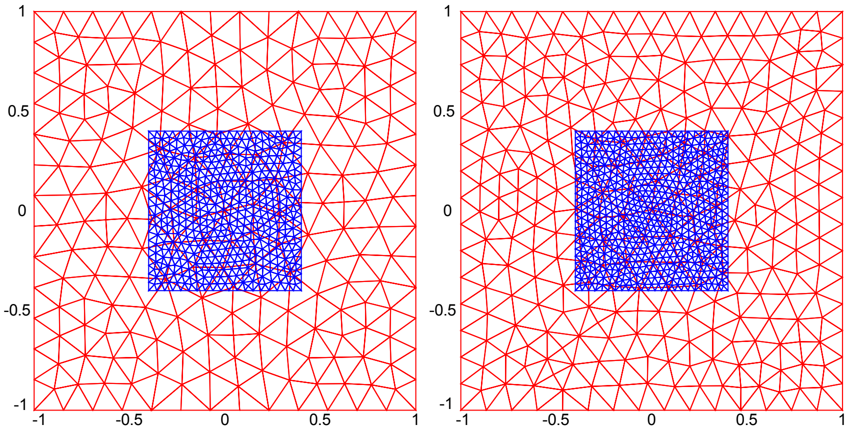

Figure (4.4): *Computational meshes employed in the numerical solution of problem (4.57). Notice that the ratio H/h is kept constant during the refinement.*

In (4.59) $\chi(R)$ is a function defined as:

$$\chi(R) := \begin{cases} 1 & \text{if } R := \sqrt{x^2+y^2} \leq \epsilon_f , \\ 0 & \text{otherwise.} \end{cases} \tag{4.60}$$

while η and ϵ_f are parameters set to $\eta = 10$ and $\epsilon_f = 0.4$. Plots of either the right hand side and solution components are given in Figure 4.3.

To provide an illustration of Theorem 4.1 numerical approximations of (4.57) are computed with either standard finite element and patches of finite element techniques. The patch domain is defined to be $\Omega_1^1 := (-0.4, 0.4)^2$, while the patched space is constructed employing linear finite element for either the coarse and fine domain:

$$V := X_H^1(\Omega_0^1) + Y_h^1(\Omega_1^1) \ . \tag{4.61}$$

To characterize the accuracy of the method the *relative error on the energy-norm* is taken as a figure of merit. The results obtained for a successive refinement of either the coarse and fine triangulation (with constant ratio $H/h \approx 3.7$) are reported in Table 4.1, where efficiency is evaluated on the base of the total number of mesh nodes. Figure 4.4 displays the first two couple of coarse-fine meshes appearing in Table 4.1. Notice the constant ratio H/h maintained when refining both grids. Figure 4.5 shows a log-scale plot of the *relative energy-norm error* against the characteristic length H of the coarse mesh, where it is possible to observe:

1. a good agreement with the order-one error decay predicted by Lemma 4.1,
2. a drastic reduction of the relative a-norm error when employing the patches method.

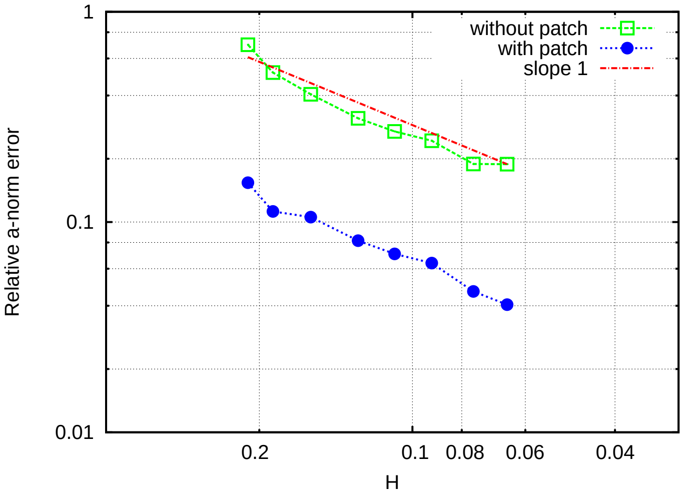

Figure (4.5): *Relative error on the energy-norm plotted against the characteristic length of the coarse grid. Notice the good agreement with the linear decay predicted by Lemma 4.1.*

Coarse mesh			**Patch mesh**		
H	# nodes	Reference error	h	# nodes	Computed error
2.10523e-01	217	6.97059e-01	5.88522e-02	483(+217)	1.53944e-01
1.88050e-01	299	5.14016e-01	4.77519e-02	652(+299)	1.12352e-01
1.58422e-01	417	4.05275e-01	4.21864e-02	931(+417)	1.05469e-01
1.27898e-01	636	3.11364e-01	3.62168e-02	1432(+636)	8.15661e-02
1.08406e-01	848	2.69749e-01	2.98711e-02	1858(+848)	7.05245e-02
9.16620e-02	1209	2.43549e-01	2.46061e-02	2563(+1209)	6.37921e-02
7.58930e-02	1673	1.88854e-01	2.11124e-02	3777(+1673)	4.67773e-02
6.51516e-02	2237	1.88382e-01	1.72072e-02	5322(+2237)	4.04827e-02

Table (4.1): *Results obtained from the numerical approximation of problem* (4.57) *with a direct approach. The reference error is obtained considering standard finite element on the coarse grid.*

As a last remark it is worth to note that the error obtained using the first couple of coarse-fine grids (483+217 total mesh nodes) with the patch method is smaller than the one obtained with standard finite element on the coarse grid having 2237 nodes. This behavior suggests that the patches method permits a great reduction on the number of unknowns for a fixed accuracy on the approximate solution of a diffusion-reaction problem when multi-scale features appear.

Chapter summary In this chapter the patches of finite element method (firstly introduced in literature by Wagner et al.) was presented as a proper approach towards the discretization of the PDE appearing in the definition of the thermal element model established in Chapter 2. As an original contribution, the method was extended to cope with an arbitrary hierarchy of domains. A novel modification to this approach devised to resolve internal and boundary layer in the case of reaction-dominant PDEs will be addressed in Appendix D.

5

Numerical solution of the coupled system

As the coupled electro-thermal system derived in Chapter 2 does not generally admit closed-form solutions, the purpose of Chapter 5 is to outline a strategy to approximate this solution numerically.

A first step toward this aim is given in Section 5.1 treating the discretization of the full PDAE system. A general multi-step method is employed to time discretize the system and provide a set of non-linear algebraic equations for each time point. Some means to obtain efficiency improvements within this framework are referenced here. In Section 5.2 it is shown how to solve non-linear algebraic equation systems resorting to Newton's method. In particular, a technique [1] to improve computational efficiency in the case the non-linear equation system is to be assembled on a per element basis is introduced and applied to the set of discretized equations derived in Section 5.1. This contextualization permits to sketch the most commonly adopted algorithmic structure in transient circuit simulation softwares, based on the concept of *elemental stamp*. The latter is nothing but a table-like diagram that completely characterize a particular element, uniquely defining its contributions to the Jacobian and residual during each Newton's iteration. To conclude the chapter, the stamp associated with a linear thermal element is derived in Section 5.3 in the case the method introduced in Chapter 4 is used to space discretize the PDE appearing in its constitutive relations.

5.1 Discretization of the electro-thermal model

In Chapter 2 a model was proposed to describe electro-thermal effects at the system level. The derivation of this model, merging the usual lumped description of electrical device behavior with a spatially distributed description of thermal diffusion, was mainly guided by the need to fit usual circuit simulator structures imposed by

---

[1] This technique is widely known as *by-pass* technique in the circuit simulation field.

MNA. This effort led to the definition of a particular *thermal element* in Section 2.4, embedding a PDE in its constitutive relations to properly describe thermal effects occurring in a 2D/3D domain. The overall system of equations stemming from the semi-discretized model was then formulated with the element-wise notation (2.39) (reported below for easiness of reference) to stress the assembly-by-element structure still shared with standard MNA:

$$\begin{aligned} \sum_{m=1}^{M} A_m \big[D_m \dot{\mathbf{r}}_m + \mathbf{J}_m(A_m^T \mathbf{n}, \mathbf{r}_m; t) \big] &= 0 \ , \\ B_m \dot{\mathbf{r}}_m + \mathbf{Q}_m(A_m^T \mathbf{n}, \mathbf{r}_m; t) &= 0 \qquad m = 1, \ldots, M. \end{aligned} \tag{5.1}$$

When dealing with practical applications it is of course not feasible to search for closed-form solutions of problem (5.1) in a time interval $[0, \mathrm{t}_1]$ and supplied with consistent initial conditions $\mathbf{n}(0)$ and $\mathbf{r}_m(0)$: a suitable time discretization becomes thus necessary to compute a numerical approximation of both $\mathbf{n}(t)$ and $\mathbf{r}_m(t)$. This subject is treated in the following, while a discussion concerning a proper space-discretization of the thermal element is left to Section 5.3.

Time discretization Assume, for sake of simplicity, that a p-step linear multi-step method of the form:

$$\dot{y}(t_k) + f(y(t_k), t_k) \approx \sum_{j=0}^{p} \alpha_j y(t_{k-j}) + h \sum_{j=0}^{p} \beta_j f(y(t_{k-j}), t_{k-j}) = 0 \tag{5.2}$$

is adopted to discretize (5.1), where the coefficients α_j and β_j depend on the particular method employed and the time step h is supposed to be constant (for a deeper characterization of these methods and a description of usual initialization procedures refer to [51,74]). Notice that the general concepts presented here would essentially still hold if different time-stepping techniques (e.g. DIRK or ROW methods [51]) were to be adopted, but the required modifications to the arguments presented below exceed the scope of the present section. Assuming $k > p$, then a set of difference equations is obtained when discretizing system (5.1) in agreement to (5.2). The balance part reads then:

$$\sum_{m=1}^{M} A_m \Big[D_m \sum_{j=0}^{p} \alpha_j \mathbf{r}_m(t_{k-j}) + h \sum_{j=0}^{p} \beta_j \mathbf{J}_m(A_m^T \mathbf{n}(t_{k-j}), \mathbf{r}_m(t_{k-j}); t_{k-j}) \Big] = 0 \ , \tag{5.3}$$

while the constitutive relation part becomes ($m = 1, \ldots, M$):

$$B_m \sum_{j=0}^{p} \alpha_j \mathbf{r}_m(t_{k-j}) + h \sum_{j=0}^{p} \beta_j \mathbf{Q}_m(A_m^T \mathbf{n}(t_{k-j}), \mathbf{r}_m(t_{k-j}); t_{k-j}) = 0 \ . \tag{5.4}$$

Defining:

$$\begin{aligned} \tilde{\mathbf{J}}_m^{(k)}(A_m^T \mathbf{n}, \mathbf{r}_m) &= D_m \alpha_0 \mathbf{r}_m(t_k) + h\, \beta_0\, \mathbf{J}_m(A_m^T \mathbf{n}(t_k), \mathbf{r}_m(t_k); t_k) \ , \\ \tilde{\mathbf{Q}}_m^{(k)}(A_m^T \mathbf{n}, \mathbf{r}_m) &= B_m \alpha_0 \mathbf{r}_m(t_k) + h\, \beta_0\, \mathbf{Q}_m(A_m^T \mathbf{n}(t_k), \mathbf{r}_m(t_k); t_k) \ , \end{aligned} \tag{5.5}$$

and:

$$\begin{aligned}
\mathbf{b}_m^{(k)} &= D_m \sum_{j=1}^{p} \alpha_j \mathbf{r}_m(t_{k-j}) + h \sum_{j=1}^{p} \beta_j \mathbf{J}_m(A_m^T \mathbf{n}(t_{k-j}), \mathbf{r}_m(t_{k-j}); t_{k-j}) \ , \\
\mathbf{c}_m^{(k)} &= B_m \sum_{j=1}^{p} \alpha_j \mathbf{r}_m(t_{k-j}) + h \sum_{j=1}^{p} \beta_j \mathbf{Q}_m(A_m^T \mathbf{n}(t_{k-j}), \mathbf{r}_m(t_{k-j}); t_{k-j}) \ ,
\end{aligned} \tag{5.6}$$

it is possible to divide quantities referring to the actual time instant t_k from the ones depending on previous time points. In this way system (5.3)-(5.4) can be rewritten in the compact notation:

$$\begin{aligned}
\sum_{m=1}^{M} A_m \left[\tilde{\mathbf{J}}_m^{(k)}(A_m^T \mathbf{n}, \mathbf{r}_m) + \mathbf{b}_m^{(k)} \right] &= 0 \\
\tilde{\mathbf{Q}}_m^{(k)}(A_m^T \mathbf{n}, \mathbf{r}_m) + \mathbf{c}_m^{(k)} &= 0 \qquad m = 1, \ldots, M.
\end{aligned} \tag{5.7}$$

If the value of all variables at times $t_{k-1}, \ldots, t_{k-p}$ are known, (5.7) can be regarded as a non-linear implicit system of equations that allows to compute the values of the nodal variables and element internal variables at time t_k.

Time step adaptivity, multi-rate techniques For easiness of exposition, the algebraic system of equations (5.7) is derived under the assumption that a constant time step h is employed to time discretize (5.1). Even though a thorough analysis of the topic is out of the scope of the present chapter, it should be noticed that this assumption is generally too restrictive to be actually used in an industrial framework, where computational efficiency is a major concern. Therefore, to fulfill the usually strict performance requirements, some means to diminish the computational burden during time integration were designed, which are mainly based on the two concepts of *time step adaptivity* and *multi-rate time integration.* [2]

The first class of methods tries to reach a smaller computational load resorting to an adaption of the stepsize h based on an estimation of the *local truncation error* [12, 36, 81, 109]. In fact, as the equation systems stemming from electrical circuits are usually stiff, the benefit of a larger stepsize (once the fast transients are exhausted) greatly overcomes the cost of a numerical evaluation of the local truncation error estimator in many situations. The second category of methods employs instead time-scale separation techniques to integrate "slow" variables with a greater stepsize than "fast" ones [9,59,63,99]. Multi-rate methods provide thus a major impact on efficiency when the system under examination includes time constants that spans several orders of magnitude. This results to be often the case for digital circuits subject to high clock-rate or power circuits [72] switched at high frequency. Anyhow, although some very promising results have been shown for particular applications [10], in general the impact of state of the art multirate time-stepping approaches on the performance of coupled electrothermal simulation still needs to be fully assessed through extensive numerical tests on real life applications. Though out of the scope of the present work, further research on this issue is warranted.

---

[2] Even though only time discretization is taken into account in this paragraph, other means to improve simulation efficiency could be employed that address different aspects of the solution algorithm (e.g. the strategy used to solve the non-linear system (5.7)).

5.2 Solution of non-linear algebraic equation systems

To obtain an approximate solution to (5.7) a system of non-linear algebraic equations has to be solved. This task is usually accomplished in circuit simulators resorting to Newton-like methods, introduced in the following.

Newton's method Consider the continuously differentiable function:

$$\mathbf{F} \; : \; D \subseteq \mathbb{R}^n \to \mathbb{R}^n \; . \tag{5.8}$$

Denote with $\mathbb{J}_{\mathbf{F}}(\mathbf{y})$ the Jacobian matrix associated with $\mathbf{F}$ and evaluated at the point $\mathbf{y} \in \mathbb{R}^n$, and suppose that $\mathbf{y}^* \in \mathbb{R}^n$ such that:

$$\mathbf{F}(\mathbf{y}^*) = 0 \; , \tag{5.9}$$

has to be found. *Newton's method* to solve problem (5.9) can be formulated as follows:

- Set $\mathbf{y}^{[0]}$ to be the initial guess.
- Then for $l = 0, 1, 2, \dots$
    1. Solve:
    $$\mathbb{J}_{\mathbf{F}}(\mathbf{y}^{[l]})\, \delta\mathbf{y}^{[l]} = -\mathbf{F}(\mathbf{y}^{[l]}) \; . \tag{5.10}$$
    2. Set:
    $$\mathbf{y}^{[l+1]} = \mathbf{y}^{[l]} + \delta\mathbf{y}^{[l]} \; . \tag{5.11}$$

Newton's method presents an high sensitivity on the choice of the initial guess, and proves to be quadratically convergent if $\mathbf{y}^{[0]}$ is sufficiently close to $\mathbf{y}^*$ and the Jacobian matrix is non-singular [74, Theorem 7.1]. Of course, in practical implementations a suitable approximation of $\mathbf{y}^*$ is obtained terminating the iterative process on the base of some *stopping criteria* which involve the control of either the functional residual or the solution increment.

By-pass technique At each step of Newton's method two functional evaluations ($\mathbb{J}_{\mathbf{F}}$ and $\mathbf{F}$) and the solution of a linear system are performed. These operations require a computational effort that can be excessively high as the number of unknowns gets large. For this reason several modifications to the usual algorithm, involving an approximation of the Jacobian or an inexact solution of system (5.10), have been proposed to improve computational efficiency. When the complete system of non-linear equations (5.9) can be assembled via a per element inspection, a technique of particular interest is the so called *by-pass* technique. Consider, for the sake of simplicity, a system of the form:

$$\mathbf{F}(\mathbf{y}^*) = \sum_{m=1}^{M} A_m \mathbf{F}_m(A_m^T \mathbf{y}^*) = 0 \ , \tag{5.12}$$

where A_m is a suitable incidence matrix. Under this assumption the quantities appearing in (5.10) can be constructed as:

$$\begin{aligned} \mathbb{J}_{\mathbf{F}}(\mathbf{y}^{[l]}) &= \sum_{m=1}^{M} A_m \mathbb{J}_m(A_m^T \mathbf{y}^{[l]}) \ , \\ \mathbf{F}(\mathbf{y}^{[l]}) &= \sum_{m=1}^{M} A_m \mathbf{F}_m(A_m^T \mathbf{y}^{[l]}) \ . \end{aligned} \tag{5.13}$$

Denoting with τ the required accuracy on the Newton's method, then the by-pass technique [94] is based on the assumption that if the following inequality holds for a generic element:

$$\|A_m^T \mathbf{y}^{[l+1]} - A_m^T \mathbf{y}^{[l]}\| \leq \tau \ \|A_m^T \mathbf{y}^{[l+1]}\| \ , \tag{5.14}$$

its Jacobian and residual contributions are maintained passing from the l-th step to the $(l+1)$-th step:

$$\begin{aligned} \mathbb{J}_m(A_m^T \mathbf{y}^{[l+1]}) &:= \mathbb{J}_m(A_m^T \mathbf{y}^{[l]}) \ , \\ \mathbf{F}_m(A_m^T \mathbf{y}^{[l+1]}) &:= \mathbf{F}_m(A_m^T \mathbf{y}^{[l]}) \ . \end{aligned} \tag{5.15}$$

In this way for each element satisfying (5.14) two functional evaluations are avoided at each iteration step. Notice that dividing the elements in the two set for which (5.14) hold or hold not, then it is possible to interpret by-pass technique as an adaptive multirate approach. The main difference when compared to usual multi-rate is that in this case the partitioning among "latent" and "active" part is done on a per element basis, rather than directly on nodal variables. In fact at each Newton's step the method can be written as:

$$\begin{aligned} &\left(\sum_{m=1}^{M_l} A_m \mathbb{J}_m(A_m^T \mathbf{y}^{[l]}) + \sum_{m=M_l+1}^{M_l+M_a} A_m \mathbb{J}_m(A_m^T \mathbf{y}^{[l]}) \right) \delta\mathbf{y}^{[l]} = \\ -&\left(\sum_{m=1}^{M_l} A_m \mathbf{F}_m(A_m^T \mathbf{y}^{[l]}) + \sum_{m=M_l+1}^{M_l+M_a} A_m \mathbf{F}_m(A_m^T \mathbf{y}^{[l]}) \right) \ , \end{aligned} \tag{5.16}$$

where M_a denotes the number of *active* elements, whose contributions are actually evaluated, while M_l denotes the number of *latent* elements, whose contributions are maintained from the previous Newton's iteration.

Application to the discretized electro-thermal system Before proceeding with the application of the numerical scheme described so far to the discretized electro-thermal system, it is necessary to point out that the content of the remaining part of this section and of the whole Section 5.3 requires a good knowledge of the usual algorithmic structure adopted in transient circuit simulation softwares. The reader interested in a gentle introduction to this topic can refer to [42, Chapter 1]. That being said, in order to apply Newton's method to system (5.7), define the following residuals:

$$\begin{aligned} \mathbf{F}_m^{[l]} &:= \tilde{\mathbf{J}}_m^{(k)}(A_m^T \mathbf{n}^{[l]}, \mathbf{r}_m^{[l]}) + \mathbf{b}_m^{(k)} \ , \\ \mathbf{G}_m^{[l]} &:= \tilde{\mathbf{Q}}_m^{(k)}(A_m^T \mathbf{n}^{[l]}, \mathbf{r}_m^{[l]}) + \mathbf{c}_m^{(k)} \ , \end{aligned} \tag{5.17}$$

and the corresponding Jacobians:

$$\begin{aligned} \mathbb{J}_{m,\mathbf{n}}^{[l]} &:= \left.\frac{\partial \tilde{\mathbf{J}}_m^{(k)}}{\partial A_m^T \mathbf{n}}\right|_{\mathbf{n}=\mathbf{n}^{[l]}} \ , \quad & \mathbb{J}_{m,\mathbf{r}}^{[l]} &:= \left.\frac{\partial \tilde{\mathbf{J}}_m^{(k)}}{\partial \mathbf{r}_m}\right|_{\mathbf{r}_m=\mathbf{r}_m^{[l]}} \ , \\ \mathbb{Q}_{m,\mathbf{n}}^{[l]} &:= \left.\frac{\partial \tilde{\mathbf{Q}}_m^{(k)}}{\partial A_m^T \mathbf{n}}\right|_{\mathbf{n}=\mathbf{n}^{[l]}} \ , \quad & \mathbb{Q}_{m,\mathbf{r}}^{[l]} &:= \left.\frac{\partial \tilde{\mathbf{Q}}_m^{(k)}}{\partial \mathbf{r}_m}\right|_{\mathbf{r}_m=\mathbf{r}_m^{[l]}} \ . \end{aligned} \tag{5.18}$$

With this notation introduced, the l-th Newton's iteration reads:

$$\begin{aligned} \left[\sum_{m=1}^{M} A_m \mathbb{J}_{m,\mathbf{n}}^{[l]}\right] \delta\mathbf{n}^{[l]} + \left[\sum_{m=1}^{M} A_m \mathbb{J}_{m,\mathbf{r}}^{[l]}\, \delta\mathbf{r}_m^{[l]}\right] &= -\sum_{m=1}^{M} A_m \mathbf{F}_m^{[l]} \ , \\ \mathbb{Q}_{m,\mathbf{n}}^{[l]} A_m^T\, \delta\mathbf{n}^{[l]} + \mathbb{Q}_{m,\mathbf{r}}^{[l]}\, \delta\mathbf{r}_m^{[l]} &= -\mathbf{G}_m^{[l]} \qquad m = 1, \ldots, M. \end{aligned} \tag{5.19}$$

As anticipated in Chapter 2, the possibility to assemble on a per-element basis the complete set of equations stemming from the coupled electro-thermal model remains also at the discrete level. In fact from the discussion carried out above it is possible to sketch the structure most commonly adopted in the design of a software package for transient circuit simulation. To implement the algorithm outlined so far a program must contain three basic components:

1. a *time-stepper* responsible for time-step selection and for computing the coefficients α_j and β_j of the time discretization
2. a *non-linear solver* responsible for solving, at each time-step, system (5.7) by iteratively assembling and solving the linear system (5.19),
3. a set of *element evaluators* that provide the non-linear solver with the local Jacobian matrices and residuals needed to assemble the linear system corresponding to each Newton iteration.

These local contributions are commonly referred to as *stamps* and are feasible to be represented in a table-like format:

	$A_m^T \mathbf{n}$	$\mathbf{r}_m$	
KCL	$\mathbb{J}_{m,\mathbf{n}}^{[l]}$	$\mathbb{J}_{m,\mathbf{r}}^{[l]}$	$\mathbf{F}_m^{[l]}$,
CR	$\mathbb{Q}_{m,\mathbf{n}}^{[l]}$	$\mathbb{Q}_{m,\mathbf{r}}^{[l]}$	$\mathbf{G}_m^{[l]}$,

where the acronym CR stands for "constitutive relations". The application of by-pass technique can be also formalized resorting to the stamp notation. In this case, during each element evaluation, the following steps are performed:

- If the inequalities:

$$\|A_m^T \mathbf{n}^{[l+1]} - A_m^T \mathbf{n}^{[l]}\| \leq \tau \|A_m^T \mathbf{n}^{[l+1]}\| \quad , \quad \|\mathbf{r}_m^{[l+1]} - \mathbf{r}_m^{[l]}\| \leq \tau \|\mathbf{r}_m^{[l+1]}\| \ , \tag{5.20}$$

  hold, then it is assumed:

$$\begin{aligned} \mathbb{J}_{m,\mathbf{n}}^{[l+1]} &:= \mathbb{J}_{m,\mathbf{n}}^{[l]} \ , & \mathbb{J}_{m,\mathbf{r}}^{[l+1]} &:= \mathbb{J}_{m,\mathbf{r}}^{[l]} \ , & \mathbf{F}_m^{[l+1]} &:= \mathbf{F}_m^{[l]} \ , \\ \mathbb{Q}_{m,\mathbf{n}}^{[l+1]} &:= \mathbb{Q}_{m,\mathbf{n}}^{[l]} \ , & \mathbb{Q}_{m,\mathbf{r}}^{[l+1]} &:= \mathbb{Q}_{m,\mathbf{r}}^{[l]} \ , & \mathbf{G}_m^{[l+1]} &:= \mathbf{G}_m^{[l]} \ . \end{aligned} \tag{5.21}$$

- Otherwise the Jacobian and residual contributions are computed as specified in the *element evaluator*.

5.3 Evaluation of the thermal element

To conclude the chapter, the construction of the *thermal element stamp* is discussed. Assuming the thermal element to be the M-th element of the system, the nodal variables associated with it read:

$$A_M^T \mathbf{n} = \boldsymbol{\theta} = [\theta_1, \ldots, \theta_{K+1}]^T \ , \tag{5.22}$$

where K is the number of thermally active regions, θ_k $(k = 1, \ldots, K)$ are the mean temperatures over these regions and θ_{K+1} represents the environment temperature. Introducing the power density vector:

$$\mathbf{p} = [p_1, \ldots, p_K]^T \ , \tag{5.23}$$

and the vector of the n_T unknowns stemming from the space discretization of the distributed temperature field $T(\mathbf{x}, t)$:

$$\mathbf{T} = \left[\mathbf{T}_C, \mathbf{T}_1, \ldots, \mathbf{T}_K\right]^T \ , \tag{5.24}$$

then the set of the thermal element internal variables reads:

$$\mathbf{r}_M = \begin{bmatrix} \mathbf{p} \\ \mathbf{T} \end{bmatrix} \ . \tag{5.25}$$

The particular structure of $\mathbf{T}$ in (5.24) arise from a space discretization via the patches of finite element method defined in Chapter 4. Notice that, even though the following discussion will remain essentially the same in the case of multiple patch layers, for the sake of simplicity only a single level of patches is assumed here. Defining:

$$\boldsymbol{\Omega} \in \mathbb{R}^{K+1 \times K} \quad \text{such that} \quad \boldsymbol{\Omega} := \begin{bmatrix} |\Omega_1| & \cdots & 0 \\ \vdots & \ddots & \vdots \\ 0 & \cdots & |\Omega_K| \\ -|\Omega_1| & \cdots & -|\Omega_K| \end{bmatrix} \ , \tag{5.26}$$

then it is possible to provide an explicit formulation for the stamp entries referring to KCL:

$$\begin{aligned}
\mathbb{J}^{[l]}_{M,\mathbf{n}} &\in \mathbb{R}^{K+1\times K+1} \quad \text{with} \quad \mathbb{J}^{[l]}_{M,\mathbf{n}} := \begin{bmatrix} 0 \end{bmatrix} \;, \\
\mathbb{J}^{[l]}_{M,\mathbf{r}} &\in \mathbb{R}^{K+1\times K+n_T} \quad \text{with} \quad \mathbb{J}^{[l]}_{M,\mathbf{r}} := \begin{bmatrix} \mathbf{\Omega} & 0 \end{bmatrix} \;, \\
\mathbf{F}^{[l]}_{M} &\in \mathbb{R}^{K+1} \quad \text{with} \quad \mathbf{F}^{[l]}_{M} := \mathbf{\Omega}\; \mathbf{p}^{[l]} \;.
\end{aligned} \tag{5.27}$$

The definition of the entries referring to the thermal element constitutive relations is a bit more involved. Assume $\{\phi_j, j = 1, \ldots, n_T\}$ to represent the full basis set associated with the space discretized vector $\mathbf{T}$ and define:

$$\begin{aligned}
M_{\boldsymbol{\theta}} &\in \mathbb{R}^{K\times K+1} \quad \text{with} \quad M_{\boldsymbol{\theta}} := \begin{bmatrix} 1 & \cdots & 0 & 0 \\ \vdots & \ddots & \vdots & 0 \\ 0 & \cdots & 1 & 0 \end{bmatrix} \;, \\
M_{\mathbf{T}} &\in \mathbb{R}^{K\times n_T} \quad \text{with} \quad [M_{\mathbf{T}}]_{ij} := \frac{1}{|\Omega_i|}(\phi_j, \mathbf{1}_{\Omega_i}) \;.
\end{aligned} \tag{5.28}$$

The discretized version of relation (2.20) linking junction temperatures to the distributed temperature field reads then:

$$M_{\boldsymbol{\theta}}\boldsymbol{\theta} - M_{\mathbf{T}}\mathbf{T} = 0 \;. \tag{5.29}$$

Lastly the discretization of the PDE describing heat-diffusion has to be considered. Denote with:

$$\begin{aligned}
B &\in \mathbb{R}^{n_T\times K+1} \quad \text{with} \quad B := \begin{bmatrix} 0 & \cdots & 0 & b_1 \\ \vdots & \ddots & \vdots & \vdots \\ 0 & \cdots & 0 & b_{n_T} \end{bmatrix} \;, \\
P &\in \mathbb{R}^{n_T\times K} \quad \text{with} \quad [P]_{ij} := (\mathbf{1}_{\Omega_j}, \phi_i) \;,
\end{aligned} \tag{5.30}$$

the matrices accounting respectively for boundary conditions and for heat generation. Notice that only the last column of B may have non-zero entries, as boundary conditions depend only on the environment temperature. Assume finally A and C to be the stiffness and mass matrix stemming from patches of finite element method (for more insight on the construction of these matrices the interested reader is referred to Chapter 4). [3] The space discretized formulation of heat-diffusion equation reads then:

$$C\dot{\mathbf{T}} + A\mathbf{T} + P\mathbf{p} + B\boldsymbol{\theta} = 0 \;. \tag{5.31}$$

---

[3] Not to unnecessarily involve the notation, heat-diffusion it is assumed here to be properly described by a linear PDE. However, the extension of the following to the non-linear case implies only different evaluations of mass and stiffness matrix depending on vector $\mathbf{T}$.

Applying the multi-step time discretization (5.2) with constant stepsize to (5.30) and (5.31) it is possible to write the Jacobian contributions as:

$$\begin{aligned} \mathbb{Q}^{[l]}_{M,\mathbf{n}} &\in \mathbb{R}^{K+n_T\times K+1} \quad \text{with} \quad \mathbb{Q}^{[l]}_{M,\mathbf{n}} := \begin{bmatrix} M_{\boldsymbol{\theta}} \\ h\beta_0 B \end{bmatrix} , \\ \mathbb{Q}^{[l]}_{M,\mathbf{r}} &\in \mathbb{R}^{K+n_T\times K+n_T} \quad \text{with} \quad \mathbb{Q}^{[l]}_{M,\mathbf{r}} := \begin{bmatrix} 0 & M_{\mathbf{T}} \\ h\beta_0 P & (\alpha_0 C + h\beta_0 A) \end{bmatrix} , \end{aligned} \tag{5.32}$$

while defining:

$$\mathbf{g}_{(k)} = \sum_{j=1}^{p} \alpha_j C \mathbf{T}_{(k-j)} + h \sum_{j=1}^{p} \beta_j \left(A\mathbf{T}_{(k-j)} + P\mathbf{p}_{(k-j)} + B\boldsymbol{\theta}_{(k-j)} \right) , \tag{5.33}$$

gives the following expression for the residual $\mathbf{G}^{[l]}_M \in \mathbb{R}^{K+n_T}$:

$$\mathbf{G}^{[l]}_M = - \begin{bmatrix} 0 \\ h\beta_0 B\boldsymbol{\theta}^{[l]} + h\beta_0 P\mathbf{p}^{[l]} + (\alpha_0 C + h\beta_0 A)\mathbf{T}^{[l]} + \mathbf{g}_{(k)} \end{bmatrix} . \tag{5.34}$$

Schur-complement evaluation of the thermal element The thermal element evaluator described in the previous paragraph provides the non-linear solver with a *sparse stamp*, due to the fact that a PDE is used to describe heat-diffusion (see Chapter 6 or Chapter 7 for sparsity patterns examples). This feature is however not always desired. In fact many industrial circuit simulators, though allowing for a sparse structure of the global matrix in system (5.19), permit only a *dense representation* of the individual stamps. In this case, to effectively employ the thermal element and avoid a dramatic *fill-in* in the global matrix [74, Chapter 4], a different strategy than the one presented above should be employed. One possibility is in this sense to resort to a Schur-complement evaluation of the thermal element.

Taking into account the linear thermal element discussed above, then it is possible to write its contribution to the non-linear system (5.7) in a compact notation as:

$$\begin{bmatrix} B_{\boldsymbol{\theta}\boldsymbol{\theta}} & B_{\boldsymbol{\theta}\mathbf{r}} \\ B_{\mathbf{r}\boldsymbol{\theta}} & B_{\mathbf{r}\mathbf{r}} \end{bmatrix} \begin{bmatrix} \boldsymbol{\theta}(t_k) \\ \mathbf{r}_M(t_k) \end{bmatrix} + \begin{bmatrix} 0 \\ \mathbf{g}_{(k)} \end{bmatrix} = \begin{bmatrix} \tilde{\mathbf{J}}^{(k)}_M (A^T_M \mathbf{n}, \mathbf{r}_M) + \mathbf{b}^{(k)}_M \\ 0 \end{bmatrix} , \tag{5.35}$$

with:

$$\begin{aligned} B_{\boldsymbol{\theta}\boldsymbol{\theta}} &\in \mathbb{R}^{K+1\times K+1} \quad \text{with} \quad B_{\boldsymbol{\theta}\boldsymbol{\theta}} := \begin{bmatrix} 0 \end{bmatrix} , \\ B_{\boldsymbol{\theta}\mathbf{r}} &\in \mathbb{R}^{K+1\times K+n_T} \quad \text{with} \quad B_{\boldsymbol{\theta}\mathbf{r}} := \begin{bmatrix} \boldsymbol{\Omega} & 0 \end{bmatrix} , \\ B_{\mathbf{r}\boldsymbol{\theta}} &\in \mathbb{R}^{K+n_T\times K+1} \quad \text{with} \quad B_{\mathbf{r}\boldsymbol{\theta}} := \begin{bmatrix} M_{\boldsymbol{\theta}} \\ h\beta_0 B \end{bmatrix} , \\ B_{\mathbf{r}\mathbf{r}} &\in \mathbb{R}^{K+n_T\times K+n_T} \quad \text{with} \quad B_{\mathbf{r}\mathbf{r}} := \begin{bmatrix} 0 & M_{\mathbf{T}} \\ h\beta_0 P & (\alpha_0 C + h\beta_0 A) \end{bmatrix} . \end{aligned} \tag{5.36}$$

$B_{\mathbf{rr}}$ can be shown to be invertible by the arguments of Theorem 3.2 and Theorem 3.3, so that:

$$\mathbf{r}_M(t_k) = -B_{\mathbf{rr}}^{-1}(B_{\mathbf{r}\boldsymbol{\theta}}\boldsymbol{\theta}(t_k) + \mathbf{g}_{(k)}) \ . \tag{5.37}$$

Substituting (5.37) into the first line of (5.35) reads:

$$(B_{\boldsymbol{\theta\theta}} - B_{\boldsymbol{\theta}\mathbf{r}}B_{\mathbf{rr}}^{-1}B_{\mathbf{r}\boldsymbol{\theta}})\,\boldsymbol{\theta}(t_k) - B_{\boldsymbol{\theta}\mathbf{r}}B_{\mathbf{rr}}^{-1}\mathbf{g}_{(k)} = \tilde{\mathbf{J}}_M^{(k)}(A_M^T\mathbf{n}, \mathbf{r}_M) + \mathbf{b}_M^{(k)} \ . \tag{5.38}$$

It is now evident how a *dense* Jacobian contribution:

$$\mathbb{J}_{M,\mathbf{n}}^{[l]} \quad \in \quad \mathbb{R}^{K+1\times K+1} \quad \text{with} \quad \mathbb{J}_{M,\mathbf{n}}^{[l]} \quad := \quad (B_{\boldsymbol{\theta\theta}} - B_{\boldsymbol{\theta}\mathbf{r}}B_{\mathbf{rr}}^{-1}B_{\mathbf{r}\boldsymbol{\theta}}) \ , \tag{5.39}$$

of size $(K+1)\times(K+1)$ and a residual contribution:

$$\mathbf{F}_M^{[l]} \quad \in \quad \mathbb{R}^{K+1} \quad \text{with} \quad \mathbf{F}_M^{[l]} \quad := \quad \mathbb{J}_{M,\mathbf{n}}^{[l]}\boldsymbol{\theta}^{[l]} - B_{\boldsymbol{\theta}\mathbf{r}}B_{\mathbf{rr}}^{-1}\mathbf{g}_{(k)} \ , \tag{5.40}$$

of size $(K+1)\times 1$ can be provided by the thermal element evaluator to the non-linear solver, regardless of the number of mesh nodes. Differently from the *sparse stamp* approach, this one requires the ability to solve a linear system during the element evaluation phase. An efficient implementation can turn this constraint into an advantage if specialized solvers are used for the heat-diffusion equation. In the last case, in fact, the PDE part of the thermal element is treated in an optimal way, while a *sparse stamp* would have left all the computational burden onto the circuit solver, which is indeed optimized for MNA-like equations.

Chapter summary In this chapter a suitable algorithm to approximate numerically the model established in Part I and analyzed in Part II has been proposed. A general multi-step method was employed to time discretize the system, while Newton's method was used to solve the resulting non-linear algebraic equations. The stamp associated with the novel thermal element was discussed in details and two approaches returning respectively a sparse and a dense Jacobian contribution were presented. Numerical examples to validate the algorithm will be given in Part IV.

Part IV

Numerical validation

6
CMOS inverter

As a preliminary validation of the method proposed in the thesis, results obtained by its application to a simple benchmark problem are presented in this chapter. Particular attention is given to the reduced number of unknowns stemming from the patched finite element method, if compared to a standard approach, and to the natural way in which mutual heating is taken into account by the method. Notice that in this and in the following chapter a simple backward Euler scheme is adopted to time-discretize the coupled system.

6.1 Description of the circuit

Consider the CMOS-inverter circuit represented in Figure 6.1. This circuit constitutes the basic building-block of the whole digital electronics. Its logical behavior is that of the `NOT` function, i.e. an high output corresponds to a low input and vice-versa. It can be noticed that the electro-thermal schematic consists of two MOS-FETs (denoted by M_3 and M_4), two DC voltage source (denoted by V_1 and V_6), an input voltage source (denoted by V_2) and a distributed thermal element (denoted by T_5).

The two MOS-FETs are modeled by a simplified version of the classic Shichman-Hodges model [85] with an added temperature pin, as reported in [8]. The actual parameters used in the simulations are copied in Table 6.1. The impact of temperature

	W/L	μ_0	θ_0	V_{th}	r_d	C_{gb}	C_{gd}	C_{gs}	C_{sb}	C_{db}
nMOS	5	1e5	300	.1	1e6	1e−11	1e−12	1e−12	1e−12	1e−12
pMOS	5	1e5	300	−.1	1e6	1e−11	1e−12	1e−12	1e−12	1e−12

Table (6.1): *Parameters of the simplified Shichman-Hodges MOS-FET models employed in the simulation. Notice that the employed parameters are academic and not derived from technological considerations.*

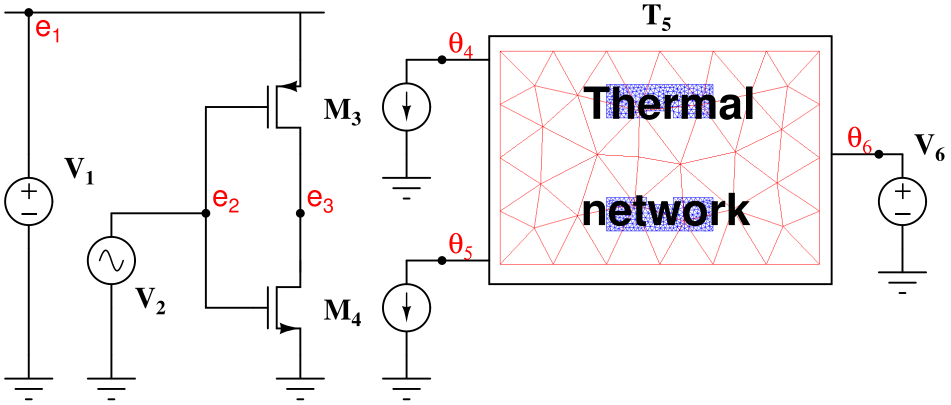

Figure (6.1): *CMOS-inverter electro-thermal network. Inside the thermal element the 2D mesh used for the approximation of heat diffusion on a distributed domain is shown. Notice that θ_4 is the junction temperature referring to the p-channel MOS-FET M_3, while θ_5 is the one referring to the n-channel MOS-FET M_4. Finally θ_6 refers to the environment temperature.*

is represented by a temperature dependent carrier mobility:

$$\mu(\theta) = \mu_0 \left(\frac{\theta}{\theta_0}\right)^{-3/2} , \tag{6.1}$$

where μ denotes the electron mobility for the n-channel transistor M_4 and the hole mobility for the p-channel transistor M_3 and μ_0 is the value of μ at the reference temperature θ_0. The total dissipated Joule-power is given by the simple expression:

$$P = i_{ds} v_{ds} , \tag{6.2}$$

where i_{ds} denotes the current flowing in the controlled current source appearing in the transistor model and v_{ds} is the drain-to-source-voltage. Notice that (6.2) fits the assumptions made in Section 3.3 as P depends on node potentials and junction temperatures.

The thermally active regions on the IC substrate (blue meshes in Figure 6.1) are taken to roughly correspond to the channel region of the transistors. Figure 6.2 and Figure 6.3 show respectively a standard conforming triangulation and a patched triangulation of the 2D layout. It can be seen that, while maintaining the same mesh refinement in the channel regions, the patched mesh greatly reduces the number of unknowns. The adopted thermal element is supposed to be linear with constant coefficients. The corresponding parameters are given in Table 6.2, while a plot of the thermal element stamp sparsity-pattern is provided in Figure 6.4.

It should be noticed that the values used for this simulation are not meant to mimic any type of existing technology. The only purpose of this academic example is to show

$\hat{c}_v$	$\hat{\kappa}$	$\hat{c}$	$\hat{\alpha}$
1.5e−6	1.5e−6	1	1e1

Table (6.2): *Thermal element parameters employed in the simulation of the CMOS-inverter circuit. Notice that the employed parameters are academic and not derived from technological considerations.*

the merits of the approach proposed in the thesis on a relatively simple problem. A more complex application will be treated then in Chapter 7.

6.2 Simulation results

A transient simulation of the response of the circuit to a 1 kHz sinusoidal input signal is performed [20, 21]. The plot in Figure 6.5 shows the voltage waveforms and the corresponding values of the device temperatures. As is expected the junction temperatures θ_4 and θ_5 are close to the ambient temperature value $\theta_6 = 300K$ when the output is either in the ON or in the OFF state, as in such situation only small leakage currents flow in the devices, while the current flowing during the ON-to-OFF or OFF-to-ON transitions generates a relatively more significant heating. Figure 6.6 depicts the temperature distribution in the IC substrate at different instants during an OFF-to-ON transition. It can be noted that the heat produced mainly by the p-channel device (above), diffuses through the substrate and affects the n-channel device (below).

Chapter summary An application of the algorithm depicted in Part III to a simple CMOS inverter circuit has been shown. Particular attention has been given to the reduced number of unknowns stemming from the patched finite element method, and to the way in which electrical and thermal variables interact in the coupled system. In the next chapter an application to a more realistic benchmark will be provided.

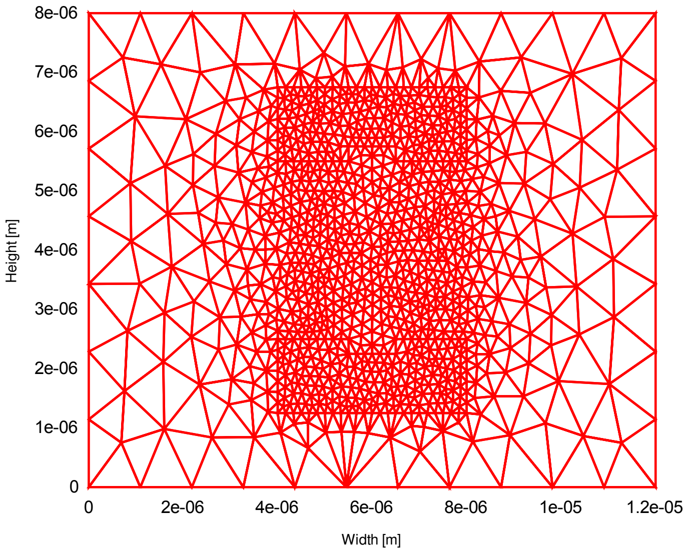
8e-06
7e-06
6e-06
5e-06
4e-06
3e-06
2e-06
1e-06
0
Height [m]
0
2e-06
4e-06
6e-06
8e-06
1e-05
1.2e-05
Width [m]

Figure (6.2): *Globally conforming triangulation of 2D chip-layout: 1052 nodes, 2066 elements and 1052 unknowns.*

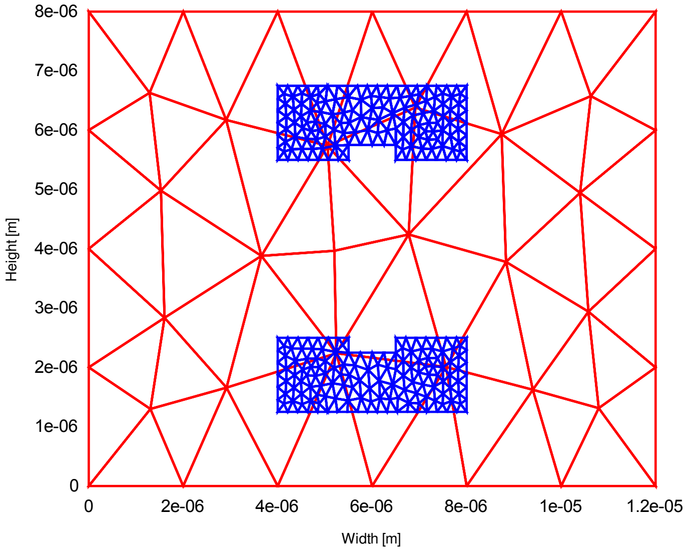
8e-06
7e-06
6e-06
5e-06
4e-06
3e-06
2e-06
1e-06
0
Height [m]
0
2e-06
4e-06
6e-06
8e-06
1e-05
1.2e-05
Width [m]

Figure (6.3): *Patched triangulation of 2D chip-layout: 339 nodes, 550 elements and 237 unknowns.*

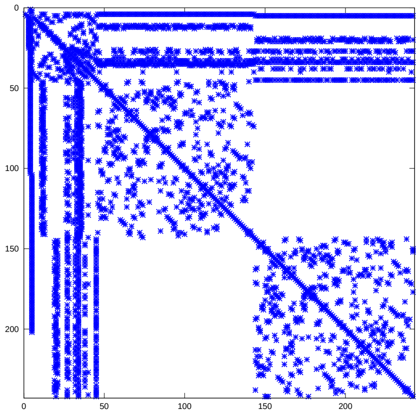

Figure (6.4): *Thermal element stamp sparsity pattern. Notice that the usage of a PDE in the thermal element constitutive relations produces an highly sparse stamp contribution to the overall system.*

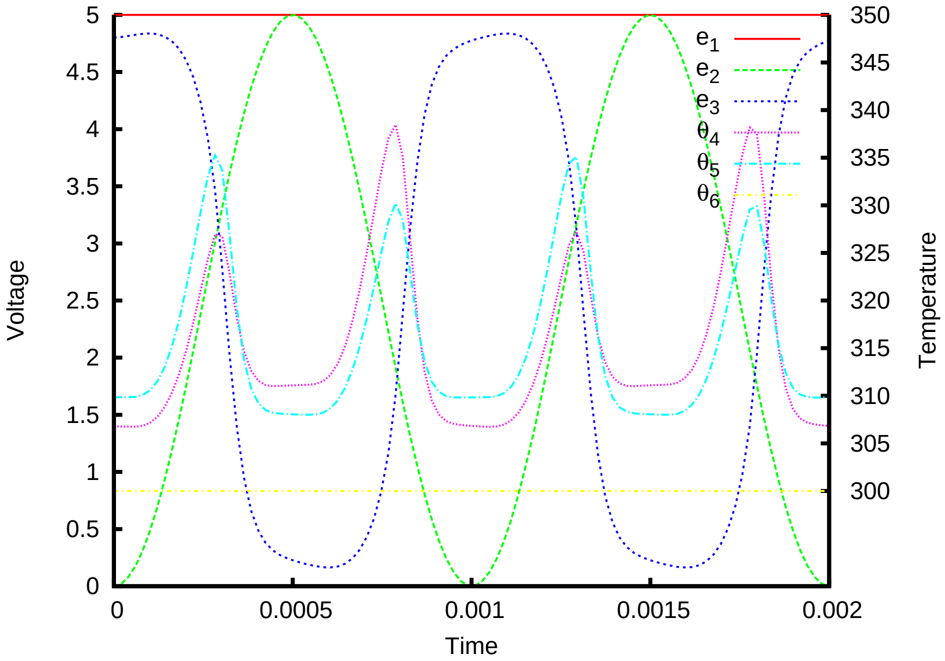

Figure (6.5): *Node voltages and junction temperatures plotted against time for two periods of an input sine voltage at the frequency of* 1 *kHz. A simple backward Euler scheme was adopted to time discretize the coupled system.*

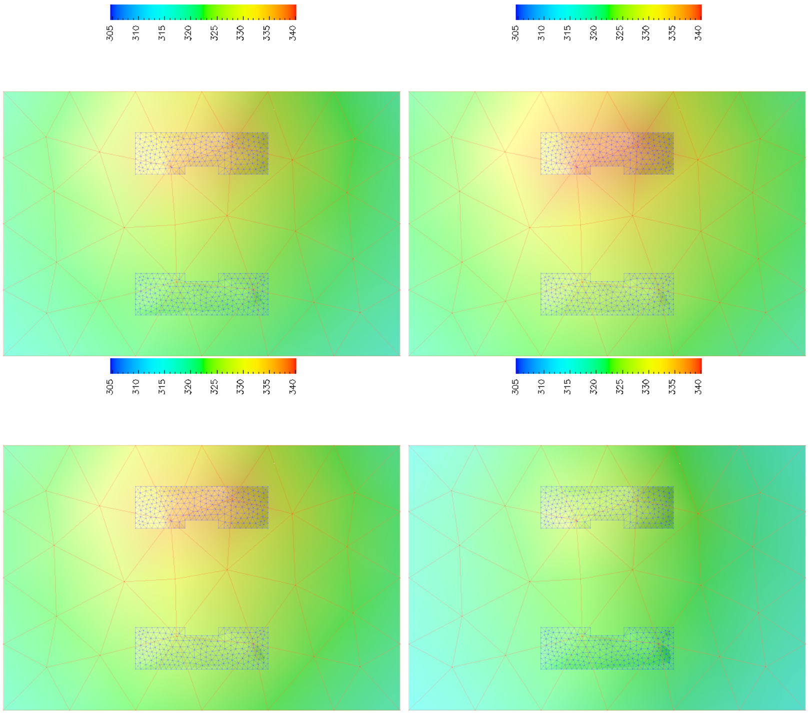

Figure (6.6): *Subsequent snapshots of the distributed temperature field taken during the first switching phase. Notice that the heat produced mainly by the p-channel device (above), diffuses through the substrate and affects the n-channel device (below)*

7

Power nMOS-FET

In this chapter the application of the method discussed in the thesis to a slight simplification of an industrial n-channel MOS-FET designed for power application is proposed. This problem, constituting a major step toward a real industrial test-case, is chosen because of the regularity of its layout that easily permits to show an important characteristic of the method, i.e. the possibility to replicate a fine mesh associated with a thermally active area at different positions in the die. This feature gives the possibility, in an industrial implementation, to create a library of electro-thermal devices in which a pre-computed mesh of their active region is included, diminishing the computational effort and possibly permitting a performance gain if an optimization of the relative device placement is to be performed.

7.1 Description of the device

As a second benchmark a simplification of the MOS-FET described in [11] is taken into account. This device is a vertical n-channel MOS-FET, mainly used for power applications (e.g lighting or high-frequency dc-dc converter). A sketch of its cross-section is shown in Figure 7.1. As it can be seen, the technology employed for its fabrication exploits only one metal layer (source contact) and one polysilicon layer (gate interconnects). The drain contact, not visible in Figure 7.1, is placed at the bottom of the die. To avoid the turn-on of the parasitic npn bipolar transistor, the source is short circuited to the body via the source metal layer.

A simplified layout of the device is shown in Figure 7.2, where several elementary transistors cells are connected in parallel to permit an high current handling capability. The *active device regions* are organized in rows, due to the fabrication technology, and the external signal is transmitted to each elementary cell through the polysilicon gate interconnects. Source metal covers almost all the device surface. The only exceptions are constituted by the regions of the *gate metal fingers* and of the *external gate metal*: here the metal layer is used to create low-resistance gate connections to overcome the poor conductivity of the polysilicon layer. Anyhow, as space has to be left toward the center to allow connection of the source bond wires, these fingers cannot extend from the upper to the lower part of the layout. Some elementary cells are thus left without a direct metal connection causing an higher delay as the gate signal has to reach the basic cells passing through the polysilicon layer.

In [11] a distributed electrical network, which allowed to observe local maxima in the current density distribution, was introduced to model the nMOS-FET. The main idea was to exploit the concepts employed for high frequency modeling of microstrips to describe the electrical behavior of polysilicon and metal interconnects of a power device. Hence the layout design information is used to generate a *lumped-element distributed circuit model* feasible to be analyzed by any spice-like circuit simulator. The resulting netlist has a hierarchical and scalable structure based upon three basic building blocks, representing respectively:

1. metal over passive area,
2. polysilicon over passive area,
3. polysilicon over active area.

For a thorough description of the model the interested reader is referred to [11]. In [44] the model proposed in [11] is extended to account for the self-heating of the cells, still the dependence of the electrical characteristics of each cell on the dissipated power remains purely local. The non-locality introduced in our model by the distributed thermal element provides a further extension as it allows to account for mutual-heating effects previously neglected [22].

7.2 Simulation results

A transient simulation of the turn-off switching of the device is performed to test the proposed method. The set-up employed to investigate its characteristics is reported in Figure 7.3. The input voltage waveform is a step function going from 10V to 0V at $t = 3 \times 10^{-9}$ sec.

The electrical behavior of the power n-channel MOS-FET is described by the same *lumped-element distributed approach* presented in [11], the only difference being in the complexity of the active cell model. In fact a simplified Shichman-Hodges model with an added temperature pin (introduced in Chapter 6) is employed here to describe the elementary transistor cells. Notice that the parameter values used in the following, though fitted to provide realistic results, do not stem from any existing technology. The electrical network is scaled to contain 24 × 24 active cells and 6 metal fingers, as shown in [11, Figure 1(b)]. The values used for each of the basic cells are gathered in Table 7.1, while the parameters of the Shichman-Hodges model are given in Table 7.2.

A picture of the mesh underlying the distributed thermal element is reported in Figure 7.4: a coarse grid covers the 4mm × 4mm die, while a fine one is replicated at each active region position. The model employed to describe heat diffusion is supposed

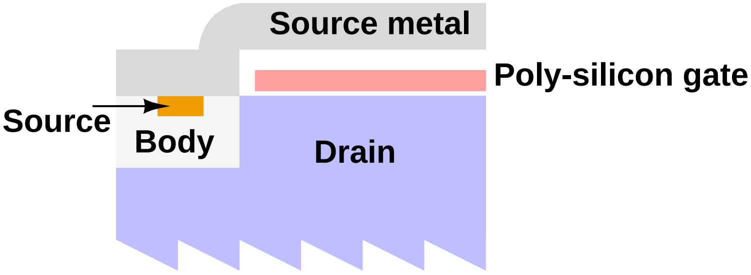
Source metal
Poly-silicon gate
Source
Body
Drain

Figure (7.1): *Sketch of the cross-section of the power n-channel MOS-FET. Notice that only one metal layer and one polysilicon layer are employed during the fabrication process. The drain contact is placed at the bottom of the die.*

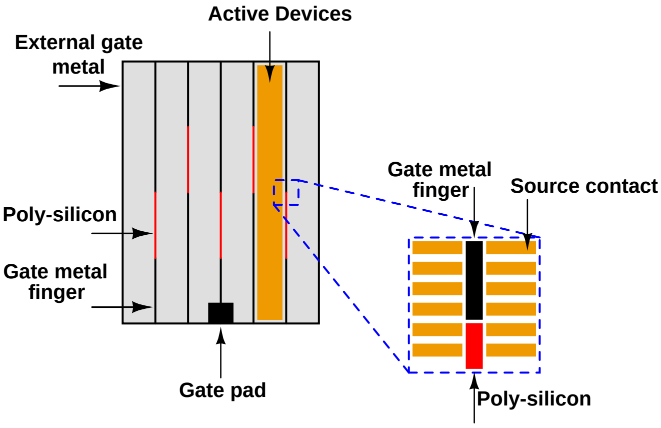
Active Devices
External gate metal
Poly-silicon
Gate metal finger
Gate pad
Gate metal finger
Source contact
Poly-silicon

Figure (7.2): *Schematic layout of the power n-channel MOS-FET. Several active cells are connected in parallel to achieve the required current handling capability. The external gate signal reaches every cell passing through metal fingers (low resistance) or polysilicon interconnects (high resistance).*

	R (series)	L (series)	R (ground)	C (ground)
Metal (passive)	1e1	1e−15	1e12	1e−13
PolySi (passive)	1e2	1e−6	1e12	1e−12
PolySi (active)	1e2	1e−6	-	-

Table (7.1): *Basic cell parameters employed in the simulation of the n-channel MOS-FET turn-off transient. See [11] for more details.*

W/L	μ_0	θ_0	V_{th}	r_d	C_{gb}	C_{gd}	C_{gs}	C_{sb}	C_{db}
2.2	1e6	300	.5	1e9	1e−12	1e−15	1e−15	1e−15	1e−15

Table (7.2): *Parameters of the simplified Shichman-Hodges MOS-FET model used to describe the behavior of each active cell. Notice that the employed parameters are academic and not derived from technological considerations.*

to be linear with constant coefficients (see Table 7.3). Finally the sparsity pattern of the thermal element stamp is given in Figure 7.5.

In Figure 7.6 the total dissipated power and the mean temperature of the device are plotted against time during a turn-off transient. As expected to a lowering of the power corresponds a cooling of the device; however these two effects exhibit different relaxation times. The power densities and junction temperatures of the cells are shown respectively in Figure 7.7 and Figure 7.8 for six different time-points defined in Figure 7.6. It can be clearly seen a delay in the propagation of the signal from the gate-pad in the lower part of the die to the single cells, and the presence of an hot-spot in the central upper part of the die for $t = t_2$ and $t = t_3$. Moreover the presence of a non-negligible temperature gradient over the device area is detected at times $t = t_1$ and $t = t_2$. Furthermore the different spatial distribution of heat density and temperature are an indication that non-local effects may not be negligible in estimating the device performance.

Chapter summary The algorithm presented in Part III was here applied to a realistic benchmark. The possibility to replicate a fine mesh associated with a particular

$\hat{c}_v$	$\hat{\kappa}$	$\hat{c}$	$\hat{\alpha}$
1e−4	2e−2	1e3	4e4

Table (7.3): *Parameters of the thermal element employed in the simulation of the power n-channel MOS-FET turn-off. Notice that the employed parameters are academic and not derived from technological considerations.*

lumped device at different positions in the die was stressed. As a last remark it should be noticed that the implementation of the method in an industrial environment would provide a final practical validation. In this case a study of the trade-off between mesh refinement and solution accuracy would be of great interest, as well as a comparison against measurement data. Toward this aim a work is on-going to implement the algorithm in `TITAN` (Infineon circuit simulator).

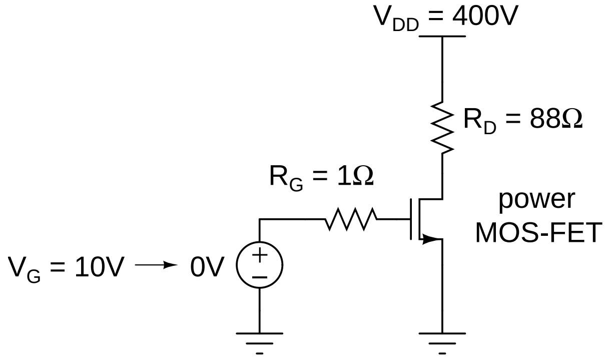
V_{DD} = 400V
R_D = 88Ω
R_G = 1Ω
power MOS-FET
V_G = 10V ⟶ 0V
+
−

Figure (7.3): *Circuit used to simulate the turn-off switching of the power n-channel MOS-FET. The input signal switches at* $t = 3 \times 10^{-9}$ *sec.*

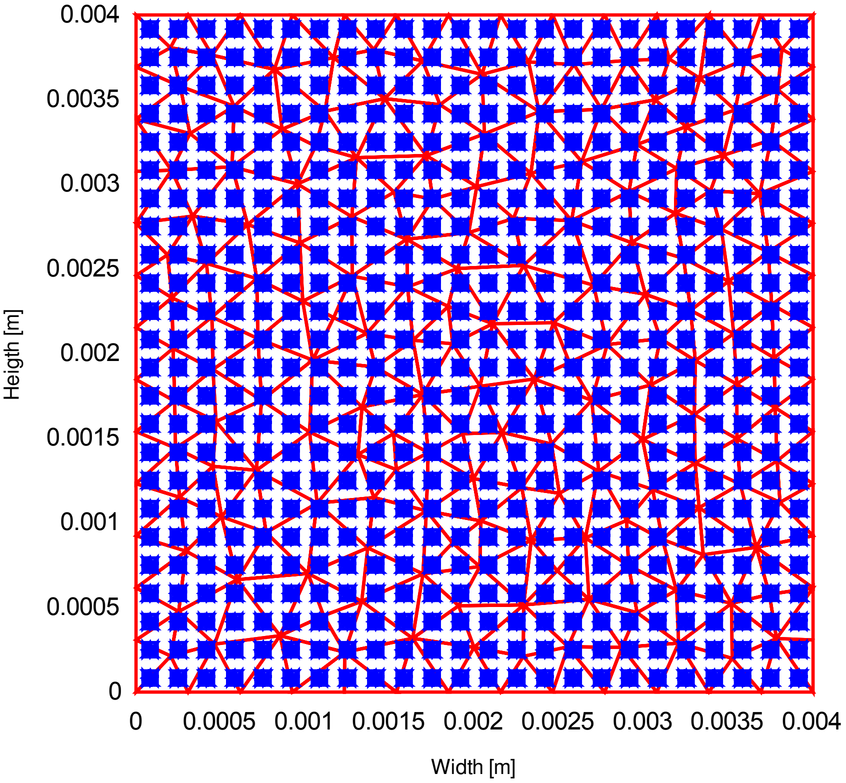
0.004
0.0035
0.003
0.0025
0.002
0.0015
0.001
0.0005
0
Heigth [m]
0
0.0005
0.001
0.0015
0.002
0.0025
0.003
0.0035
0.004
Width [m]

Figure (7.4): *Non-conforming meshes for the whole CHIP and the basic cells. The nMOS-FET model is here scaled to 576 active cells. A coarse grid (in red) covers the* 4*mm* × 4*mm die, while a fine one (in blue) is replicated at each active region position.*

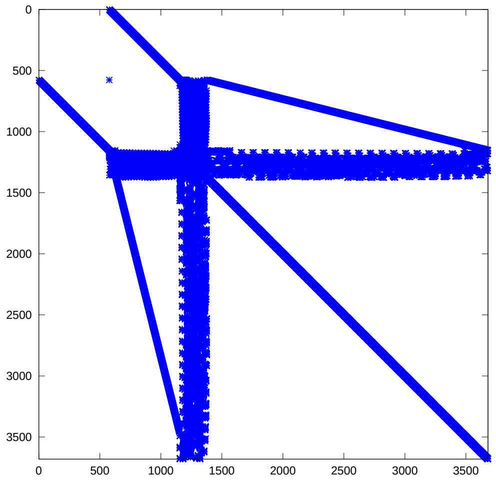

Figure (7.5): *Sparsity pattern of the thermal element stamp. As noted in the previous chapter, the usage of a PDE in the thermal element constitutive relations produces an highly sparse stamp contribution to the overall system.*

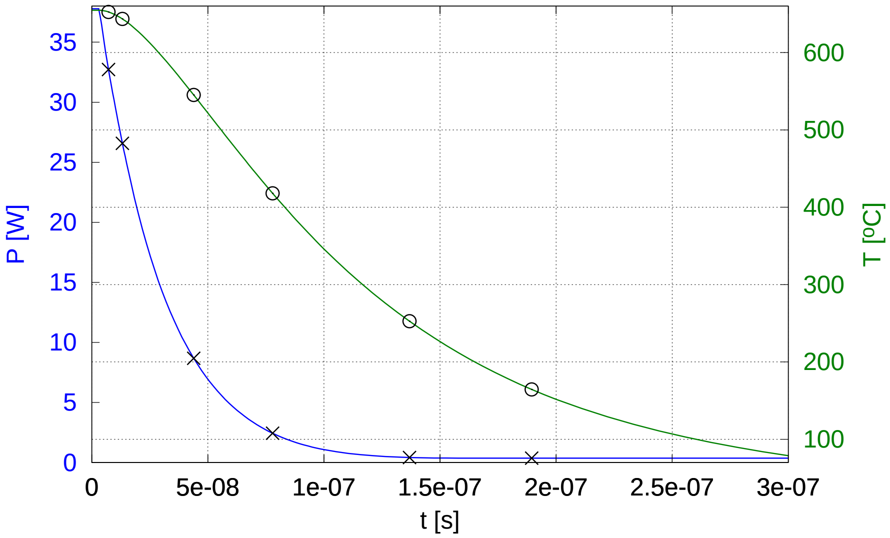

Figure (7.6): *Total dissipated power and mean temperature plotted against time for a turn-off transient. The sampled points refer to the snapshots presented in Figure 7.7 and Figure 7.8. A simple backward Euler scheme was adopted to time discretize the coupled system.*

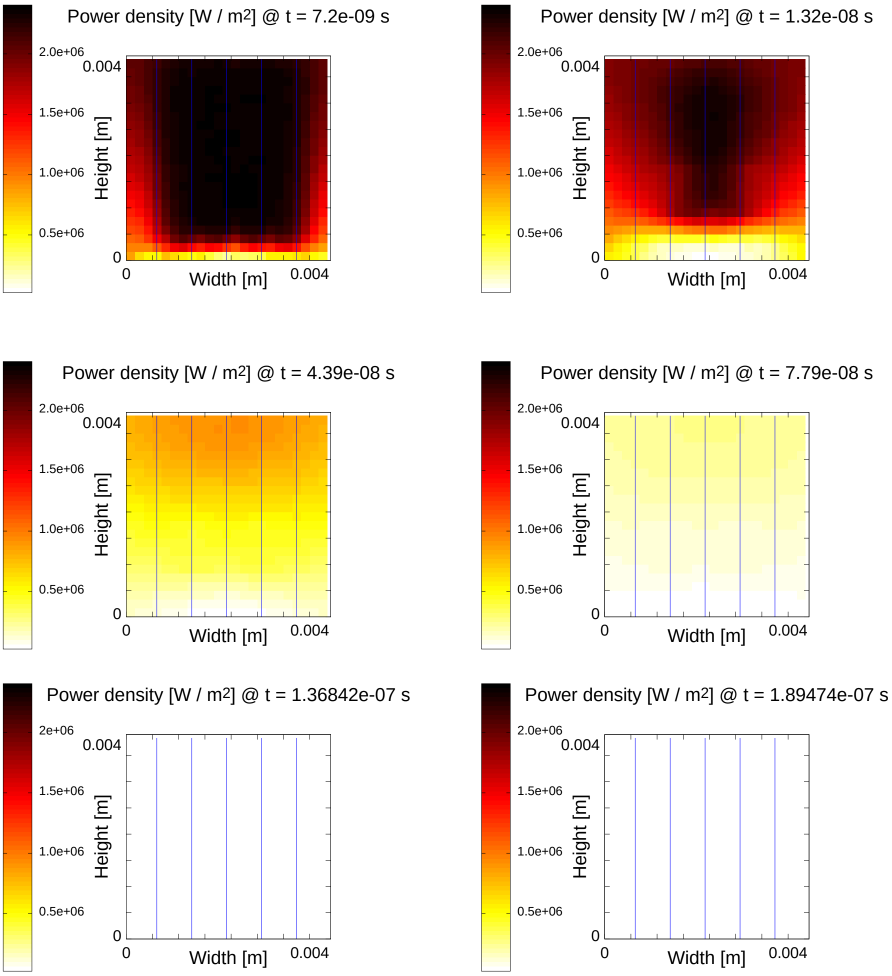

Figure (7.7): *Snapshots of the active cell power densities at the time points t_1, t_2, t_3, t_4, t_5, and t_6 defined in Figure 7.6. Notice that, due to the academic nature of the problem data, only the qualitative behavior of the solution is of interest here.*

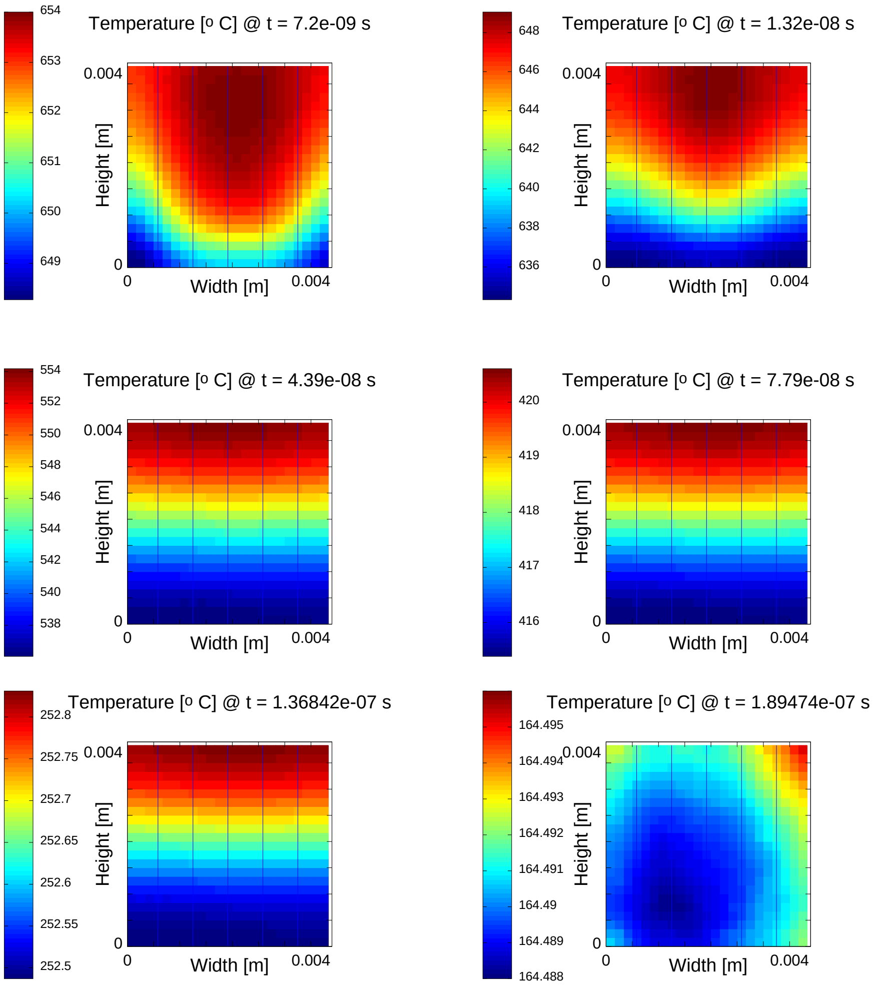

Figure (7.8): *Snapshots of the active cell junction temperatures at the time points* t_1, t_2, t_3, t_4, t_5, *and* t_6 *defined in Figure 7.6. Notice that, due to the academic nature of the problem data, only the qualitative behavior of the solution is of interest here.*

Part V

Appendix

A

Graph theory

Further details on graph theory can be found in [28].

A.1 Basic definitions

Definition A.1 (Graph, Directed graph)**.** *A pair of sets V and E is called graph if it satisfies:*

$$E \subseteq V \times V, \tag{A.1}$$

The elements of V are called nodes *or* vertices *of the graph, while the elements of E are called* branches *or* edges*. The graph will be denoted with $G = (V, E)$. If branches are given an orientation, then the graph is said to be* directed.

Definition A.2 (Path, Connected graph)**.** *A non empty graph $P = (V, E)$ is called a* path *if it is of the form:*

$$V = \{x_0, x_1, \dots, x_k\} \quad , \quad E = \{x_0x_1, x_1x_2, \dots, x_{k-1}x_k\}, \tag{A.2}$$

x_0 and x_k will be referred as the ending nodes of the path, while $x_1, \dots, x_{k-1}$ as the inner nodes. If a non-empty graph is such that any two of its nodes can be linked by a path, then the graph is said to be connected*, otherwise* unconnected.

Definition A.3 (Cycle / Loop)**.** *Given a path $P = (V, E)$ with $k \geq 3$ we call:*

$$C := (V, E') \tag{A.3}$$

a cycle *if $E' := E + \{x_kx_0\}$.*

Definition A.4 (Cutset)**.** *A set of branches $F \subset E$ of a connected graph $G = (V, E)$ is called a* cutset *if:*

- *removing all the branches $f \in F$ from G leads to an unconnected graph.*

- *removing all the branches $f \in F$ but one from G leaves the graph connected.*

Definition A.5 (Incidence matrix)**.** *Given a directed graph with n nodes and m branches, a matrix $A \in \mathbb{R}^{n \times m}$ is called incidence matrix of the graph if:*

$$a_{ij} = \begin{cases} +1 & \text{if branch } j \text{ leaves node } i, \\ -1 & \text{if branch } j \text{ enters node } i, \\ 0 & \text{otherwise.} \end{cases} \tag{A.4}$$

Notice that the matrix A is not a full-rank matrix by construction. To obtain a full-rank matrix a row must be eliminated from A. It is common practice in circuit modeling to neglect the row corresponding to the ground node. The matrix obtained in this way is called *reduced* incidence matrix.

A.2 Kirchhoff's laws

Kirchhoff's voltage law and Kirchhoff's current law can also be expressed in terms of graph notions [15]:

Statement A.1 (Kirchhoff's voltage law)**.** *The algebraic sum of voltage drops around any cycle of the circuit graph is always zero, i.e.:*

$$A^T \mathbf{e} = \mathbf{v} \ , \tag{A.5}$$

where A is the incidence matrix of the graph, $\mathbf{e}$ the node voltage vector and $\mathbf{v}$ the voltage drops vector.

Statement A.2 (Kirchhoff's current law)**.** *The algebraic sum of branch currents traversing each cutset of the circuit graph is always zero. As a particular case we find:*

$$A\mathbf{j} = 0 \ , \tag{A.6}$$

where A is the incidence matrix of the graph and j is the branch current vector.

Note that $\mathbf{e}$ are quantities living on circuit graph nodes, while $\mathbf{j}$ and $\mathbf{v}$ are quantities living on graph branches.

$\mathcal{B}$

DAE theory

The general form of a DAE system can be expressed as:

$$\mathcal{F}\left(\frac{d\mathbf{x}}{dt}, \mathbf{x}, t\right) = 0, \tag{B.1}$$

where:

$$\mathcal{F} : \mathbb{R}^n \times \mathbb{R}^n \times \mathbb{R} \to \mathbb{R}^n, \tag{B.2}$$

and $\partial_y \mathcal{F}(\mathbf{y}, \mathbf{x}, t)$ is singular. Constituting a generalization to ODEs concept, DAEs behavior mainly differs in two points:

1. some components of the solution may be determined by constraints, so that initial values must be chosen consistently,

2. some part of the DAE may require additional smoothness, i.e. it must be differentiable a sufficient number of time.

To categorize in a precise manner the "distance" of a given DAE system to an ODE system various *index* concepts have been introduced in literature.

B.1 Linear DAEs with constant coefficients: Kronecker index

A linear DAE system with constant coefficients has the form:

$$A\dot{\mathbf{x}}(t) + B\mathbf{x}(t) = \mathbf{f}(t), \tag{B.3}$$

with $A, B \in \mathbb{R}^{n\times n}$.

Theorem B.1 (Kronecker form)**.** *If A and B form a regular matrix pencil [51], then there exist non-singular matrices U and V such that:*

$$UAV = \begin{bmatrix} I & 0 \\ 0 & N \end{bmatrix} \quad , \quad UBV = \begin{bmatrix} C & 0 \\ 0 & I \end{bmatrix} \ . \tag{B.4}$$

N is nilpotent of index μ, due to the way it is constructed.

Definition B.1 (Kronecker index)**.** *If A and B in* (B.3) *form a regular matrix pencil, then the* Kronecker index *of the corresponding DAE is said to be* 0 *if A is invertible, and μ otherwise.*

B.2 Extension of index concepts to non-linear DAEs

The Kronecker index concept presented for linear DAEs with constant coefficients can be generalized to a wide variety of concepts when treating the case of a non-linear DAE of the form (B.1).

Definition B.2 (Differentiation index [37,38])**.** *Suppose μ is the minimum number of analytical differentiations:*

$$\mathcal{F}\left(\frac{d\mathbf{x}}{dt}, \mathbf{x}, t\right) = 0 \quad , \quad \frac{d}{dt}\mathcal{F}\left(\frac{d\mathbf{x}}{dt}, \mathbf{x}, t\right) = 0 \ , \ldots , \ \frac{d^{\mu}}{dt^{\mu}}\mathcal{F}\left(\frac{d\mathbf{x}}{dt}, \mathbf{x}, t\right) = 0 \ , \tag{B.5}$$

such that it is possible to extract an explicit ODE system from the the set of equations (B.5)*. Then μ is said to be the* differentiation *(or differential) index of system* (B.1)*.*

Definition B.3 (Perturbation index [51])**.** *Equation* (B.1) *has* perturbation index μ *along a solution x on a closed interval $\mathcal{I} = [0, T]$ if μ is the smallest integer such that for functions $\hat{x}$ having a (sufficiently small) defect:*

$$\mathcal{F}\left(\frac{d\hat{\mathbf{x}}}{dt}, \hat{\mathbf{x}}, t\right) = \boldsymbol{\delta}(t) \ , \tag{B.6}$$

there exists on $\mathcal{I}$ an estimate:

$$\|\hat{\mathbf{x}}(t) - \mathbf{x}(t)\| \le C\left(\|\hat{\mathbf{x}}(0) - \mathbf{x}(0)\| + \sum_{\alpha=1}^{\mu} \max_{t\in(0,T)} \left\|\boldsymbol{\delta}^{\alpha-1}(t)\right\|\right) \ . \tag{B.7}$$

In [47] it is proved that differentiation and perturbation index are always equal for DAE systems stemming from MNA, while in [29] it is proved that differentiation and tractability index coincide and that, under certain assumptions, an electrical circuit cannot exceed index two.

C
PDE theory

C.1 Function spaces

Definition C.1 ($\mathbb{L}^p(\Omega)$ spaces)**.** *Let $\Omega \subset \mathbb{R}^d$ be an open set, $d \geq 1$, and consider in Ω the Lebesgue measure. For $1 \leq p \leq \infty$ it is possible to define the sets of measurable functions:*

$$\begin{aligned} \mathbb{L}^p(\Omega) &:= \left\{ u \text{ measurable} \mid \int_\Omega |u(\mathbf{x})|^p d\mathbf{x} < \infty \right\} \qquad 1 \leq p < \infty, \\ \mathbb{L}^p(\Omega) &:= \left\{ u \text{ measurable} \mid \operatorname{ess\,sup}_{\mathbf{x}\in\Omega} |u(\mathbf{x})| < \infty \right\} \quad p = \infty. \end{aligned} \tag{C.1}$$

The space $\mathbb{L}^p(\Omega)$ is a Banach space if endowed with the norm:

$$\begin{aligned} \|u\|_{\mathbb{L}^p(\Omega)} &:= \left(\int_\Omega |u(\mathbf{x})|^p d\mathbf{x} \right)^{\frac{1}{p}} \quad 1 \leq p < \infty, \\ \|u\|_{\mathbb{L}^\infty(\Omega)} &:= \operatorname{ess\,sup}_{\mathbf{x}\in\Omega} |u(\mathbf{x})| \qquad p = \infty. \end{aligned} \tag{C.2}$$

Furthermore the space $\mathbb{L}^2(\Omega)$ is an Hilbert space, endowed with the scalar product:

$$(u, v)_{\mathbb{L}^2(\Omega)} := \int_\Omega u(\mathbf{x}) v(\mathbf{x}) d\mathbf{x}. \tag{C.3}$$

Further details on Lebesgue spaces can be found in [78, Chapter 3].

Definition C.2 (Sobolev spaces)**.** *Let k be a non-negative integer and $1 \leq p \leq \infty$. Then it is possible to define the Sobolev space:*

$$W^{k,p}(\Omega) := \{ u \in \mathbb{L}^p(\Omega) \mid D^{\boldsymbol{\alpha}} u \in \mathbb{L}^p(\Omega) \textit{ for } |\boldsymbol{\alpha}| < k \}, \tag{C.4}$$

where $\boldsymbol{\alpha}$ is a non-negative multi-index defined as in [75, Chapter 1, pag.6]

The space $W^{k,p}(\Omega)$ is a Banach space if endowed with the norm:

$$\begin{aligned} \|u\|_{W^{k,p}(\Omega)} &:= \left(\sum_{|\boldsymbol{\alpha}|\leq k} \|D^{\boldsymbol{\alpha}}u\|^p_{\mathbb{L}^p(\Omega)}\right)^{\frac{1}{p}} \quad 1 \leq p < \infty, \\ \|u\|_{W^{k,p}(\Omega)} &:= \operatorname{ess\,sup}_{\boldsymbol{\alpha}\leq k} \|D^{\boldsymbol{\alpha}}u\|_{\mathbb{L}^\infty(\Omega)} \quad p = \infty. \end{aligned} \tag{C.5}$$

The associated seminorm will be denoted with $|u|_{W^{k,p}(\Omega)}$. When $p = 2$ the Sobolev space $W^{k,2}(\Omega)$ is indeed an Hilbert space, usually denoted as $\mathbb{H}^k(\Omega)$. The corresponding scalar product results to be:

$$(u, v)_{\mathbb{H}^k(\Omega)} := \sum_{|\boldsymbol{\alpha}|\leq k} (D^{\boldsymbol{\alpha}}u, D^{\boldsymbol{\alpha}}v)_{\mathbb{L}^2(\Omega)}. \tag{C.6}$$

It will be useful in the following to define:

$$\mathbb{H}^1_0(\Omega) := \{v \in \mathbb{H}^1(\Omega) \mid v = 0 \text{ on } \partial\Omega\} \subset \mathbb{H}^1(\Omega) \ . \tag{C.7}$$

A thorough treatment of Sobolev spaces and their properties (including a mathematically sound definition of the trace space $\mathbb{H}^{1/2}(\Omega)$) can be found in [1].

C.2 Variational formulation of elliptic problems

In the following a variational formulation is derived for the model problem:

$$\begin{aligned} \mathcal{L}\, T(\mathbf{x}) &= f(\mathbf{x}) \quad \text{in } \Omega, \\ T(\mathbf{x}) + \alpha \frac{\partial\, T(\mathbf{x})}{\partial\, \mathbf{n}_{\mathcal{L}}} &= g(\mathbf{x}) \quad \text{on } \partial\Omega, \end{aligned} \tag{C.8}$$

where $f(\mathbf{x}) \in \mathbb{L}^2(\Omega)$, $\alpha \geq 0$ and the elliptic operator:

$$\mathcal{L}\, T(\mathbf{x}) := -\sum_{i,j=1}^{d} D_i \Big[\kappa_{ij}(\mathbf{x}) D_j T(\mathbf{x})\Big] + c(\mathbf{x})T(\mathbf{x}), \tag{C.9}$$

was defined in Section 3.1. A deeper treatment of the subject can be found in [30].

Homogeneous Dirichlet BC In this case it is assumed that $g \equiv 0$ and $\alpha = 0$. Defining then the bilinear form:

$$a(T, v) := \int_\Omega \big(\sum_{i,j=1}^{d} \kappa_{ij}(\mathbf{x})\ D_j T\ D_i v\big)\ d\mathbf{x} + \int_\Omega c(\mathbf{x})\ T\ v\ d\mathbf{x}, \tag{C.10}$$

as in (3.4), the weak formulation of (C.8) reads:

$$\text{find } T \in \mathbb{H}^1_0(\Omega)\ :\ a(T, v) = (f, v)_{\mathbb{L}^2(\Omega)} \quad \forall v \in \mathbb{H}^1_0(\Omega). \tag{C.11}$$

Non-homogeneous Dirichlet BC This is the case for $\alpha = 0$ but $g \in \mathbb{H}^{1/2}(\partial\Omega) \neq 0$. A possible way to analyze the problem is presented in [75, Chapter 6, pag. 166]. The function g is extended in the whole Ω. Denote with $\tilde{g}$ this extension and assume:

$$T = \tilde{T} + \tilde{g} \ . \tag{C.12}$$

Then $\tilde{T} \in \mathbb{H}^1_0(\Omega)$ and:

$$a(T, v) = a(\tilde{T} + \tilde{g}, v) = (f, v)_{\mathbb{L}^2(\Omega)} \ . \tag{C.13}$$

Moving all the known terms to the right hand-side, the equivalent homogeneous problem for $\tilde{T}$ is obtained:

$$\text{find } \tilde{T} \in \mathbb{H}^1_0(\Omega) \ : \ a(\tilde{T}, v) = (f, v)_{\mathbb{L}^2(\Omega)} - a(\tilde{g}, v) \quad \forall v \in \mathbb{H}^1_0(\Omega). \tag{C.14}$$

This problem can be solved as in the previous case. Notice that the requirement:

$$g \in \mathbb{H}^{1/2}(\partial\Omega) \ ,$$

is the weakest one ensuring the well posedness of (C.14) (for the definition of the space $\mathbb{H}^{1/2}(\partial\Omega)$ see [1, Chapter 7]).

Robin BC The last case of interest for the thesis, is when $\alpha > 0$ and $g \in \mathbb{L}^2(\partial\Omega)$. In this case a variational formulation of the problem reads:

$$\text{find } T \in \mathbb{H}^1(\Omega) \ : \ a(T, v) + \frac{1}{\alpha}(T, v)_{\mathbb{L}^2(\partial\Omega)} = (f, v)_{\mathbb{L}^2(\Omega)} + \frac{1}{\alpha}(g, v)_{\mathbb{L}^2(\partial\Omega)} \quad \forall v \in \mathbb{H}^1(\Omega). \tag{C.15}$$

Again, the requirement $g \in \mathbb{L}^2(\partial\Omega)$ is the weakest one ensuring the well posedness of (C.15).

D

Resolution of diffusion-reaction equation layers

Diffusion-reaction equations with non-smooth coefficients can possibly exhibit thin internal and boundary layers where the solution varies rapidly. This could be the case, for instance, of the PDE used in Chapter 2 to describe heat diffusion at the system level if the distributed thermal capacitance or diffusivity result to be discontinuous. Layer resolving methods for this type of problems in one dimension are either based on fitted difference operators or on fitted meshes. Among those of the latter class, methods based on Shishkin-type meshes [31] are especially attractive because of their simplicity. Their applicability to multidimensional problems is, though, constrained by the difficulty of generating structured conforming meshes for general domain geometries.

In the following a novel numerical method to resolve internal and boundary layers is devised, based on the same mesh structure presented in Chapter 4. This gives the possibility to reduce the requirements on mesh generation software when strong local refinement is needed to capture features of the solution that appear on different scales. To validate the proposed algorithm numerical results on a problem, which can be seen as a 2D extension of the problem derived in [25], are presented.

D.1 Model problem exhibiting internal layers

Assume the open bounded domain $\Omega \subset \mathbb{R}^d$ $(d = 1, 2)$ to be partitioned into two subdomains Ω_1, Ω_2 such that:

$$\begin{array}{ccccc} \Omega_1 & \cap & \Omega_2 & \equiv & \emptyset \, , \\ \bar{\Omega}_1 & \cup & \bar{\Omega}_2 & \equiv & \bar{\Omega} \, . \end{array} \tag{D.1}$$

Define the internal interface to be:

$$\Gamma := \Omega \setminus (\Omega_1 \cup \Omega_2) \, . \tag{D.2}$$

Let the external boundary be defined as:

$$\partial\Omega \equiv \Gamma_N \cup \Gamma_D \ , \tag{D.3}$$

with the Neumann and Dirichlet part satisfying the requirements:

$$\begin{array}{ccccc} \Gamma_N & \cap & \Gamma_D & \equiv & \emptyset \ , \\ \Gamma_D & \cap & \Omega_1 & \neq & \emptyset \ , \\ \Gamma_D & \cap & \Omega_2 & \neq & \emptyset \ . \end{array} \tag{D.4}$$

The model problem considered in the following reads:

$$\begin{cases} -\text{div}\ \sigma(u) + ru = f & \text{in } \Omega \setminus \Gamma \ , \\ \sigma(u) = \varepsilon\kappa_i \nabla u, \ \kappa_i > 0 & \text{in } \Omega_i \quad i = 1, 2 \ , \\ u|_{\Gamma_D} = g_D, & \sigma(u) \cdot n|_{\Gamma_N} = 0 \ , \end{cases} \tag{D.5}$$

where the reaction term r and the right hand side f are defined as:

$$r = \begin{cases} r_1 \geq \beta > 0 \text{ in } \Omega_1 \ , \\ r_2 \equiv 0 \text{ in } \Omega_2 \ , \end{cases} \qquad f = \begin{cases} f_1 \text{ in } \Omega_1 \ , \\ f_2 \text{ in } \Omega_2 \ . \end{cases} \tag{D.6}$$

Furthermore the constraint that u and the component of $\sigma(u)$ along the direction normal to Γ be continuous over all Γ holds. In (D.5) $\varepsilon > 0$ is a small perturbation parameter, n denotes the outward unit normal to $\partial\Omega$ and n_i the outward unit normal to $\partial\Omega_i$. For the sake of simplicity and to prevent the appearance of boundary layers occurring in u we impose the further boundary condition:

$$g_D|_{\Gamma_D \cap \partial\Omega_1} = \left.\frac{f}{r}\right|_{\Gamma_D \cap \partial\Omega_1} \ . \tag{D.7}$$

D.2 Solution decomposition

Problem (D.5) can be restated in a multidomain formulation introducing:

$$\begin{cases} -\text{div}\ \sigma(v_i) + r_i v_i = f_i & \text{in } \Omega_i \quad i = 1, 2, \\ v_i|_{\Gamma_D \cap \partial\Omega_i} = g_D|_{\Gamma_D \cap \partial\Omega_i} \quad , \quad \sigma(v_i) \cdot n_i|_{\Gamma_N \cap \partial\Omega_i} = 0 \ , & \\ v_i|_{\Gamma} = \left.\dfrac{f_1}{r_1}\right|_{\Gamma} =: g_\Gamma \ , & \end{cases} \tag{D.8}$$

and:

$$\begin{cases} -\text{div}\ \sigma(w_1) + r_1 w_1 = 0 \ , & \text{in } \Omega_1, \\ w_1|_{\partial\Omega_1 \cap \Gamma_D} = 0 \quad , \quad \sigma(w_1) \cdot n_p|_{\partial\Omega_p \cap \Gamma_N} = 0 \ , & \end{cases} \tag{D.9}$$

$$\begin{cases} -\text{div }\sigma(w_2) = 0 \ , & \text{in } \Omega_2, \\ w_2|_{\partial\Omega_2 \cap \Gamma_D} = 0 \quad , \quad \sigma(w_2) \cdot n_2|_{\partial\Omega_2 \cap \Gamma_N} = 0 \ , & \end{cases} \tag{D.10}$$

Furthermore the following conditions at the internal interface are required:

$$\begin{cases} \displaystyle\sum_{i=1,2} (\sigma(v_i) + \sigma(w_i)) \cdot n_i|_\Gamma = 0 \ , \\ w_1|_\Gamma = w_2|_\Gamma =: w_\Gamma \ . \end{cases} \tag{D.11}$$

The solution u of (D.5) is related to v_i, w_i by:

$$\begin{aligned} u|_{\Omega_i} &= v_i + w_i \quad , \quad i = 1, 2 \ , \\ u|_\Gamma &= g_\Gamma + w_\Gamma \ , \end{aligned} \tag{D.12}$$

The case where $d = 1$ is of particular interest. In this case Ω reduces to an interval $(a, b) \subset \mathbb{R}$ and without loss of generality we can assume $a = 0, b = 1$. Furthermore Γ will be a single point in $\mathbb{R}$ s.t. $0 < \Gamma < 1$ thus:

$$\begin{aligned} \Omega_1 &\equiv (0, \Gamma) \ , \\ \Omega_2 &\equiv (\Gamma, 1) \ . \end{aligned} \tag{D.13}$$

Assume finally that:

$$\partial\Omega \equiv \Gamma_D \equiv \{0, 1\} \quad , \quad \Gamma_N \equiv \emptyset \quad , \quad g_D(0) = \frac{f(0)}{g_D(0)} \ . \tag{D.14}$$

Following the arguments in [25] it is possible to state the following:

Lemma D.1. *Let* $d = 1$ *and* k *be an integer satisfying* $0 \le k \le 4$. *Then the solution* u *of the problem* (D.8)-(D.12) *satisfies the pointwise bounds*

$$\begin{cases} \left|\dfrac{d^k v_1}{dx^k}(x)\right| \le C + C\varepsilon^{1-\frac{k}{2}} e^{-(\Gamma - x)\sqrt{\beta/\varepsilon}}, & \forall x \in \Omega_1 \\ \left|\dfrac{d^k v_2}{dx^k}(x)\right| \le C, & \forall x \in \Omega_2 \end{cases}$$

$$\begin{cases} \left|\dfrac{d^k w_1}{dx^k}(x)\right| \le C\varepsilon^{-\frac{k}{2}} e^{-(\Gamma - x)\sqrt{\beta/\varepsilon}}, & \forall x \in \Omega_1 \\ \left|\dfrac{d^k w_2}{dx^k}(x)\right| \le C, & \forall x \in \Omega_2 \end{cases}$$

where C *is a constant independent of* ε.

Notice that the term w_1 in (D.12) is negligible at a distance to the left of Γ, which is proportional to $\sqrt{\varepsilon}$.

D.3 Discretization of the model problem

To construct a parameter-uniform numerical method [31] the quantity τ_ε, which represents the *width of the interior layer*, is introduced. Define the *interior layer region* as the subdomain:

$$\Omega_p(\tau_\varepsilon) := \left\{ x \in \Omega_1, |\min_{y\in\Gamma} |x-y| \leq \tau_\varepsilon \right\} \ . \tag{D.15}$$

Following very closely the presentation of [56] the following spaces are introduced:

$$\begin{cases} S_i \equiv \left\{ u \in H^1(\Omega_i) |\ u|_{\partial\Omega_i\cap\Gamma_D} = g|_{\partial\Omega_i\cap\Gamma_D}\ ,\ u|_\Gamma = g_\Gamma \right\}\ , \\ \mathcal{V}_i \equiv \left\{ u \in H^1(\Omega_i) |\ u|_{(\partial\Omega_i\cap\Gamma_D)\cup\Gamma} = 0 \right\}\ , \end{cases} \qquad i = 1,2$$

$$\begin{cases} Z_2 \equiv \left\{ u \in H^1(\Omega_2) |\ u|_{\partial\Omega_2\cap\Gamma_D} = 0 \right\}\ , \\ Z_p \equiv \left\{ u \in H^1(\Omega_p) |\ u|_{\partial\Omega_p\setminus(\Gamma_N\cup\Gamma)} = 0 \right\}\ , \\ \mathcal{V}_p \equiv \left\{ u \in H^1(\Omega_p) |\ u|_{\partial\Omega_p\setminus\Gamma_N} = 0 \right\}\ . \end{cases} \tag{D.16}$$

Let $\mathcal{T}_i^h$ $(i = 1,2,p)$ indicate a quasi-uniform, conforming triangulation [75, Chapter 3] of Ω_i and:

$$\begin{aligned} S_i^h &\subset S_i \quad i = 1,2, \\ \mathcal{V}_i^h &\subset \mathcal{V}_i \quad i = 1,2,p, \\ Z_i^h &\subset Z_i \quad i = 2,p, \end{aligned} \tag{D.17}$$

be continuous finite element spaces consisting of functions that are linear on each element of $\mathcal{T}_i^h$. Away from Γ it is not required any correspondence between the nodes of $\mathcal{T}_p^h$ and those of $\mathcal{T}_1^h$. For sake of simplicity, though, it is assumed for the triangulations $\mathcal{T}_i^h$ to be constructed in such a way that $\mathcal{T}_1^h \cup \mathcal{T}_2^h$ be a globally conforming triangulation of Ω and $\mathcal{T}_p^h \cup \mathcal{T}_2^h$ be a globally conforming triangulation of $\Omega_p \cup \Omega_2$, so that the mesh nodes located on the interface Γ are the same in all three meshes (see Figure D.1). A consequence of this assumption is that the traces on Γ of the functions in any of the sets Z_i^h and S_i^h all belong to the same space T^h; the functions in T^h are piece-wise linear functions defined on Γ. The discretization of problem (D.8), (D.9), (D.10), (D.11) asks for finding:

$$\begin{aligned} v_i^h &\in S_i^h \qquad i = 1,2\ , \\ w_1^h &\in Z_p^h\ , \\ w_2^h &\in Z_2^h\ , \\ \Phi_{\Gamma,i}^h, \Psi_{\Gamma,i}^h &\in T^h \qquad i = 1,2\ , \end{aligned} \tag{D.18}$$

such that:

$$\begin{cases} B_i(\nu, v_i^h) = L_i(\nu) \quad \forall \nu \text{ in } \mathcal{V}_i^h, \\ B_i(\nu, v) = (\nabla \nu, \sigma(v))_{\Omega_i} + (\nu, rv)_{\Omega_i} - (\nu, \Phi_{\Gamma,i}^h)_\Gamma \qquad i = 1, 2, \\ L_i(\nu) = (\nu, f)_{\Omega_i} \ , \end{cases} \tag{D.19}$$

$$\begin{cases} A_p(\nu, w_1^h) = 0 \quad \forall \nu \text{ in } \mathcal{V}_p^h \ , \\ A_p(\nu, w) = (\nabla \nu, \sigma(w))_{\Omega_p} + (\nu, rw)_{\Omega_p} - (\nu, \Psi_{\Gamma,1}^h)_\Gamma \ , \end{cases} \tag{D.20}$$

$$\begin{cases} A_2(\nu, w_2^h) = 0 \quad \forall \nu \text{ in } \mathcal{V}_2^h \ , \\ A_2(\nu, w) = (\nabla \nu, \sigma(w))_{\Omega_2} - (\nu, \Psi_{\Gamma,2})_\Gamma \ , \end{cases} \tag{D.21}$$

$$\begin{cases} \displaystyle\sum_{i=1,2} (\nu, \Phi_{\Gamma,i} + \Psi_{\Gamma,i})_\Gamma = 0, \quad \forall \nu \in T^h \ , \\ w_1^h\big|_\Gamma = w_2^h\big|_\Gamma \ . \end{cases} \tag{D.22}$$

The solution to the initial problem results to be:

$$\begin{aligned} u^h\big|_{\Omega_1 \setminus \Omega_p} &= v_1^h\big|_{\Omega_1 \setminus \Omega_p} \ , \\ u^h\big|_{\Omega_2} &= v_2^h\big|_{\Omega_2} + w_2^h\big|_{\Omega_2} \ , \\ u^h\big|_{\Omega_p} &= v_1^h\big|_{\Omega_p} + w_1^h\big|_{\Omega_p} \ . \end{aligned} \tag{D.23}$$

The associated algebraic problem consists in solving the following sequence of linear systems:

$$\begin{cases} B_{II}^1 \mathbf{v}_I^1 = \mathbf{f}_I^1 - B_{I\Gamma}^1 \mathbf{g}_\Gamma \\ B_{II}^2 \mathbf{v}_I^2 = \mathbf{f}_I^2 - B_{I\Gamma}^2 \mathbf{g}_\Gamma \end{cases} , \quad \begin{cases} \mathbf{\Phi}^1 = \mathbf{f}_\Gamma^1 - B_{\Gamma I}^1 \mathbf{v}_I^1 - B_{\Gamma\Gamma}^1 \mathbf{g}_\Gamma \\ \mathbf{\Phi}^2 = \mathbf{f}_\Gamma^2 - B_{\Gamma I}^2 \mathbf{v}_I^2 - B_{\Gamma\Gamma}^2 \mathbf{g}_\Gamma \end{cases} , \tag{D.24}$$

$$\begin{bmatrix} A_{II}^p & A_{I\Gamma}^p & 0 \\ A_{\Gamma I}^p & A_{\Gamma\Gamma}^p + A_{\Gamma\Gamma}^2 & A_{\Gamma I}^2 \\ 0 & A_{I\Gamma}^2 & A_{II}^2 \end{bmatrix} \begin{bmatrix} \mathbf{w}_I^p \\ \mathbf{w}_\Gamma \\ \mathbf{w}_I^2 \end{bmatrix} = \begin{bmatrix} \mathbf{0} \\ -\left(\mathbf{\Phi}^1 + \mathbf{\Phi}^2\right) \\ \mathbf{0} \end{bmatrix} \tag{D.25}$$

Where the subscript I indicates the degrees of freedom relative to internal mesh nodes while the subscript Γ denotes degrees of freedom relative to the internal nodes.

To complete the definition of the discretization algorithm a formula for τ_ε needs to be prescribed. To this end, let us again focus our attention on the case $d = 1$ and assume $\Omega \equiv (0, 1)$ as in the previous paragraph. In such a case, if the standard lumping technique is adopted for the matrices corresponding to the zero-order terms in (D.19)-(D.21), the algebraic equations in (D.24)-(D.25) become identical to those that would arise in a Centered Finite Difference discretization. Using the methods of analysis in [23, 25], one can establish the following:

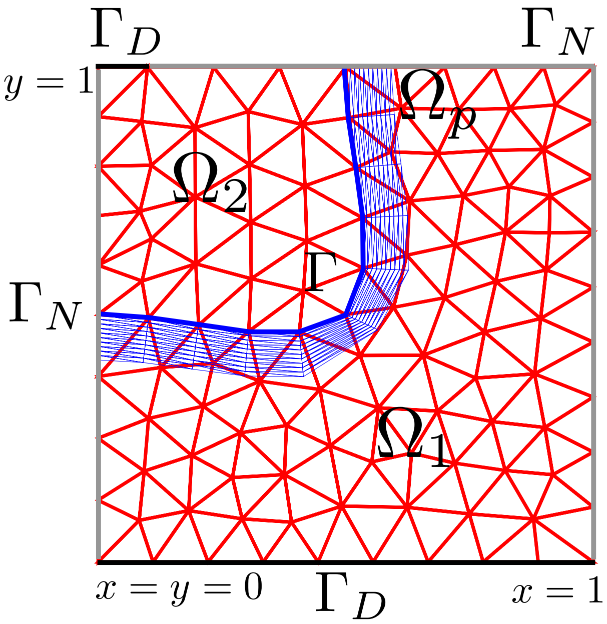

Figure (D.1): *Computational domain and mesh for the test case of Example D.1. The number of mesh points is $N = 117$, while the adopted diffusion coefficient is $\varepsilon = 1.5 \times 10^{-3}$. Finally the width of the interior layer results to be $\tau_\varepsilon = 9.16 \times 10^{-2}$.*

Theorem D.1. *Let $d = 1$ and $\tau_\varepsilon := \min\left\{d,\ 2\sqrt{\frac{\varepsilon_1}{\beta}}\ln N\right\}$. Then:*

$$\|u - u^h\|_\infty \leq C\frac{\ln N}{N}\ ,\ \|u^{h\prime} - u'\|_{\infty,\Omega\setminus\Omega_p} \leq \frac{\ln N}{N}\ ,\ \sqrt{\varepsilon}\|u^{h\prime} - u'\|_{\infty,\Omega_p} \leq C\frac{(\ln N)^2}{N}\ ,$$

where C is a constant independent of ε and of the number of mesh points N.

Although the bounds in Theorem D.1 have only been established in the case of $d = 1$, the numerical results in Example D.1 suggest that similar error estimates may also hold for $d = 2$.

Example D.1 (2D diffusion-reaction equation exhibiting an internal layer)**.** As a test case a problem with $d = 2$ in the domain pictured in Figure D.1 is considered, where:

$$\begin{aligned} r_1 = f_1 &= 1 \quad \text{in}\Omega_1\ , \\ r_2 = f_2 &= 0 \quad \text{in}\Omega_2\ , \\ g_D &= 1 \quad \text{on}\Gamma_D \cap \Omega_1\ , \\ g_D &= 0 \quad \text{on}\Gamma_D \cap \Omega_2\ . \end{aligned} \tag{D.26}$$

Figure D.2(a) and Figure D.2(b) show the solution of the test problem as computed by the algorithm of Section D.3 and by a standard piece-wise linear finite element discretization on a single quasi-uniform triangulation over the whole domain Ω, respectively. By comparing the plots in Figure D.3(a) and Figure D.3(b) one may notice that, while the error produced by the standard approximation has a non-trivial dependence on both the number of degrees of freedom N and on the singular perturbation parameter ε, for the algorithm proposed here the error, at least for small enough ε is a function of N alone.

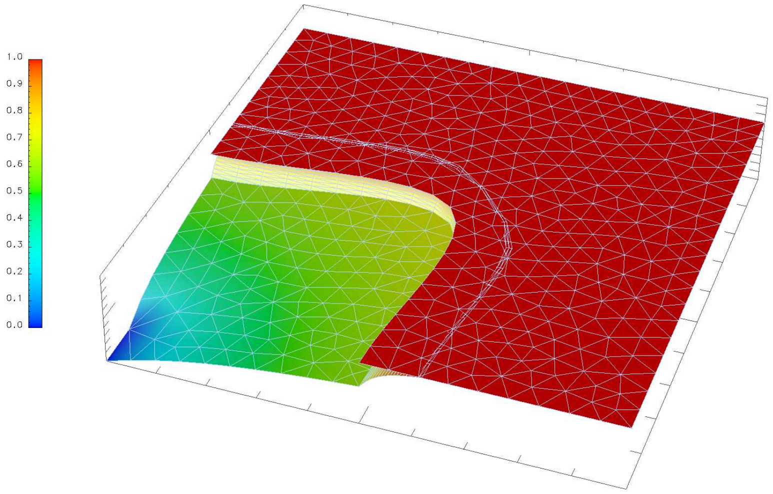

(a) Computed solution of the test problem for $\varepsilon = 1.5 \times 10^{-3}$ and $N = 456$ with the algorithm described in Section D.3. Note that in Ω_p both the solution u and the regular component v_1 are shown.

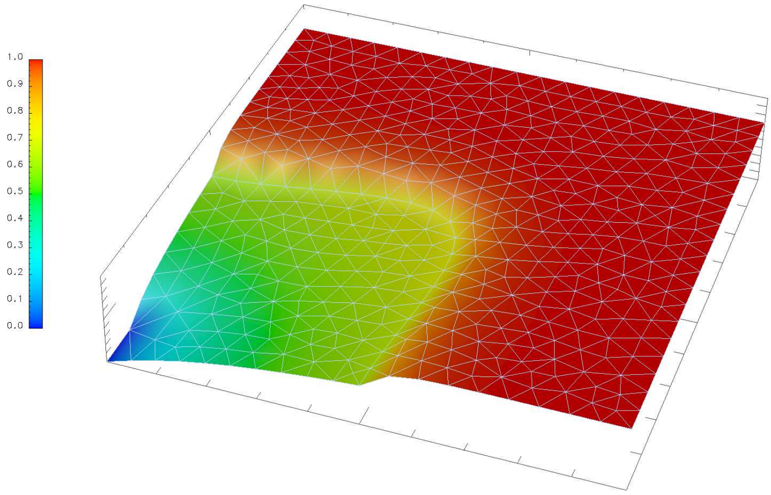

(b) Computed solution u of the test problem of Example D.1 for $\varepsilon = 1.5 \times 10^{-3}$ and $N = 456$ with standard finite element, on a quasi-uniform mesh.

Figure (D.2): *Computed solutions of the test problem of Example D.1.*

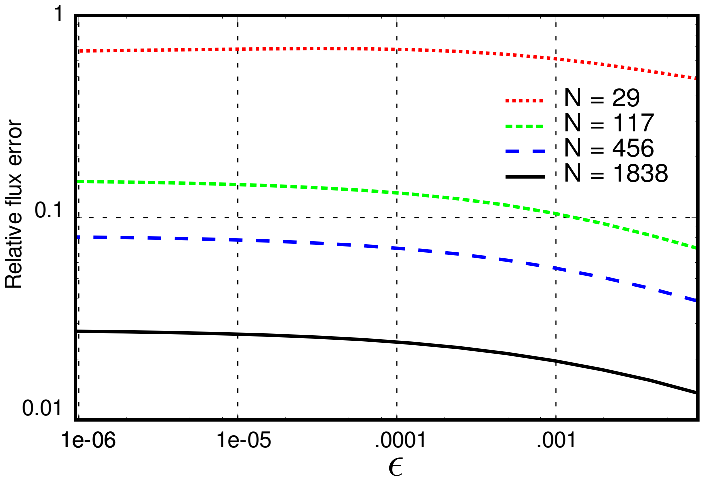

(a) Relative error in the flux Q computed by the algorithm of Section D.3

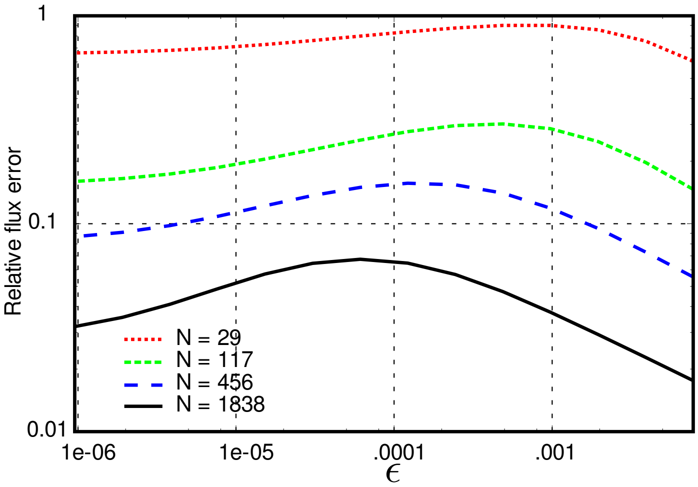

(b) Relative error in the flux Q computed on a quasi-uniform mesh

Figure (D.3): *Relative error in the flux Q for the test problem in Example D.1.*

Part VI

Summary and Bibliography

Summary

The last few CMOS technology generations exhibit a clear trend towards an increase in power consumption, strongly correlated to the decrease in the feature sizes imposed by pure *geometrical scaling*. It is foreseen that this trend will be further exacerbated in the near future, with industry approaching the theoretical limits of CMOS scaling. In fact all the technological solutions developed to maintain the same rate of improvements in circuit performance share the side-effect of a greater thermal insulation in the produced SoC or SiP, thus posing major heat dissipation problems. An accurate electro-thermal analysis is predicted to become a key factor to a reliable and cost-effective design and thus CAD tools are required to provide dependable means to simulate coupled electro-thermal effects. To this end, a new strategy to perform electro-thermal simulations at the system level is proposed in the thesis.

As a high-degree of integration inside the design flow is a major industry requirement, the mathematical model underlying the proposed approach was derived to fit the usual MNA structure. In fact, exploiting the similarities in the physical description of electrical current-flow and heat power-flow, heat diffusion at the system level is accounted for by a novel *thermal element*, embedding a 2D/3D diffusion-reaction PDE in its constitutive relations. The geometry upon which the PDE is casted is feasible to be defined on the base of available layout or package information, permitting thus to automate the extraction procedure inside an industrial environment. Coupling to the electrical network is then obtained by enforcing instantaneous energy conservation. The overall PDAE system is then formulated with a non-standard *element-wise notation*, which proves to be better suited to stress the hierarchical assembly structure adopted in actual implementations of MNA.

Analytical considerations are then provided in the case of a *linear* thermal element driven by external independent sources. Theorems proving existence and uniqueness of the solution are given either for the elliptic case and for the parabolic case. Besides their theoretical nature, these new results hold also a practical importance as they

provide a validation of a possible implementation of the thermal element in either admittance or conductance form. Finally the well posedness of a particular type of coupled electro-thermal system is also proved.

The numerical approximation of the thermal element model requires an efficient handling of spatial multi-scale issues. To this end two methods employing unstructured non-nested grids are presented. The first one (Chapter 4) is a particular finite element approach, firstly introduced by Wagner et al. (*patches of finite element method*). The original contribution of the thesis is in this case constituted by an extension of the method to cope with an arbitrary hierarchy of domains. A suitable formalism is devised to properly describe this extension, and *a-priori bounds* reflecting the asymptotic rate of convergence are provided. The second one (Appendix D) is a novel method to resolve internal layers in the case of reaction-dominant PDEs. The approach is introduced and analyzed on a 1D model problem, and then a sound extension to 2D case and complex geometry is provided with an illustrative example. A complete characterization of the thermal element stamp, obtained employing the first of the two methods, is then given.

Finally, the approach proposed in the thesis is tested on two numerical examples. The first one is a simple CMOS-inverter circuit, while the second one is a more realistic problem derived from the *distributed lumped-element description* of a power device. In both examples it is possible to see the reduced number of unknowns stemming from the patched finite element method (if compared to a standard finite element approach), and the natural way in which mutual heating is accounted for by the method proposed in the thesis. Furthermore, the power device example shows the possibility for the patched finite element method to associate a fine mesh with each thermally active device and deploy it at different positions in the die, providing thus a considerable gain during the mesh generation phase.

The results achieved in the thesis motivate further investigations in either theoretical and applied directions. From the modeling perspective a major improvement would be given by a suitable modification of the method to allow for the coupling with other refined description of physical phenomena (e.g. distributed description of semiconductor devices and transmission lines behaviors). From the analytical point of view a desirable contribution would be the extension of the theorems appearing in Chapter 3 to the non-linear case. Regarding the numerical discretization of the model two issues (out of the scope of the present research) are of major concern, namely the extension of the patched finite element method to account for advection fields and the development of a suitable multi-rate scheme to improve efficiency in the case largely different time-scales appear in the model. Lastly, the implementation of the method in an industrial environment to test its practical applicability on real designs will provide a final engineering validation. With this respect a work is on-going to integrate the thermal element inside `TITAN` (circuit simulator of Infineon AG).

Bibliography

[1] R. A. Adams and J. J. F. Fournier, *Sobolev spaces*, vol. 140 of Pure and applied mathematics, Elsevier Science, 2nd edition ed., 2003.

[2] A. Akturk, N. Goldsman, and G. Metze, *Self-consistent modeling of heating and MOSFET performance in 3-D integrated circuits*, Electron Devices, IEEE Transactions on, 52 (2005), pp. 2395–2403.

[3] G. Alì, A. Bartel, M. Culpo, and C. de Falco, *Analysis of a PDE thermal element model for electrothermal circuit simulation*, in Proceedings of Scientific Computing in Electrical Engineering (SCEE) 2008 (to appear), Mathematics in Industry, Springer-Verlag, 2009.

[4] S. S. Attar, M. Yagoub, and F. Mohammadi, *New electro-thermal integrated circuit modeling using coupling of simulators*, Electrical and Computer Engineering, 2006. CCECE '06. Canadian Conference on, (2006), pp. 1218–1222.

[5] P. Bagnoli, C. Casarosa, M. Ciampi, and E. Dallago, *Thermal resistance analysis by induced transient (TRAIT) method for power electronic devices thermal characterization. I. Fundamentals and theory*, Power Electronics, IEEE Transactions on, 13 (1998), pp. 1208–1219.

[6] K. Banerjee, S.-C. Lin, and N. Srivastava, *Electrothermal engineering in the nanometer era: from devices and interconnects to circuits and systems*, in ASP-DAC '06: Proceedings of the 2006 conference on Asia South Pacific design automation, Piscataway, NJ, USA, 2006, IEEE Press, pp. 223–230.

[7] K. Banerjee, S. Souri, P. Kapur, and K. Saraswat, *3-D ICs: a novel chip design for improving deep-submicrometer interconnect performance and systems-on-chip integration*, Proceedings of the IEEE, 89 (2001), pp. 602–633.

[8] A. Bartel, *Partial Differential-Algebraic Models in Chip Design - Thermal and Semiconductor Problems*, PhD thesis, TU Munich, 2004. VDI Verlag.

[9] A. Bartel and M. Günther, *A multirate W-method for electrical networks in state-space formulation*, J. Comput. Appl. Math., 147 (2002), pp. 411–425.

[10] A. Bartel and M. Günther, *From SOI to Abstract Electric-Thermal-1D multiscale modeling for first order thermal effects*, Mathematical and Computer Modelling of Dynamical Systems, 9 (2003), pp. 25 – 44.

[11] T. Biondi, G. Greco, M. Allia, S. Liotta, G. Bazzano, and S. Rinaudo, *Distributed modeling of layout parasitics in large-area high-speed silicon power devices*, Power Electronics, IEEE Transactions on, 22 (2007), pp. 1847–1856.

[12] R. Brayton, F. Gustavson, and G. Hachtel, *A new efficient algorithm for solving differential-algebraic systems using implicit backward differentiation formulas*, Proceedings of the IEEE, 60 (1972), pp. 98–108.

[13] H. Brezis, *Analyse Fonctionnelle - Thorie et Applications*, Masson, 1983.

[14] Y.-K. Cheng, P. Raha, C.-C. Teng, E. Rosenbaum, and S.-M. Kang, *ILLIADS-T: an electrothermal timing simulator for temperature-sensitive reliability diagnosis of CMOS VLSI chips*, Computer-Aided Design of Integrated Circuits and Systems, IEEE Transactions on, 17 (1998), pp. 668–681.

[15] L. Chua, C. Desoer, and E. Kuh, *Linear ad Nonlinear Circuits*, Mc Graw-Hill, New York, 1987.

[16] L. O. Chua and P. M. Lin, *Computer-Aided Analysis for Electronic Circuits*, Prentice Hall, Englewood Cliffs, 1975.

[17] S. Clemente, *Transient thermal response of power semiconductors to short power pulses*, Power Electronics, IEEE Transactions on, 8 (1993), pp. 337–341.

[18] L. Codecasa, D. D'Amore, and P. Maffezzoni, *Modeling the thermal response of semiconductor devices through equivalent electrical networks*, Circuits and Systems I: Fundamental Theory and Applications, IEEE Transactions on, 49 (2002), pp. 1187–1197.

[19] ———, *Compact modeling of electrical devices for electrothermal analysis*, Circuits and Systems I: Fundamental Theory and Applications, IEEE Transactions on, 50 (2003), pp. 465–476.

[20] M. Culpo and C. de Falco, *Dynamical iteration schemes for coupled simulation in nanoelectronics*, in PAMM, Proceedings in Applied Mathematics and Mechanics 2008, Wiley, 2009, pp. 10065 – 10068.

[21] ———, *Dynamical iteration schemes for multiscale simulation in nanoelectronics*, in PAMM, Proceedings in Applied Mathematics and Mechanics 2008, Wiley, 2009, pp. 10061 – 10064.

[22] M. Culpo, C. de Falco, G. Denk, and S. Voigtmann, *Automatic thermal network extraction and multiscale electro-thermal simulation*, in Proceedings of Scientific Computing in Electrical Engineering (SCEE) 2008 (to appear), Mathematics in Industry, Springer-Verlag, 2009.

[23] M. Culpo, C. de Falco, and E. O'Riordan, *Patches of finite elements for singularly-perturbed diffusion reaction equations with discontinuous coefficients*, in Progress in Industrial Mathematics at ECMI 2008 (to appear), Mathematics in Industry, Springer-Verlag, 2010.

[24] V. De and S. Borkar, *Technology and design challenges for low power and high performance*, in ISLPED '99: Proceedings of the 1999 international symposium on Low power electronics and design, New York, NY, USA, 1999, ACM, pp. 163–168.

[25] C. de Falco and E. O'Riordan, *Singularly perturbed reaction–diffusion equation with discontinuous diffusion coefficient*, International Journal of Numerical Analysis and Modeling (to appear), 6 (2009).

[26] R. Deheuvels, *Formes quadratiques et groupes classiques*, Presses Universitaires de France, Paris, 1981.

[27] C. A. Desoer and E. S. Kuh, *Basic Circuit Theory*, McGraw-Hill, New York, 1969. Chapter 12.

[28] R. Diestel, *Graph Theory*, Springer-Verlag, New York, 2000.

[29] D. Estévez Schwarz and C. Tischendorf, *Structural analysis of electric circuits and consequences for MNA*, International Journal of Circuit Theory and Applications, 28 (2000), pp. 131–162.

[30] L. Evans, *Partial Differential Equations*, American Mathematichal Society, 1998.

[31] P. A. Farrel, A. F. Hegarty, J. J. H. Miller, E. O'Riordan, and G. I. Shishkin, *Robust Computational Techniques for Boundary Layers*, Chapman and Hall/CRC Press, Boca Raton, 2000.

[32] U. Feldmann, M. Günther, and J. ter Maten, *Handbook of Numerical Analysis*, vol. XIII, North-Holland, 2005, ch. Modelling and discretization of circuit problems.

[33] U. Feldmann, M. Miyake, T. Kajiwara, and M. Miura-Mattausch, *On local handling of inner equations in compact models*, in Proceedings of Scientific Computing in Electrical Engineering (SCEE) 2008 (to appear), Mathematics in Industry, Springer-Verlag, 2009.

[34] D. P. Foty, *MOSFET modeling with SPICE: principles and practice*, Prentice-Hall, Inc., Upper Saddle River, NJ, USA, 1997.

[35] K. Fukahori and P. Gray, *Computer simulation of integrated circuits in the presence of electrothermal interaction*, Solid-State Circuits, IEEE Journal of, 11 (1976), pp. 834–846.

[36] C. Gear, *Simultaneous numerical solution of differential-algebraic equations*, Circuit Theory, IEEE Transactions on, 18 (1971), pp. 89–95.

[37] C. W. Gear, *Differential-algebraic equations index transformations*, SIAM J. Sci. Stat. Comput., 9 (1988), pp. 39–47.

[38] ——, *Differential algebraic equations, indices, and integral algebraic equations*, SIAM Journal on Numerical Analysis, 27 (1990), pp. 1527–1534.

[39] R. Glowinski, J. He, A. Lozinski, J. Rappaz, and J. Wagner, *Finite element approximation of multi-scale elliptic problems using patches of elements*, Numer. Math., 101 (2005), pp. 663–687.

[40] R. Glowinski, J. He, J. Rappaz, and J. Wagner, *Approximation of multiscale elliptic problems using patches of finite elements*, C. R. Math. Acad. Sci. Paris, 337 (2003), pp. 679–684.

[41] ——, *A multi-domain method for solving numerically multi-scale elliptic problems*, C. R. Math. Acad. Sci. Paris, 338 (2004), pp. 741–746.

[42] T. Grasser, *Mixed-Mode Device Simulation*, PhD thesis, Technischen Universität Wien Fakultät für Elektrotechnik, 1999.

[43] T. Grasser and S. Selberherr, *Fully coupled electrothermal mixed-mode device simulation of SiGe HBT circuits*, Electron Devices, IEEE Transactions on, 48 (2001), pp. 1421–1427.

[44] G. Greco and C. Rallo, *Xa integration in custom power mosfet analysis flow*, in SNUG 2008 proceedings, Feb. 2008. `http://www.snug-universal.org`.

[45] E. Griepentrog and R. März, *Differential-Algebraic Equations and Their Numerical Treatment*, Teubner Verlagsgesellschaft, Leipzig, 1986.

[46] D. Grier, *The innovation curve [Moore's law in semiconductor industry]*, Computer, 39 (2006), pp. 8–10.

[47] M. Günther, *Ladungsorientierte Rosenbrock-Wanner-Methoden zur numerischen Simulation digitaler Schaltungen*, VDI-Verlag, Düsseldorf, 1995.

[48] M. Günther and U. Feldmann, *CAD-based electric-circuit modeling in industry. I. Mathematical structure and index of network equations*, Surveys Math. Indust., 8 (1999), pp. 97–129.

[49] ——, *CAD-based electric-circuit modeling in industry. II. Impact of circuit configurations and parameters*, Surveys Math. Indust., 8 (1999), pp. 131–157.

[50] G. Hachtel, R. Brayton, and F. Gustavson, *The sparse tableau approach to network analysis and design*, Circuit Theory, IEEE Transactions on, 18 (1971), pp. 101–113.

[51] E. Hairer and G. Wanner, *Solving Ordinary Differential Equations II*, Springer Series in Computational Mathematics, Springer Verlag, Berlin, 1996.

[52] C. W. Ho, A. Ruehli, and P. Brennan, *The modified nodal approach to network analysis*, Circuits and Systems, IEEE Transactions on, 22 (Jun 1975), pp. 504–509.

[53] J. T. Hsu and L. Vu-Quoc, *A rational formulation of thermal circuit models for electrothermal simulation. I. Finite element method [power electronic systems]*, Circuits and Systems I: Fundamental Theory and Applications, IEEE Transactions on, 43 (1996), pp. 721–732.

[54] ——, *A rational formulation of thermal circuit models for electrothermal simulation. II. Model reduction techniques [power electronic systems]*, Circuits and Systems I: Fundamental Theory and Applications, IEEE Transactions on, 43 (1996), pp. 733–744.

[55] Y. Huang and J. Xu, *A conforming finite element method for overlapping and nonmatching grids*, Mathematics of Computation, 72 (2003), pp. 1057–1066.

[56] T. J. R. Hughes, G. Engel, L. Mazzei, and M. G. Larson, *The continuous Galerkin method is locally conservative*, J. Comput. Phys., 163 (2000), pp. 467–488.

[57] International Roadmap Commitee, *International Technology Roadmap for Semiconductors 2007 - Executive Summary*, tech. rep., ITRS, 2007.

[58] ——, *International Technology Roadmap for Semiconductors 2007 - Modeling and Simulation*, tech. rep., ITRS, 2007.

[59] T. Kato and T. Kataoka, *Computer-aided analysis of a power electronic circuit by a new multirate method*, Power Electronics Specialists Conference, 1998. PESC 98 Record. 29th Annual IEEE, 2 (1998), pp. 1076–1083 vol.2.

[60] Y. Kosaku, *Functional Analysis*, Springer-Verlag, 1980.

[61] J. C. Ku and Y. Ismail, *On the scaling of temperature-dependent effects*, Computer-Aided Design of Integrated Circuits and Systems, IEEE Transactions on, 26 (2007), pp. 1882–1888.

[62] S.-S. Lee and D. Allstot, *Electrothermal simulation of integrated circuits*, Solid-State Circuits, IEEE Journal of, 28 (1993), pp. 1283–1293.

[63] E. Lelarasmee, A. Ruehli, and A. Sangiovanni-Vincentelli, *The waveform relaxation method for time-domain analysis of large scale integrated circuits*, Computer-Aided Design of Integrated Circuits and Systems, IEEE Transactions on, 1 (1982), pp. 131–145.

[64] P. Leturcq, J.-M. Dorkel, A. Napieralski, and E. Lachiver, *A new approach to thermal analysis of power devices*, Electron Devices, IEEE Transactions on, 34 (1987), pp. 1147–1156.

[65] P. Li, L. T. Pileggi, M. Asheghi, and R. Chandra, *Efficient full-chip thermal modeling and analysis*, in ICCAD '04: Proceedings of the 2004 IEEE/ACM International conference on Computer-aided design, Washington, DC, USA, 2004, IEEE Computer Society, pp. 319–326.

[66] J. H. Lienhard IV and J. H. Lienhard V, *A Heat Transfer Textbook*, 3rd ed., 2006. `http://web.mit.edu/lienhard/www/ahtt.html`.

[67] J. Lin, M. Shen, M.-C. Cheng, and M. Glasser, *Efficient thermal modeling of SOI MOSFETs for fast dynamic operation*, Electron Devices, IEEE Transactions on, 51 (2004), pp. 1659–1666.

[68] J. L. Lions and E. Magenes, *Problèmes aux limites non Homogènes et Applications*, vol. 1, Paris, dunod ed., 1968.

[69] G. Massobrio and P. Antognetti, *Semiconductor Device Modeling with SPICE*, Mc Graw-Hill, 2nd ed., Apr. 1993.

[70] E. Mollick, *Establishing Moore's law*, Annals of the History of Computing, IEEE, 28 (2006), pp. 62–75.

[71] A. Osman, M. Osman, N. Dogan, and M. Imam, *An extended tanh law MOSFET model for high temperature circuit simulation*, Solid-State Circuits, IEEE Journal of, 30 (1995), pp. 147–150.

[72] S. Pekarek, O. Wasynczuk, E. Walters, J. Jatskevich, C. Lucas, N. Wu, and P. Lamm, *An efficient multirate simulation technique for power-electronic-based systems*, Power Systems, IEEE Transactions on, 19 (2004), pp. 399–409.

[73] T. Quarles, D. Pederson, R. Newton, A. Sangiovanni Vincentelli, and C. Wayne, *Spice3 version 3f5 users guide*, tech. rep., EECS Department, University of California, Berkeley, 1994.

[74] A. Quarteroni, R. Sacco, and F. Saleri, *Numerical Mathematics*, Springer - Applied mathematics, 2nd edition ed., 2006.

[75] A. Quarteroni and A. Valli, *Numerical approximation of Partial Differential Equations*, Computational Mathematics, Springer, 1997.

[76] V. Rezzonico, *Multiscale algorithm with patches of finite elements and applications*, PhD thesis, EPFL, Lausanne, Mar. 2006.

[77] V. Rezzonico, A. Lozinski, M. Picasso, J. Rappaz, and J. Wagner, *Multiscale algorithm with patches of finite elements*, Math. Comput. Simulation, 76 (2007), pp. 181–187.

[78] W. Rudin, *Real and Complex Analysis*, Mc Graw-Hill, 1970.

[79] ——, *Functional analysis*, Mc Graw Hill Science, Mc Graw-Hill, 1991.

[80] T. Sakurai and A. Newton, *Alpha-power law MOSFET model and its applications to CMOS inverter delay and other formulas*, Solid-State Circuits, IEEE Journal of, 25 (1990), pp. 584–594.

[81] R. Saleh and J. White, *Accelerating relaxation algorithms for circuit simulation using waveform-newton and step-size refinement*, Computer-Aided Design of Integrated Circuits and Systems, IEEE Transactions on, 9 (1990), pp. 951–958.

[82] S. Salsa, *Equazioni a derivate parziali*, Springer UNITEXT, Springer-Verlag, Italia, 2007.

[83] A. Sangiovanni-Vincentelli, *The tides of EDA*, Design and Test of Computers, IEEE, 20 (2003), pp. 59–75.

[84] R. Schaller, *Moore's law: past, present and future*, Spectrum, IEEE, 34 (1997), pp. 52–59.

[85] H. Shichman and D. Hodges, *Modeling and simulation of insulated-gate field-effect transistor switching circuits*, Solid-State Circuits, IEEE Journal of, 3 (Sep 1968), pp. 285–289.

[86] A. Shousha and M. Aboulwafa, *A generalized tanh law MOSFET model and its applications to CMOS inverters*, Solid-State Circuits, IEEE Journal of, 28 (1993), pp. 176–179.

[87] J. Silvester, *Determinants of block matrices*, The Mathematical Gazette, 84 (2000), pp. 460–467.

[88] T. Skotnicki, J. Hutchby, T.-J. King, H.-S. Wong, and F. Boeuf, *The end of CMOS scaling: toward the introduction of new materials and structural changes to improve MOSFET performance*, Circuits and Devices Magazine, IEEE, 21 (2005), pp. 16–26.

[89] V. Szekely, A. Poppe, A. Pahi, A. Csendes, G. Hajas, and M. Rencz, *Electro-thermal and logi-thermal simulation of VLSI designs*, Very Large Scale Integration (VLSI) Systems, IEEE Transactions on, 5 (1997), pp. 258–269.

[90] V. Szekely and K. Tarnay, *Accurate algorithm for temperature calculation of devices in nonlinear-circuit-analysis programs*, Electronics Letters, 8 (1972), pp. 470–472.

[91] C. Tischendorf, *Coupled systems of differential algebraic and partial differential equations in circuit and device simulation. Modeling and numerical analysis*, Habilitationsschrift, Humboldt-Univ. zu Berlin, 2004.

[92] R. Viswanath et al., *Thermal performance challenges from silicon to systems*, Intel Technology journal 3rd quarter, (2000).

[93] A. Vladimirescu and S. Liu, *The simulation of MOS integrated circuits using SPICE2*, tech. rep., EECS Department, University of California, Berkeley, 1980.

[94] S. Voigtmann. "Private communication".

[95] ——, *General linear methods for integrated circuit design*, PhD thesis, Humboldt-Universität zu Berlin, Mathematisch-Naturwissenschaftliche Fakultät II, 2006.

[96] J. Wagner, *Finite element methods with patches and applications*, PhD thesis, EPFL, Lausanne, 2006.

[97] T.-Y. Wang and C. Chen, *Thermal-ADI - a linear-time chip-level dynamic thermal-simulation algorithm based on alternating-direction-implicit (ADI) method*, Very Large Scale Integration (VLSI) Systems, IEEE Transactions on, 11 (2003), pp. 691–700.

[98] T.-Y. Wang and C. C.-P. Chen, *3-D Thermal-ADI: a linear-time chip level transient thermal simulator*, Computer-Aided Design of Integrated Circuits and Systems, IEEE Transactions on, 21 (2002), pp. 1434–1445.

[99] J. White, F. Odeh, A. L. Sangiovanni-Vincentelli, and A. Ruehli, *Waveform relaxation: Theory and practice*, tech. rep., EECS Department, University of California, Berkeley, 1985.

[100] S. Wünsche, C. Clauss, P. Schwarz, and F. Winkler, *Electro-thermal circuit simulation using simulator coupling*, Very Large Scale Integration (VLSI) Systems, IEEE Transactions on, 5 (1997), pp. 277–282.

[101] J. Xu, *Iterative methods by space decomposition and subspace correction*, SIAM Review, 34 (1992), pp. 581–613.

[102] ——, *The method of subspace corrections*, J. Comp. Appl. Math., 128 (2001), pp. 335–362.

[103] J. Xu and L. Zikatanov, *The method of alternating projections and the method of subspace corrections in Hilbert space*, Journal of The American Mathematical Society, 15 (2002), pp. 573–597.

[104] Y. Yang, C. Zhu, Z. P. Gu, L. Shang, and R. P. Dick, *Adaptive multi-domain thermal modeling and analysis for integrated circuit synthesis and design*, in ICCAD '06: Proceedings of the 2006 IEEE/ACM international conference on Computer-aided design, New York, NY, USA, 2006, ACM, pp. 575–582.

[105] F. Yu, M.-C. Cheng, P. Habitz, and G. Ahmadi, *Modeling of thermal behavior in SOI structures*, Electron Devices, IEEE Transactions on, 51 (2004), pp. 83–91.

[106] E. Zeidler and L. Boron, *Nonlinear Functional Analysis and Its Applications*, vol. 2 A, Springer-Verlag, 1989.

[107] Y. Zhan and S. Sapatnekar, *High-efficiency Green function-based thermal simulation algorithms*, Computer-Aided Design of Integrated Circuits and Systems, IEEE Transactions on, 26 (2007), pp. 1661–1675.

[108] ——, *A high efficiency full-chip thermal simulation algorithm*, Computer-Aided Design, 2005. ICCAD-2005. IEEE/ACM International Conference on, (6-10 Nov. 2005), pp. 635–638.

[109] M. Zhuang and W. Mathis, *Research on stepsize control in the BDF method for solving differential-algebraic equations*, Circuits and Systems, 1994. ISCAS '94., 1994 IEEE International Symposium on, 5 (1994), pp. 229–232 vol.5.

[110] O. Zienkiewicz and R. Taylor, *The Finite Element Method*, vol. 1 - The Basis, Butterworth - Heinemann, 5th ed., 2000.

List of Figures

1.1 Scope of ET-engineering 11
1.2 Schematic of the $\mu A709$ Operational Amplifier 15
1.3 Electro-thermal simulation of ICs: automated design flow 16

2.1 Drawing of a k-pins element with oriented current vector 20
2.2 CMOS inverter: electrical schematic 23
2.3 CMOS inverter: electro-thermal schematic 24
2.4 Shichman-Hodges MOS-FET model 27
2.5 MOS-FET with added temperature node 28
2.6 Thermal element mesh 29
2.7 CMOS inverter: voltage source set-up 36
2.8 CMOS inverter: n-channel MOS-FET set-up 37

4.1 Hierarchical domains 70
4.2 Domains violating hypothesis of Definition 4.3 71
4.3 Solution and rhs components for Example 4.1 79
4.4 Computational meshes employed in the numerical solution of problem (4.57) 80
4.5 Relative error on the energy-norm plotted against characteristic mesh length 81

6.1 CMOS-inverter: electro-thermal network 96
6.2 CMOS-inverter: globally conforming triangulation of 2D chip-layout . . 98
6.3 CMOS-inverter: patched triangulation of 2D chip-layout 98
6.4 CMOS-inverter: sparsity pattern of the thermal element stamp 99
6.5 CMOS-inverter: node voltages and junction temperatures for 1 kHz sine 99
6.6 CMOS-inverter: snapshots of distributed temperature field 100

7.1 Power nMOS-FET: cross-section 103
7.2 Power nMOS-FET: layout 103
7.3 Power nMOS-FET: simulation setup 106
7.4 Power nMOS-FET: non-conforming meshes for the whole CHIP and the basic cells 106
7.5 Power nMOS-FET: sparsity pattern of the thermal element stamp . . . 107
7.6 Power nMOS-FET: total dissipated power vs. mean temperature during turn-off 107
7.7 Power nMOS-FET: power densities snapshots at different time points . 108
7.8 Power nMOS-FET: junction temperatures snapshots at different time points 109

D.1 Computational domain and mesh for the test case of Example D.1 . . . 126
D.2 Computed solutions of the test problem of Example D.1. 128
D.3 Relative error in the flux Q for the test problem in Example D.1. 129

List of Tables

4.1 Results for the numerical approximation of problem (4.57) 81

6.1 CMOS-inverter: Shichman-Hodges MOS-FET model parameters 95
6.2 CMOS-inverter: thermal element parameters 97

7.1 Power nMOS-FET: basic cell parameters 104
7.2 Power nMOS-FET: Shichman-Hodges MOS-FET model parameters . . 104
7.3 Power nMOS-FET: thermal element parameters 104

Index

analytical models, 14

brute-force models, 14

CMOS inverter
  electrical balance, 22
  electro-thermal balance, 23
coercivity, 42
conservation laws, 19
continuity, 42
coupled ET system
  by-pass technique, 86
  element-wise formulation, 31
  elemental stamp, 87
  non-linear algebraic system, 86
  time discretization, 83

electrical device, 24
electro-thermal engineering, 9–12
  macro-scale effects, 11
  micro-scale effects, 10
electro-thermal simulation, 12–15
  analytical models, 14
  brute-force models, 14
  other approaches, 15
  RC-network fitting, 14
  relaxation methods, 13
  requirements, 12
  V-cycle methodology, 12
ellipticity, 42

finite element
  hierarchical domain families, 69
  interpolation estimates, 71
  patched space, 67
  patched space definition, 70
  resolution of internal and boundary layers, 121
  triangular FEM spaces, 68
  triangulation, 68

incidence matrix, 21

Kirchhoff's current law, 20
Kirchhoff's voltage law, 25

Lax-Milgram lemma, 43

macro-scale effects, 11
micro-scale effects, 10
MNA
  DAE formulation, 26
  element-wise formulation, 31
  incidence matrix, 21

modeling, 19–33
    conservation laws, 19
    constitutive relations, 24–31
    coupled system, 31
    electrical device, 24
    electro-thermal device, 27
    modified nodal analysis, 25
    thermal element, 28
modified nodal analysis, 25
Moore's law, 9
MOS-FET model
    Shichman-Hodges, 26

Newton's method, 86
    by-pass technique, 86

patches of finite element, 67–82
    approximation of a DR-PDE, 72
    direct solution procedure, 77
    interpolation estimates, 71
    iterative solution procedure, 78
    mixed integrals, 76

RC-network fitting, 14
relaxation methods, 13

scaling, 10
    equivalent, 10
    functional diversification, 10
    geometrical, 10
system level ET simulation
    coupled system, 31
    overview and setting, 15–17
    thermal element, 28

thermal element, 28–31
    2D heat diffusion, 31
    3D heat diffusion, 30
    analysis, 41
    interface, 29
    stamp, 89
    weak formulation of heat diffusion, 42
triangular finite element spaces, 68
triangulation, 68

V-cycle methodology, 12

well posedness of the coupled system, 54
well posedness of the thermal element
    elliptic case, 43
    parabolic case, 48